University of Calgary

PRISM Repository **https://prism.ucalgary.ca**

The Vault Open Theses and Dissertations

2018-05-11

Investigating the role of the cell envelope in E. coli relating to silver sensitivity and resistance

Westersund, Connor

Westersund, C. (2018). Investigating the role of the cell envelope in E. coli relating to silver sensitivity and resistance (Master's thesis, University of Calgary, Calgary, Canada). Retrieved from https://prism.ucalgary.ca. doi:10.11575/PRISM/31922

http://hdl.handle.net/1880/106641

Downloaded from PRISM Repository, University of Calgary

University of Calgary

Investigating the role of the cell envelope in *E. coli* relating to silver sensitivity and resistance

by

Connor Westersund

A THESIS

SUBMITTED TO THE FACULTY OF GRADUATE STUDIES

IN PARTIAL FULFILMENT OF THE REQUIREMENTS FOR THE

DEGREE OF MASTER OF SCIENCE

GRADUATE PROGRAM IN BIOLOGICAL SCIENCES

CALGARY, ALBERTA

MAY, 2018

© Connor Westersund 2018

Abstract

Silver (I) is an antimicrobial agent that has established antimicrobial activity, yet the mechanism of action is unclear. This thesis follows up on an observation that Ag^+ ions cause the cell membrane to separate from the cell wall in *Escherichia coli*. Data from a chemical genomic screen was utilized, identifying 6 Ag-responsive cells with single gene deletions (*damX*, *rodZ*, *minC*, *sanA*, *ybhO*, *tolB*), which are genes involved in maintenance of the cell envelope. When these mutants were grown in the presence of Ag^+, cells demonstrated extensive cell envelope damage as seen by transmission electron microscopy. Evaluation of kill curves, some mutants conferred resistance and others sensitivity to silver in comparison to wildtype. From the data collected, it was recognized that functions around cell wall and transport across the cell membranes have roles in both silver resistance and sensitivity.

Acknowledgements

Compiling this thesis work was not only a terrific way to reflect on the work completed along with its associated trials and tribulations, but it also reminded me of all the individuals that helped me along the way. I am indebted to my supervisor Dr. Raymond J. Turner, whose mentorship, tutelage, friendship, and above all else, his unselfish support to help develop not only my skills as a research scientist, but my professional skills as well, has made me forever grateful. To my supervisor committee, Dr. Joe Harrison and Dr. Lashitew Gedamu, I am very grateful for your valued guidance, encouragement, and friendship over the years. Thank you to the neutral chair Dr. Douglas G Muench for your continued support and guidance. Thank you to the internal examiner Dr. Michael David Parkins for his time and much appreciated feedback regarding this thesis.

I was very fortunate over the duration of my time in graduate studies to work with many great colleagues, most notably current and former Turner lab members including: Dr. Joe Lemire, Natalie Gugala, Niklas Janzing, Nadia Monych, Sean Booth, Damon Brown, Rajni Pushpker, Elena Piacenza, and Alessandro Presentato. I will treasure the time, and the journey that we shared together, and be forever thankful for all your support, intellectual input, and scientific discussions.

Last but certainly not least, I would not be here completing my masters and recently accepted into the Rutgers School of Dental Medicine, without the unwavering love and support from my family and friends. I wish to express my upmost gratitude to my brothers Chase and Cole and especially to my parents Curtis and Claudia, for always supporting me and providing me the means to pursue my goals and dreams. Special thanks to my girlfriend Chloe, for her continued love, patience, and encouragement. The contributions and sacrifices you have made were instrumental to my success, and I thank you.

Table of Contents

Page

Abstract ii

Acknowledgements iii

List of Tables vii

List of Figures and Illustrations viii

List of Symbols, Abbreviations, Nomenclatures xv

CHAPTER ONE: INTRODUCTION

1.1 Metal antimicrobials 1

1.2 The metal antimicrobial, silver (Ag^{+}) 6

1.3 Hypothesis and aims. 8

CHAPTER TWO: METHODS

2.0 Materials and media 10

2.1.1 Bacterial strains 10

2.1.2 Chemicals and reagents 12

2.1.3 Medium and culture conditions 12

2.1.4 Antimicrobial metal stock solutions 12

2.1.5 Stock antibiotics solutions 13

2.1.6 Plasmids and vectors 14

2.1.7 Optical density 15

2.1.8 Chemically competent *E. coli* cells preparation and transformation 15

2.1.9 Biofilm production 16

2.1.10 Primers 17

2.2 Red-recombinase mediated gene replacement 20

2.3 Complementation 21

2.4 Culture density analysis 22

2.4.1 Bacterial growth curves 22
2.4.2 Inoculation and growth 22
2.5 Evaluation of different metal exposure-responses of BW25113 *E. coli* 23
2.5.1 Metal exposure-response curves 23
2.5.2 Generating the metal exposure-response toxicity curve 23
2.5.3 Growing subcultures, inoculum preparation and preparation of antimicrobial challenge plate 24
2.5.4 Viable cell counts.....28
2.5.5 Preparation of antimicrobial challenge plate and manual counts of (CFU/ mL) for viable cell counts.....28
2.5.6 Crystal violet assay 29
2.5.7 Crystal violet dye exposure and biofilm cultivation 29
2.6 Microscopy 30
2.6.1 Confocal laser scanning microscopy 30
2.6.2 Microscopy biofilm production 30
2.6.3 Conducting confocal laser scanning microscopy.....31
2.6.4 Transmission electron microscopy 31
2.6.5 Whole cell transmission electron microscopy preparation 32
2.6.6 Scanning electron microscopy 32
2.6.7 Sputter deposition/coating and fixing of *E. coli* biofilms for SEM Imaging 33
2.7 High throughput metal resistance profiling 34
2.7.1 Disk diffusion assay.....34
2.7.2 Preparation of Inoculum and placement of antimicrobial disks 34

CHAPTER THREE: RESULTS

3.1 Choice of cell envelope associated genes 35
3.2 Chromosomal disruptions.....35

3.2.1 MG1655Δ*rodZ* knockout mutant and Ag^{+} exposure-response.....35
3.2.2 MG1655Δ*ispG* knockout mutant.....39
3.2.3 MG1655Δ*mreB* knockout mutant.....40
3.3 Plasmid based complementation and comparative analysis 40
3.4 Bacterial growth curves 44
3.5 Cell viability Assay (CFU/mL) for planktonic *E. coli* cells 47
3.5.1 Cell viability (CFU/mL) for *E. coli* biofilms……..……..50
3.6 Microscopy 52
3.8.3 Transmission electron microscopy analysis of treated and untreated *E. coli* biofilms 52
3.8.4 Silver nanomaterial structure 56
3.7 Disk diffusion assay.....58

CHAPTER FOUR: DISCUSSION

4.1 Toxin exposure-response of the respective cellular envelope associated Ag-responsive genes 60
4.2 Effects of Ag^{+} on *E. coli* planktonic cell morphology.....69
4.3 Conclusion 70
References.....140
Appendices A.....86
B.1 Complementation: Genomic DNA isolation, ligation to the InsTAclone cloning vector, and restriction enzyme digestion 87
Appendices B.....97
Appendices C.....99
Appendices D.....103
Appendices E 109
Appendices F 118

List of Tables

Table 2.0: Associated genotypes of *E. coli* strains used within this study 11

Table 2.1: All plasmids and vectors used in the work of this thesis 14

Table 2.2: Primers utilized throughout this thesis 18

Table 3.0: Minimal Biocidal Concentrations (MBC) and Minimal Inhibitory Concentrations (MIC) 39

Table 3.1. Minimal Biocidal Concentrations (MBC) and Minimal Biofilm Eradication Concentrations (MBEC) 51

Table 3.2: Detection of metal toxicity by use of disk diffusion susceptibility test illustrating displaying the zones of inhibition 125

Table F-1: Indicating the appropriate metal infused into sterile antimicrobial disks 219

List of Figures

Figure 1.0: General schematic of metal ion toxicity mechanisms: Mechanisms include: Ros generation causing DNA, protein and lipid damage; inhibition and disruption of membrane transport; impaired membrane function; redox reactions with thiol groups in proteins and enzymes resulting in enzyme damage and dysfunction. 4

Figure 1.1: Illustration of general metal ion resistance in bacteria. Mechanisms include: extracellular or intracellular sequestration of the metal; reduction in permeability; alteration of target sites; enzymic detoxification or efflux of the metal ions; acquisition of foreign DNA coding from antibiotic resistance; Mutations in the chromosome leading to resistance.....5

Figure 2.0: preparation of the antimicrobial challenge plate with highest metal challenge concentration being 50 µM. Using a sterile 96 well microtiter plate, the following steps described in section (*2.5.4*) illustrate how to aseptically prepare the challenge plate for toxin exposure-response analysis. The above microtiter plate represents a serial two-fold dilution gradient of a single antimicrobial challenge plate. This plate outline is kept the same for all three metal challenges. Rows B-D consisted of three technical replicates of one *E. coli* strain, while rows E-G consisted of another strain. In total there were 4 antimicrobial challenge plates for each of the metal challenges $AgNO_3$, AgSD, and $CuSO_4$. SC= sterility growth control (0.9% Saline), GC= Growth control of one *E. coli* strain. GC=Growth control of one *E. coli* strain.....26

Figure 2.1: preparation of the antimicrobial challenge plate with highest metal challenge concentration being 256 µM. Rows B-D consisted of three technical replicates of one *E. coli* strain, while rows E-G consisted of another strain. The above microtiter plate represents a serial two-fold dilution gradient of a single antimicrobial challenge plate. In total there were 4 antimicrobial challenge plates for each of the metal challenges $AgNO_3$, AgSD, and $CuSO_4$ (Table 2.2). SC= sterility growth control (0.9% Saline), GC= Growth control.GC= Growth control of one *E. coli* strain. GC=Growth control of one *E. coli* strain.....27

Figure 3.0: Agarose gel to confirm amplification of the gene replacement allele using the template plasmids pKD13 and pKD32 and *rodZ* KO and RC primers (Table 2.2). The primers have 5' 18-50 nt-homology extension, which recognize *E. coli* K-12 MG1655 chromosome, as well having 3' primers with sequence homology that matches the template plasmid. Successful reactions (Lanes: 6-10) produce a single clean PCR product that is 1.29 (Cm^R) or 1.4 kbp (Kn^R) (lane 5) in size relative to the antibiotic cassette from the template plasmids.....37

Figure 3.1: Confirmation of Flp-mediate excision of the FRT-flanked Cm^R antibiotic resistance cassette. MG1655Δ*rodZ*:: FRT-Cm^R-*FRT* insertion mutants were subjected to Flp-mediated excision of the antibiotic resistance cassette by electroporating pCP20 into the positive insertion mutants. Flp excision of the antibiotic resistance (Cm^R) cassette was accomplished by incubating the transformants at 30°C overnight and then at 43°C following antibiotic selection. The deletion mutants were confirmed via PCR using the OS and OAS primers (Table 2.2). Clean mutants should produce a band at approximately 412bp (180 OS and ORF + 146 OAS and ORF). Unsuccessful deletion mutants will have a banding pattern equal to about 1113bp – about the size of the undeleted gene or the intact antibiotic resistance cassette (1293bp).....38

Figure 3.2: Showing agarose gel containing the products of the ligation reaction of *rodZ* insert (1,014 bp) into the low copy number Amp-resistant expression vector pMS119EH$_A$ (3,967bp). Successful ligation (A) produced a product band roughly ~4,981 bp (3,967bp pMS119EH$_A$ + 1,014 bp *rodZ*) in size (lane 5 and 6). The subsequent digestion of the successful ligation products in lanes 5 and 6 in the top gel can be visualized in the (B) gels lane 2. After digestion from restriction enzymes HindIII and XbaI, two bands representing pMS119EH$_A$ (3,967bp) and (1,014 bp) *rodZ* are present.

.....42

Figure 3.3: Metal response curves of the gene deletion mutant K-12 MG1655*ΔrodZ*, the plasmid based complementation transformant MG1655Δ*rodZ::*pMS119EH$_A$::*rodZ*, and wildtype K-12 MG1655 *E. coli* cells. The three bacterial strains were subjected to 16-hour growth in the presences of three different metals antimicrobial challenges $AgNO_3$, AgSD, and $CuSO_4$ (Table 2.2). The average OD_{600}nm of three biological trials each containing three technical replicates was recorded utilizing a SpectraMax Plus 384 Microplate Reader. The solid black line represents K-12 MG1655 cultures, the dotted black line represents K-12 MG1655*ΔrodZ*, and dotted red line represents MG1655Δ*rodZ::*pMS119EH$_A$::*rodZ*.
.....43

Figure 3.4: Growth curve average of 3 biological trials each containing 3 technical trails, which measured the OD_{600} by SpectraMax Plus 384 Microplate Reader of the 7 different K-12 BW25113 *E. coli* strains (Table 2.0) 45

Figure 3.5: Growth curve of the average of 3 biological trials each containing 3 technical trails, which measured OD_{600} readings of BW25113 Δ*rodZ* and BW25113 Δ*damX* being compared to wildtype BW25113 cells. The results confirmed that all strains achieved a similar growth pattern, however, mutants appeared to have a prolonged *lag phase*.

.....46

Figure 3.6: log-kill CFU/mL generated for K-12 BW25113Δ*damX* and wildtype *E. coli* planktonic cells exposed to three antimicrobial metals $AgNO_3$, AgSD, and $CuSO_4$ (Table 2.2). The Δ*damX* cells were exposed to a 256 µM two-fold antimicrobial gradient (Figure 2.4) for a 24 hour period. These cultures were then diluted in dilution plates and 20 µL of culture was aliquoted onto 1.25% (w/v) LB agar plates (Figure 2.5). CFU/mL was calculated by multiplying the number of viable bacteria colonies by its respective dilution factor, divided by the total volume of the culture (180 µL). The CFU/mL was then expressed using logarithmic notation. 49

Figure 3.7: External cell morphologies of 1.0% phosphotungstic acid stained wildtype and BW25113Δ*damX E. coli* planktonic cells untreated (A and C) and pre-treated with 50 µM $AgNO_3$ treated (B and D) observed by transmission electron microscopy. Images A and B, are wildtype cells imaged at 15000x mag, and images C and C, were BW25113Δ*damX* cells taken at 9600 x magnification. Red arrows indicated electron-dense particles that were commonly found in treated TEM samples and areas of cell membrane separation. Some treated cells displayed either localized or complete separation of the cell membrane from the cell wall. plumes of cellular debris were also witnessed with accompanied electron-translucent cytoplasm and cellular disruption.

.....54

Figure 3.8: Internal cell envelope structures of planktonic of 1.0% phosphotungstic acid stained wildtype and BW25113 *E. coli* cells untreated (A and C) and pre-treated with 50 µM $AgNO_3$ (B and D) observed by transmission electron microscopy. 55

Figure 4.0: The identified silver resistant and sensitive genes proteins product and their relative cellular roles within the organism *E. coli.* Contents of the cell are not to scale. Notation defines genes that are silver sensitive or resistant as determined in this study. PG: Peptidoglycan, OMP: Outer membrane porin 61

Figure A-1: A agarose gel illustrating the successful amplification of the *rodZ* gene through PCR from the genomic DNA of K-12 MG1655 *E. coli.* Well 2 contains the negative control where no genomic DNA was added to the PCR reaction, while well 3 contains the successful amplified product, which corresponds to the size of the *rodZ* gene (1,014bp). Well 4 contains digested (XbaI and HindIII) Amp- resistant expression vector pMS119EHA, which was utilized for plasmid-based complementation. 89

Figure A-2: Illustrates the 1.25% (w/v) LB +/-Amp +/- X-gal plates used for the identification of successful ligation of pTZ57R/T::*rodZ* plasmids, which was transformed into DH5α *E. coli* cells. Plates were grown overnight at 37^{o}C and plasmids were isolated using

commercial kit (section *2.1.8*) These plasmids were then subjected to gel electrophoresis (section *2.1.*9) for qualitatively analysis (Figure B-3). 90

Figure A-3: A agarose gel demonstrating the successful ligation of the *rodZ* insert to the InsTAclone (Thermo Fischer Scientific) cloning vector pTZ57R/T. Well 2 consists of the negative control circularized pTZ57R/T and corresponds to a band size of 2887bp. Wells 3, 4, and 5 represent successful ligation for their corresponding product band is roughly band around ~3,900bp (2,886bp TA vector +1,014bp *rodz* ORF). 91

Figure A-4: Demonstrates the digestion of pTZ57R/T::*rodZ* by restriction enzymes XbaI and HindIII. Well three product bands highlight the TA (2,886bp) vector (top band) and the *rodz* (1,014bp) ORF (bottom band). Wells 2 and 5 consist of the negative controls used in the comparison of the digested pTZ57R/T:: *rodZ* product. 92

Figure A-5: The successful transformation of pMS119EH$_A$::*rodZ* into K-12 MG1655Δ*rodZ E. coli* cells. K-12 MG1655Δ*rodZ* cells are unable to grow in the presence of +100 μg/mL *Amp*, unless having acquired the Amp-resistant expression vector pMS119EH$_A$::*rodZ*. These cells were cultivated and utilized for cryogenic stock, which was stored at -80^{o}C. 93

Figure A-6: A agarose gel containing the purified *rodZ* inserts (1014bp) extracted from the digestion reaction of pTZ57R/T::*rodZ* by restriction enzymes XbaI and HindIII. This gel confirmed that infact the lower band corresponded to the *rodZ* ORF and that ligation of the insert into the Amp- resistant expression vector pMS119EH$_A$ could continue. 94

Figure A-7: Plasmid map of the InsTAclone cloning vector pTZ57R/T (from Thermo Fisher Scientific). The pTZ57R/T cloning vector is linearized and ddT tailed for direct use in cloning of PCR products (section *2.3.6*), generated with *Taq*, or other DNA polymerases or polymerase mixtures, which add extra adenines to the ends of PCR products. The map and the MCS region of the vector are presented in Figure 2.1 showing where XbaI and HindIII restriction enzyme sites are located. (Prathyumnan *et al*., 2011).....95

Figure A-8: Plasmid map of *Amp*-resistant expression vector pMS119EH$_A$ (Beketskaia *et al*., 2014) utilized for plasmid complementation analysis.....96

Figure B-1: Growth curve average of three biological each containing 3 technical trails, which measured OD$_{600}$nm readings of BW25113 mutant cells.

.....97

Figure C-1: Demonstrates the exposure-response relationship between K-12 BW25113 mutant's and K-12 BW25113 wildtype planktonic cells, subjected to a 50 µM two- fold dilution antimicrobial gradient prepared on 96 well microtiter challenge plates (Figure 2.3) containing the three metal antimicrobials: $AgNO_3$, AgSD, and $CuSO_4$.

.....100

Figure C-2: Demonstrates the exposure-response relationship between K-12 BW25113 mutant's and K-12 BW25113 wildtype planktonic cells, subjected to a 256 µM two- fold dilution antimicrobial gradient prepared on 96 well microtiter challenge plates (Figure 2.4) containing the three metal antimicrobials: $AgNO_3$, AgSD, and $CuSO_4$.

.....101

Figure C-3: Demonstrates the crystal violet assay of the BW25113 mutant's and wildtype biofilm cells grown for 24 hours in M9 media. The Δ*damX* cells were exposed to a 256 µM two-fold antimicrobial gradient (Figure 2.4) of the three antimicrobial metals (Table 2.2). 102

Figure D-1: One of three biological trails of viable cell counts for the 7 *E. coli* strains challenged by $AgNO_3$ that were spot plated (20 µL) onto 1.25% (w/v) LB agar. 104

Figure D-2: One of three biological trails of viable cell counts for the 7 *E. coli* strains challenged by AgSD that were spot plated (20 µL) onto 1.25% (w/v) LB agar.....105

Figure D-3: One of three biological trails of viable cell counts for the 7 *E. coli* strains challenged by $CuSO_4$ that were spot plated (20 µL) onto 1.25% (w/v) LB agar.....106

Figure D-4: log CFU/mL values generated for K-12 BW25113 mutant and wildtype *E. coli* cells exposed to three antimicrobial metals $AgNO_3$, AgSD, and $CuSO_4$. The Δ*rodZ* cells were exposed to a 256 µM two-fold antimicrobial gradient (Figure 2.1). These cultures were then diluted in dilution plates and 20 µL of culture was aliquoted onto 1.25% (w/v) LB agar plates. The CFU/mL was calculated by multiplying the number of viable bacteria colonies by its respective dilution factor, divided by the total volume of the culture (180 µL). The CFU/mL was then expressed using logarithmic notation.....107

Figure E-1: External planktonic morphologies of 1.0% phosphotungstic acid stained wildtype BW25113 *E. coli* cells untreated (A, C, and E) and 50 µM $AgNO_3$ treated (B. D, and F) observed by TEM. Images A and B, are imaged at 5000x mag, images C and D, were

taken at 7000x mag, and images E and F, were taken at 15000x mag. Red arrows indicated electron-dense particles that were commonly found in treated TEM samples and areas of cell membrane separation. Some treated cells displayed either localized or complete separation of the cell membrane from the cell wall. plumes of cellular debris were also witnessed with accompanied electron-translucent cytoplasm and cellular disruption. 110

Figure E-2: External planktonic morphologies of 1.0% phosphotungstic acid stained BW25113Δ*minC E. coli* cells untreated (A) at 7800x magnification and 50 µM $AgNO_3$ treated (B) at 9600x magnification, observed by TEM. In untreated sample BW25113Δ*minC* confines to normal bacillus morphology. In contrast, treated BW25113Δ*minC* appear to have complete disruption and compromise of the cellular envelope. 112

Figure E-3: External planktonic morphologies of 1.0% phosphotungstic acid stained BW25113Δ*sanA E. coli* cells untreated (A) and 50 µM $AgNO_3$ treated (B) observed by TEM at 7800 x magnification. In untreated sample BW25113Δ*minC* confines to normal bacillus morphology. In contrast, treated BW25113Δ*sanA* appear to have complete disruption of the cellular envelope.....113

Figure E-4: External planktonic morphologies of 1.0% phosphotungstic acid stained BW25113Δ*ybhO E. coli* cells untreated at (A) and 50 µM $AgNO_3$ treated (B) observed by TEM at 7800 x magnification. In untreated sample BW25113Δ*ybhO* confines to normal bacillus morphology. In contrast, treated BW25113Δ*ybhO* appear to have localized disruption of the cellular envelope with plumes of cellular debris being released from cell (red arrow). 114

Figure E-5: External planktonic morphologies of 1.0% phosphotungstic acid stained BW25113Δ*tolB E. coli* cells untreated (A) and 50 µM $AgNO_3$ treated (B) observed by TEM, at 19000 x magnification. In untreated sample BW25113Δ*tolB* confines to normal bacillus morphology. In contrast, treated BW25113Δ*tolB* appear to have complete disruption of the cellular envelope……...115

Figure E-6: External planktonic morphologies of 1.0% phosphotungstic acid stained wildtype K-12 MG1655 *E. coli* cells untreated (A) and 50 µM $AgNO_3$ treated (B) observed by TEM, at 4000 x magnification and 7000X magnification respectively. In the untreated sample, wildtype K-12 MG1655 cells appear to have a normal phenotype. In contrast, the treated cells displayed either localized or complete separation of the cell membrane from the cell wall.....116

Figure E-7: External planktonic morphologies of 1.0% phosphotungstic acid stained K-12 MG1655Δ*rodZ E. coli* cells untreated (A) and 50 μM $AgNO_3$ treated (B) observed by TEM, at 5000 x magnification and 6500X magnification respectively. In the untreated cells, some of the mutant MG1655Δ*rodZ* cells displayed a mutant elongated bacillus phenotype, which was commonly found throughout the sample. In contrast the treated cells displayed either localized or complete separation of the cell membrane from the cell wall.....117

Figure F-1: Illustrates the disk diffusion assay conducted on wildtype BW25113 cells with the metals present in Table J-1. 120

Figure F-2: Illustrates the disk diffusion assay conducted on wildtype BW25113Δ*damX* cells with the metals present in Table J-2. 121

Figure F-3: Illustrates the disk diffusion assay conducted on wildtype BW25113Δ*rodZ* cells with the metals present in Table J-2.....122

Figure F-4: Illustrates the disk diffusion assay conducted on wildtype BW25113Δ*minC* cells with the metals present in Table J-2. 123

Figure F-5: Illustrates the disk diffusion assay conducted on wildtype BW25113Δ*SanA* cells with the metals present in Table J-2.....124

Figure F-6: Illustrates the disk diffusion assay conducted on wildtype BW25113Δ*ybhO* cells with the metals present in Table J-2. 125

Figure F-7: Illustrates the disk diffusion assay conducted on wildtype BW25113Δ*tolB* cells with the metals present in Table J-2.....126

Section 1.0: Symbols, Abbreviation, and Nomenclature

Abbreviation and terms	Technical definition
Ab^R	Antibiotic resistance cassette
Amp^R	Ampicillin resistance, generated from an ampicillin resistance cassette.
ATP	Adenosine triphosphate
bet	A lambda phage gene that produces a Recombination protein that functions in general recombination and in the late, rolling-circle mode of lambda DNA replication.
Biofilm(s)	Any group of microorganisms in which cells stick to each other and often also to a surface. These adherent cells become embedded within a slimy extracellular matrix that is composed of extracellular polymeric substances (EPS).
BSC	Biosafety cabinet
Cm^R	Chloramphenicol resistance, generated from a Chloramphenicol resistance cassette or a *cat* (Chloramphenicol acetyltransferase*)* gene.
CBD	Calgary Biofilm Device is a lid that fits a 96 well microtiter plate, which contains 96 polystyrene equivalent pegs.
CLSM	Confocal laser scanning microscope
DMSO	Dimethyl sulfoxide is an organosulfur compound with the formula $(CH_3)_2SO$
dNTP	nucleoside triphosphate (NTP) is a molecule containing a nucleoside bound to three phosphate groups.
dsDNA	Double stranded DNA
E. coli	*Escherichia coli*
EDTA	Ethylenediaminetetraacetic acid

EtOH	Ethanol
exo	A lambda phage gene that produces a protein exonuclease that facilitates phage DNA recombination through the double-strand break repair (DSBR) and single-strand annealing pathways
Flp	Flippase (Flp) derived from the 2 μm plasmid of baker's yeast *Saccharomyces cerevisiae*.
FRT	flippase recognition target
gam	A lambda phage gene that produces protein that protects linear double-stranded DNA from host exonuclease degradation
GC	Growth control
gDNA	Genomic DNA
g	g-force
HGT	Horizontal gene transfer
IM	Inner membrane
Kn^R	Kanamycin resistance, generated from a Kanamycin cassette.
keV	Kiloelectron volt
LB	Lysogeny broth
LPS	lipopolysaccharide
MCS	Multiple cloning site
MDR	Multidrug- resistant
NSLB	No Salt Lysogeny Broth medium
OAS	Outside antisense primer, confirmation primer that binds to the antisense (non-coding) strand of DNA 3'-5'

OD	Optical density
OD_{600}	Optical density measurement at 600 nm
OM	Outer membrane
O/N	Refers to overnight growth of culture medium
ORF	Open reading frame
OS	Outside sense primer, confirmation primer that binds to the coding strand of DNA 5'-3'
PCR	Polymerase chain reaction
Planktonic	floating as single cells in liquid medium
PVD	Physical vapor deposition
ROS	Reactive oxygen species
rpm	Revolutions per minute
RT	Room temperature
(-)/SC	Sterility control
SDS	Sodium dodecyl sulfate
SEM	Scanning electron microscope
SOC	Super optimal broth with catabolite repression recovery media
TAE	Tris-acetate-EDTA

Taq	A thermostable DNA polymerase named after the thermophilic bacterium Thermus aquaticus from which it was originally isolated from
TEM	Transmission electron microscope
UV	Ultra violet radiation
V	Volts
WT	Wildtype strain

Chapter One: Introduction

1.1 Metal antimicrobials

Metals are essential for all forms of life, fulfilling certain structural and catalytic roles in biological processes, including precursor biosynthesis, DNA replication, transcription, respiration, and response to oxidative stress (Palmer and Skaar, 2016; Lemire *et al*., 2013). For instance, transition *d*-block metals, like: manganese, iron, cobalt, nickel, and copper, have unfilled *d*-orbitals and therefore are redox active (Palmer and Skaar, 2016).

These redox-active essential metals are found ubiquitously in several types of living organisms, functioning nearly exclusively as constituents of proteins, such as enzymes, storage proteins, and transcription factors (Lemire *et al*., 2013; Porcheron *et al*., 2013). Furthermore, their finely tuned redox activity permits essential metals to transfer electrons as part of vital biological processes, such as: respiration, N fixation, and photosynthesis (Finney and O'Halloran, 2003; Lemire *et al*., 2013). Although these metals are essential for many crucial biological processes, these metals are lethal at high intracellular concentrations (Lemire *et al*., 2013). Moreover, particular non-essential metals such as: silver (Ag), mercury (Hg), lead (Pb), and tellurium (Te) have been demonstrated to be extremely toxic to most microorganisms and have bactericidal activity at exceptionally low concentrations (Harrison *et al*., 2004; Lemire *et al*., 2013; Nies, 1999).

Since metal ions demonstrate extremely potent toxicity towards bacteria and yeast, particular metals have been used for their antimicrobial properties since ancient times (Lemire *et al*., 2013). For example, vessels impregnated or made of Cu and Ag metal have been used in water disinfection and food preservation practices since the time of the Persian kings (Lemire *et al*., 2013). This implementation of metals to reduce contaminant loads of resources was then later adopted by other ancient civilizations such as the Phoenicians, Greeks, Romans, and Egyptians (Alexander, 2009; Lemire *et al*., 2013). Moreover, the medicinal use of metals has also been prevalent throughout antiquity to treat an array of different ailments such as leprosy, tuberculosis, gonorrhea, and syphilis (Lemire *et al*., 2013). However, with the discovery of penicillin by Nobel laureate Sir Alexander Fleming in the 1920s (Aminov, 2010; Clardy *et al.*, 2009; Tan and Tatsumura, 2015), and the subsequent commercial development of new antibiotic drugs, metal antimicrobials prevalence in medicine rapidly diminished (Lemire *et al*., 2013; Tan and Tatsumura, 2015).

Today, antimicrobial metal compounds can be found in wound dressings, coatings of indwelling medical devices, and as metallic surfaces (Afessa *et al*., 2010; Kollef *et al*., 2008; Saint *et al*., 1998). Nonetheless, with the emergence and rise of multi-drug resistant (MDR) bacteria accompanied by the severe decline in the rate of development of new antibiotics, a resurgence of research into alternatives antimicrobials, like metals, is generating new applications for industry, agriculture, and healthcare (Allen *et al*., 2014; Lemire *et al*., 2013). This research has led to the determination and discovery that particular metals disrupt antibiotic-resistant biofilms (Teitzel and Parsek, 2003), exert synergistic bactericidal activity with other antimicrobials (Harrison *et al*., 2008), inhibit metabolic pathways (Figure 1.0) (Middaugh *et al*., 2005; Macomber *et al*., 2011; Macomber and Elsey, 2009), and kill multidrug-resistant bacteria (Kaneko *et al.*, 2007), resulting in metal based-antimicrobials having real potential for profiling sustainability solutions to infection care and health (Turner, 2017).

However, in the era of MDR bacteria, metals unfortunately are not the end-all cure-all solution that the medical field is looking for (WHO, 2014; Hobman and Crossman, 2014). Just like with the rampant exposure to antibiotics giving rise to antibiotic resistance bacteria (Džidić *et al*., 2008; Spratt, 1994; McDermott *et al*., 2003), the natural exposure of bacteria to bioavailable metals (both essential and toxic) over the past billions of years has likely been the driver for the evolution of the ability of microorganisms to control cellular levels of these bioavailable metal ions (Hobman and Crossman, 2014). Thus, bacteria have evolved mechanisms for the acquisition of essential metals, controlling intracellular levels of metals, and eliminating those that are in excess and are deleterious (Hobman and Crossman, 2014). Microorganisms can resist metal toxicity by extracellular or intracellular sequestration of the metal, reduction in permeability, alteration of target sites, enzyme detoxification or efflux of the metal ions, highlighted in Figure 1.1. (Hobman & Brown, 1997). For example, a well characterized genetic elements, which confers resistance to silver (Ag^{+}) is the *sil* operon, which microorganisms obtain through horizontal gene transfer (HGT). This operon is comprised of a gene cassette, which includes *silP*, *silA*, *silB*, *silC*, *silR*, *silS*, *silE*, ORF105, and *silABC* (Belly and Kydd, 1982). Since their initial identification, sil genes have been identified in *Salmonella Enterobacter*, *Escherichia coli*, *Pseudomonas*, *Acinetobacter*, *Klebsiella*, and methicillin-resistant coagulase-negative *Staphylococcus aureus* (Finley *et al*., 2015). The Sil system is believed to mediate silver resistance by limiting the accumulation of silver in the cell through a combination of silver

sequestration in the periplasm (via SilE and SilF binding) and active efflux transporter SilCBA and the putative P-type ATPase transporter SilP (Randall *et al*., 2015). Although many different types of metal resistant mechanisms have been well characterized (Hobman and Crossman, 2014), there have been far fewer investigations of the biochemical and biophysical mechanisms through which metals exert toxicity in bacteria (Lemire *et al*., 2013). This area of study has been neglected and overshadowed by the complexity and metabolic diversity of microorganisms, which complicates the study of metal toxicity (Lemire *et al*., 2013). Uncovering the unique biochemical pathways and toxicity mechanisms of different metal-based antimicrobials is imperative if we are to understand why resistance to these elements evolves and to improve the design of metal-based biocide agents to kill bacterial pathogens (Allen *et al*., 2014; Hobman and Crossman, 2014; Lemire *et al*., 2013).

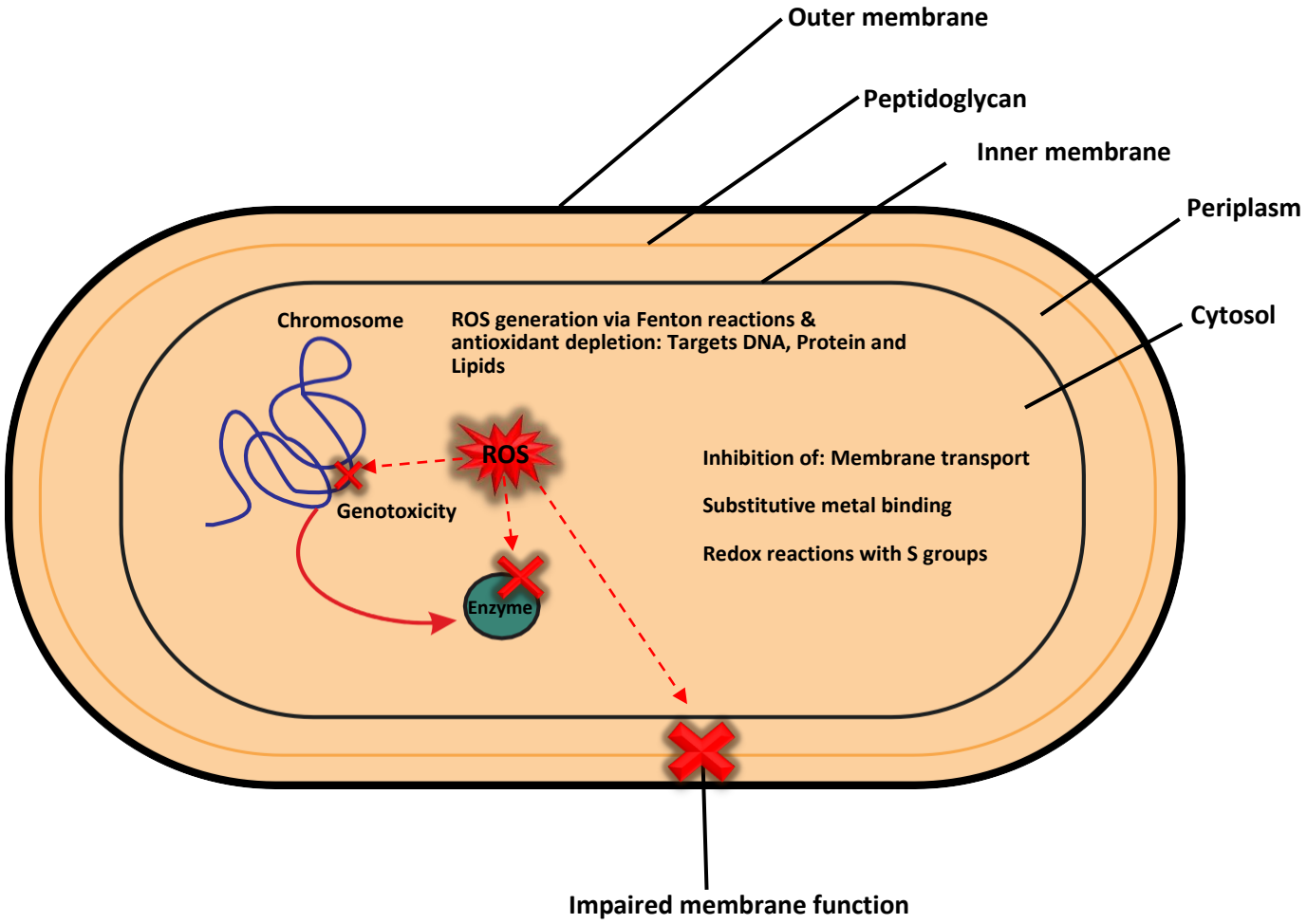

Figure 1.0: General schematic of metal ion toxicity mechanisms: Mechanisms include: ROS generation causing DNA, protein and lipid damage; inhibition and disruption of membrane transport; impaired membrane function; redox reactions with thiol groups in proteins and enzymes resulting in enzyme damage and dysfunction.

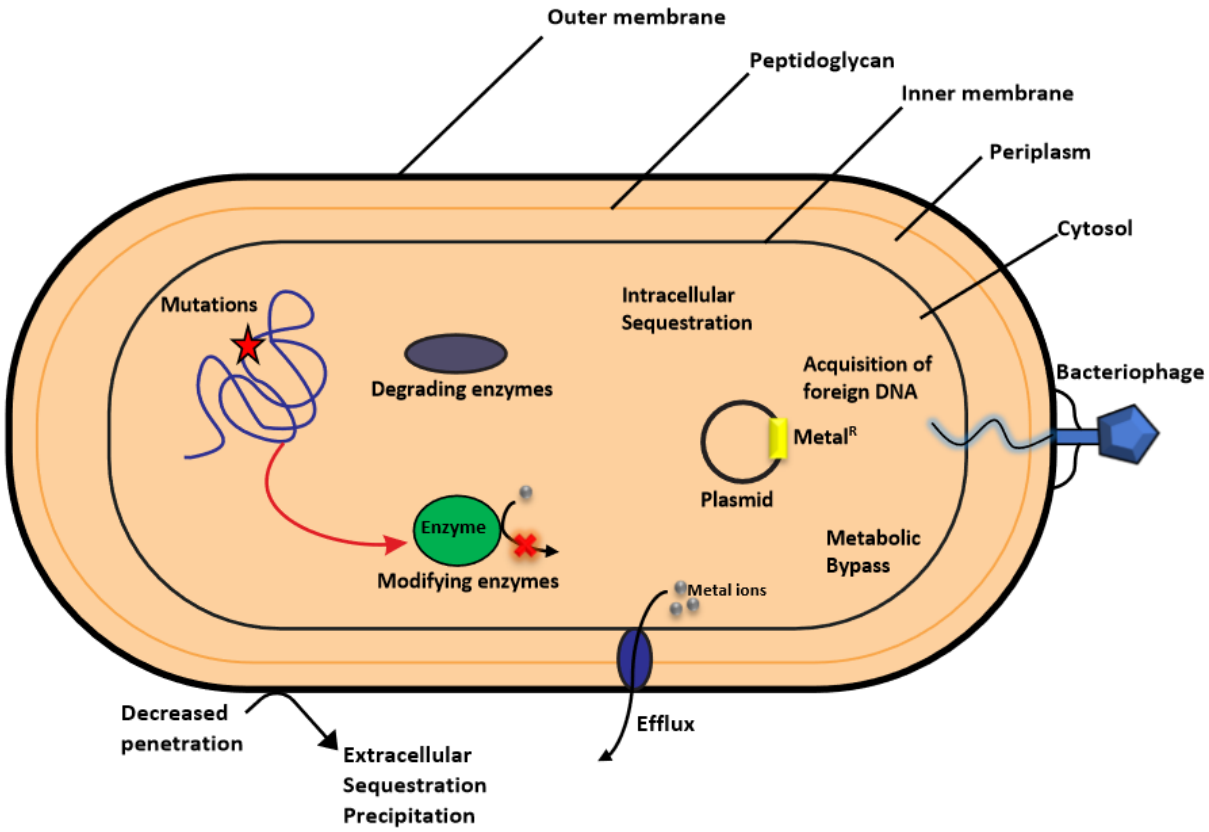

Figure 1.1: Illustration of general metal ion resistance in bacteria. Mechanisms include: extracellular or intracellular sequestration of the metal; reduction in permeability; alteration of target sites; enzyme detoxification or efflux of the metal ions; acquisition of foreign DNA coding from antibiotic resistance; Mutations in the chromosome leading to resistance.

1.2 The metal antimicrobial, silver (Ag^+)

Since ancient times, the antimicrobial activity of silver has been known to be effective against a broad range of microorganisms (Akram *et al*., 2016; Jung *et al*., 2008; Lemire *et al*., 2013). Herodotus, the Father of History, accounts that no Persian king, including Cirrus, would drink water that was not boiled and transported in flagons of silver, for the silver reduced the contaminant load of the water, while keeping it fresh for years (Alexander, 2009; Lemire *et al*., 2013). Over the millennia, silver has been utilized for variety of purposes due to its low exhibited toxicity towards eukaryotic cells in comparison to its lethality at low concentrations to prokaryotic organisms (Alexander, 2009). Now, in the 21st century, silver ions (Ag^+) are being utilized to control infection and contaminant loads in a variety of medical practices and devices, including dental restorations, coatings on indwelling medical devises (catheters and endotracheal tubes), eyedrops, and bandages. (Klasen, 2000; Lemire *et al*., 2013; Silver and Phung, 1996; Slawson *et al*., 1992). Silver has also started to become implemented into a number of nonmedical consumer products including: deodorants, toothbrushes, toilet seats, drinking glasses, and even washing machines (Jung *et al*., 2008; Turner, 2017). With silver's resurgence in applications of both the medical and consumer product fields of industry, it is surprising that the mechanisms by which silver ions (Ag^+) impose their toxicity onto microbial cells is still incomplete (Celment and Jarret, 1994). In the literature, there have been many observations of different Ag^+ cellular targets, which has led to the establishment of some mechanisms of the antimicrobial action of silver ions (Jung *et al*., 2008). What has been observed is that the antimicrobial action of silver ions is closely correlated to their interactions with thiol (sulphhydryl, R-SH) groups (Belly and Kydd, 1982; Bragg and Rainnie, 1974; Furr *et al*., 1994; Lemire *et al*., 2013). This relationship is described by the hard-soft acid base theory, which has been determined empirically and provides an ordering of transition metals according to their preferences for specific organic ligands (Jung *et al*., 2008; Lemire *et al*., 2013.) Essentially, Ag(I) is classified as a soft acid and consequently has electron-sharing affinities that can result in the energetically favorable formation of covalent bonds between soft bases, such as the sulphhydryl groups that are found in proteins (Lemire *et al*., 2013). Thus, the interaction and binding of silver ions to thiol groups in enzymes and proteins, results in their deactivation (Dakal *et al*., 2016). As a result, cells exposed to Ag^+ ions can have a depletion of antioxidant

reserves, particularly glutathione, which is responsible for preventing damage to important cellular components caused by reactive oxygen species (ROS).

Further *in vitro* experiments have revealed that micromolar concentrations of Ag^+ ions directly inactivate purified fumarase A, a member of the dehydratase family (Xu and Imlay, 2012). Additional examinations, utilizing electron paramagnetic resonance analysis and measurements of released iron confirmed that damage was directly correlated to the destruction of the [4Fe-4S] cluster, and indeed, the reconstruction of the cluster fully restored fumarase activity (Xu and Imlay, 2012). Furthermore, it is thought that the direct or indirect destruction of [4Fe-4S] clusters caused by Ag^+ ions could result in the release of additional Fenton-active Fe^{2+} into the cytoplasm, generating hydroxide (OH^-) and the highly reactive hydroxyl radical ($OH^\bullet$) (Lemire *et al*., 2013; Park *et al*., 2009; Xu *et al*., 2012). However, the precise mechanism of ROS-mediated antibacterial activity of Ag^+ is not fully clear (Pellieux *et al*., 2000).

Another established Ag^+ toxicity mechanism is silver's ability to disrupt the activity of the bacterial electron transport chain (ETC) (Bragg and Rainnie, 1974; Gorden *et al*., 2010; Lemire *et al*., 2013 Lok *et al*., 2006). In the organism *Vibrio harveyi*, Ag(I) has been demonstrated to inhibit the activity of NADH:quinone oxidoreductase (NQR), which is a component of the respiratory chain of some bacteria and generates a redox-driven transmembrane Na^+ potential by translocating Na^+(Lemire *et al*., 2013). It is proposed that Ag(I) dissipates the chemiosmotic potential of the membrane by destroying the proton motive force of the ETC, causing proton leakage through the membrane. (Dibrov *et al*., 2002; Lemire *et al*., 2013).

One observed toxicity phenotype with no established mechanism involves Ag^+ ability to jeopardize the integrity of the cellular envelope in *E. coli* and *Staphylococcus aureus* (Jung *et al*., 2008). The associated phenotype suggests that Ag^+ ions severely compromise the cell envelope, resulting in the cell lysis and separation of the cell membrane from the cell wall (Jung *et al*., 2008). What remains unclear from morphological studies examining the toxicity of Ag^+ towards the cell envelope, is that it is difficult to determine whether membrane disruption or the observed detachment of the cell wall are a cause or a consequence of cell death (Jung *et al*., 2008). Here from this thesis work, I look to add investigative insight into possible genetic determinants associated with the cell envelope of *E. coli* to be possibly involved in Ag(I) incomplete toxicology.

1.3 Hypothesis and aims

Following a similar methodology to Baryshnikova *et al*., 2010 "Quantitative analysis of fitness and genetic interactions in yeast on a genome scale", Dr. Lemire from Dr. Tuner's Microbial Biochemistry Laboratory at the University of Calgary, preformed a genetic chemical screen of the Keio collection, an ordered mutant library of *E. coli*. The Keio collection was systematically created by Baba *et al*., 2006, to contain all single-gene deletions of all non-essential genes in *E. coli* K-12. The chromosomal deletions of the Keio collection were facilitated by the Lambda Red Homologous Recombination-based technique (Baba *et al*., 2006). The Recombinase technique enabled Baba and colleagues to target 4288 open reading frames of coding genes and replace them with a kanamycin cassette flanked by FLP recombinase recognition target sites (FRT), resulting in their inactivation (Baba *et al*., 2006). The Keio collection offer researchers a new resource for systematic analyses of unknown gene functions and gene regulatory networks, but also for genome-wide testing of mutational effects and responses to antimicrobial agents in a common strain background, *E. coli* K-12 BW25113 (Baba *et al*., 2006). Dr. Lemire utilized the Keio collection to screen Keio collection *E. coli* colony size as a proxy for fitness, of 3985 confirmed non-essential *E. coli* mutants to 100µM of $AgNO_3$ infused in M9 minimal noble agar media against their unchallenged counterparts. From the genetic chemical screen, Dr. Lemire discovered over 225 mutants silver sensitive and 177 mutants to display a resistant phenotype. The Sensitive ('sicker') or resistant ('healthier') mutants were selected based on a difference of 2 standard deviations of colony size from the normal, which was determined through photographed images that were processed using software that measures colony areas in terms of pixels. Of these mutants, 20 sensitive and 4 resistant mutants were found to be involved in cell envelope homeostasis. From these 24 genes, 6 (*damX, rodZ, minC, sanA, ybhO, and tolB)* were chosen to be further characterized based of their possible collective phenotype having possible involvement in Ag(I) cell envelope toxicity mechanism.

The overarching goal of this thesis was to provide answers in regard to the cell envelope associated genetic determinants chosen from the genetic chemical screen, having potential involvement in Ag^+ mechanism of bacterial toxicity. Validation of the *E. coli* cells phenotypic responses to Ag^+ ions would provide understanding to the biochemical and genetic basis of Ag^+ toxicity. In this thesis we aimed to provide insight into specific questions:

1.) Are there genotypic differences between Keio collection BW25113 and K-12 MG1655 cells, that lead to different metal response phenotypes in the presence of metal antimicrobials?
2.) Is the growth of the wildtype and cell envelope associated Ag-responsive BW25113 and MG1655 *E. coli* cells effected while grown in the presence of Ag^+ and other metal toxins?
3.) Do Ag^+ ions effect planktonic and surface biofilms of both wildtype and cell envelope associated Ag-responsive mutant *E. coli* cells? Is the total biomass accumulation of *E. coli* Ag-responsive mutants and wildtype biofilms effected by the presence of Ag^+ ions?

We aimed to utilize a variety of microbiological techniques to answer the postulated questions. First, using similar methodology to Datsenko *et al.,* 2000, we utilized the Red-recombinase recombination method to generate chromosomal disruptions in the MG1655 genomic background of *E. coli*, aimed to be used for a genomic comparative analysis against Keio collection mutants. Second, utilizing metal exposure-response curves, I aimed to evaluate Ag^+ and a comparative metal antimicrobial Cu^{2+}, ability to inhibit the proliferation of both wildtype and cell envelope associated mutants. For the third aim, I will generate insight into answering the proposed questions from three different types of microscopy techniques: CLSM, SEM and TEM, which aim to characterize the surface morphology of biofilms (CLSM & SEM) and planktonic cell morphology (TEM) in the presence and absence of Ag^+.

It is known that the antimicrobial activity of Ag based compounds is intrinsically dependent on the formation of the Ag^+ ions (Walker and Parsons, 2014). Thus, the metal challenges that were selected for the characterization of the collective phenotyping of the Ag-responsive mutants and wild type cells were: silver nitrate ($AgNO_3$), silver sulfadiazine (AgSD), and Copper (II) sulfate ($CuSO_4$). $AgNO_3$ was chosen based of its high solubility, while AgSD was chosen based of its clinical relevance for it is frequently used as prophylactic agent in burn patients (Bessey, 2007), and $CuSO_4$ was chosen as a comparator metal antimicrobial.

Chapter Two: Methods

2.0 Materials and media

2.1.1 Bacterial strains

K-12 MG1655 and BW25113 *Escherichia coli* strains (standard laboratory strains used commonly in the study of antimicrobial resistance) were provided by National BioResource Project *E. coli* K-12 single-gene-knockout Keio Collection. The *E. coli* DH5α strain, which contained template and helper plasmids (see Table 2.0 for genotype) are available in Turner lab archive. All plasmid preparation and isolation procedures were conducted on DH5α cells containing the particular helper plasmid needed for individual experiments within this thesis work. The Red-recombinase expressing plasmid was provided by Dr. Joe Harrison (University of Calgary) K-12 MG1655::pKD46 and utilized for λ Red-recombinase gene replacement. All strains were stored at -80^{o}C in 8% (v/v) dimethyl sulfoxide (DMSO) in Lysogeny–Broth medium (pH 7.0, 5.0g NaCl, 5.0g yeast extract, and 10.0 g tryptone per litre of double distilled water (ddH_2O) in a glass vial. The individual strains and associated genotypes are depicted in the table 2.0 below.

Table 2.0: Associated genotypes of *E. coli* strains used within this study.

Strain	Genotype	Antibiotic Resistance	Function of deleted gene of interest
DH5α	F- *Φ80lacZΔM15 Δ(lacZYA-argF)U169 recA1 endA1 hsdR17 (rK–, mK+) phoA supE44 thi-1 gyrA96 relA1*	None	N/A
K-12 MG1655	F^-, $lambda^-$, *rph-1*	None	N/A
BW25113	F-, *Δ(araD-araB)567, ΔlacZ4787(::rrnB-3), λ-, rph-1, Δ(rhaD-rhaB)568, hsdR514*	None	N/A
BW25113	BW25113; Δ*damX*::Kn^R Ag^+- Resistant	Kn^R	*DamX* is a non-essential cell division protein; it contains a C-terminal SPOR domain which targets the protein to the septal ring.
BW25113	BW25113; Δ*rodZ*::Kn^R Ag^+- Sensitive	Kn^R	*rodZ* is a bitopic inner membrane protein that is involved in the maintenance of cell shape through interaction with the MreB cytoskeleton.
BW25113	BW25113; Δ*minC*::Kn^R Ag^+- Sensitive	Kn^R	The *minC-minD-minE* system acts to direct septation to the proper (central) site in the dividing *E. coli* cell.
BW25113	BW25113; Δ*sanA*::Kn^R Ag^+- Sensitive	Kn^R	Multi-copy expression of *sanA* complements the vancomycin sensitivity of an *E. coli* K-12 mutant which exhibits outer membrane permeability defects
BW25113	BW25113; Δ*ybhO*::Kn^R Ag^+- Sensitive	Kn^R	*ybhO* (*clsB*) is the second cardiolipin synthase in *E. coli*
BW25113	BW25113; Δ*tolB*::Kn^R Ag^+- Sensitive	Kn^R	*tolB* is a periplasmic component of the Tol-Pal system - a group of interacting proteins which span the cell envelope of *E. coli* K-12. The Tol-Pal system plays a role in outer membrane invagination during cell division and is important for maintaining outer membrane integrity.

* $\boldsymbol{Kn^R}$ = Kanamycin resistance, $\boldsymbol{Cm^R}$=Chloramphenicol resistance, $\boldsymbol{Amp^R}$=Ampicillin Resistance

2.1.2 Chemicals and reagents

All chemicals used in the preparation of media were supplied by Sigma Aldrich (Missouri, USA), EMD (Darmstadt, Germany), Bio-Rad Laboratories (California, USA) and BD Biosciences (New Jersey, USA). Reagents and enzymes used in cloning procedures were purchased from Thermo Fisher Scientific (Massachusetts, USA).

2.1.3 Medium and culture conditions

Throughout our studies—present and past—we have observed that the growth media chosen to culture bacterial cells is a significant factor that dictates the metal toxicity. Hence, we selected a media that provides a rich environment to ensure robust bacterial growth in each strain. Minimal salts media (M9) (10.0 mL M9 5x salts, 38.5 mL ddH_2O, 1.0 ml dextrose, 0.10 mL $MgSO_4$, and 0.005 mL $CaCl_2$) was utilized for metal susceptibility testing. The decision was made not to use rich media (high NaCl concentration) based on ionic bonding chemistry, where reducing the amount of free Cl^- ions in solution would reduce precipitation AgCl (s) and allow for more available Ag^+ ions in solution. For routine overnight starting cultures (16 or 24-hour growth), diluting cultures for screening assays, transformation, and plasmid isolation, strains were incubated in test tubes at 37°C under aerobic conditions in Lysogeny broth, M9 minimal salts media, or on LB plates (1.25% (w/v) agar). Antibiotics ampicillin (*Amp*), chloramphenicol (*Cm*), and Kanamycin (*Kn*) were added in LB medium or while pouring LB plates as required to a final concentration of 100 µg/mL, 10-34 µg/mL, and 10-25 µg/mL respectively.

2.1.4 Antimicrobial metal stock solutions

Silver nitrate ($AgNO_3$), copper (II) sulfate ($CuSO_4$), gallium (III) nitrate ($Ga(NO_3)_3 \cdot H_2O$) and nickel sulfate ($NiSO_4 \cdot 6H_2O$) were all obtained from Sigma-Aldrich (St. Louis, MO, USA). Aluminum sulfate ($Al_2(SO_4)_3 \cdot H_2O$) was obtained from Matheson Coleman and Bell (Norwood, OH, USA) and zinc sulfate ($ZnSO_4 \cdot 7H_2O$) was received from Thermo Fisher Scientific (Fair Lawn, NJ, USA). Stock solutions of $CuSO_4$, $Al_2(SO_4)_3 \cdot H_2O$ were made up to 1M, $ZnSO_4 \cdot 7H_2O$ was made up to 1.5M, $NiSO_4 \cdot 6H_2O$ to 2.5M and $AgNO_3$ to 500mM in distilled and deionized (dd)H_2O. All stock metal solutions were stored in glass vials at 21°C for no longer than two weeks.

2.1.5 Stock antibiotics solutions

Ampicillin (Sigma-Aldrich) and Kanamycin (Sigma-Aldrich) were prepared as stock solutions in double-distilled water (ddH_2O) at 100 and 25 µg/ mL respectively. Chloramphenicol (Sigma-Aldrich) was prepared in 50 % ethanol (99.8%) and treated identically to the other antibiotics. The antibiotics were syringe-filtered and stored at – 20^oC.

2.1.6 Plasmids and vectors

Table 2.1: All Plasmids and vectors used in the work of this thesis.

Vectors	Description	Source
Template plasmid λ Red recombinase		
pKD13	Amp^R and Kn^R ; plasmid markers are oriR6KγTl3$_\lambda$(Terminator), *bla*, *rgn*B (Terminator), *kan*; Accession Number AY048744	CGSC
pKD32	Amp^R and Cm^R; plasmid markers are oriR6K, tL3$_\lambda$(Terminator), *bla*, *rgn*B (Terminator), *kan*; Accession Number AY048744	CGSC
Temperature sensitive plasmid λ Red recombinase		
pCP20	Amp^R and Cm^R; (only grows at 30 °C), *[cU857](λ)ts*, *bla*, *cat*, *[Flp]*; carries the yeast Flp recombinase gene (*flp*)	CGSC
pKD46	Amp^R, *repA101*(ts), *araBp-gam-bet-exo*, *oriR101*, *bla*; more efficient that pKD20 at making gene disruptions; Accession number AY048746	CGSC
Complementation		
pTZ57R/T	Linearized pTZ57R vector with 3'-ddT overhangs for TA cloning of PCR products with blue/white screening.	Thermo Fisher Scientifc
$pMS199EH_A$	Cloning Vector- Amp^R	E. Lanka
Metal exposure-response		
pBBRIMC-2	Cloning Vector- Kn^R	M.E. Kovach

*CGSC = Coli Genetic Stock Center; Amp^R= ampicilin resistance; Cm^R = chloramphenicol resistance; Kn^R = kanamycin resistance.

2.1.7 Optical density

McFarland standards were utilized to visually approximate the concentration of cells in a suspension. The McFarland scale represents specific concentrations of CFU/mL and is used for estimating concentrations of Gram negative bacteria such as *E. coli*. Note that this estimate becomes uncertain with organisms outside the normal usage as different species of bacteria differ in size and mass. Use of this method requires calibration and validation. McFarland Standards are generally labeled 0.5 through 10 and filled with suspensions of Barium salts. The standards were created by preparing a 1.0% solution of anhydrous $BaCl_2$ and a 1.0% solution of H_2SO_4. The standards were stored in the dark, in a tightly sealed container at 20-25ºC and should be stable for approximately 6 months. The advantage of the use of these standards is that no incubation time or equipment is needed to estimate bacterial numbers. The disadvantage is that there is some subjectivity involved in interpreting the turbidity, and that the numbers are valid only for those microorganisms similar to *E. coli*.

2.1.8 Chemically competent E. coli cells preparation and transformation

Chemically competent K-12 MG1655 and BW25113 *E. coli* cells used in the study were prepared using calcium chloride method (Chan *et al.*, 2013). Overnight cultures were diluted to 1 McFarland standard d (~1.0×10^8 colony forming units(CFU) mL^{-1}) in 7.0 mL of LB and incubated aerobically at 37°C to mid-log phase until an optical density at 600 nm (OD_{600}) of 0.3-0.4 units was reached. The cultures were incubated on ice for 15 min and centrifuged at 5000 rpm for 5 min at 4°C to obtain cell pellet. The cell pellet was re-suspended in 10 mL of ice-cold 1M $CaCl_2 \cdot 2H_2O$ and incubated on ice for 1 hour. Another round of centrifugation followed by resuspension in 10 mL of ice-cold 1M $CaCl_2 \cdot 2H_2O$ and incubation on ice for 1 hour was done. After discarding the supernatant, the pellet was re-suspended in 2 mL of cold 1M $CaCl_2 \cdot 2H_2O$, 16% (v/v) glycerol 200 µL aliquots were made in sterile 1.5 mL microfuge tubes. All freshly prepared competent cells were flash frozen and stored as cryogenic stock at -80 °C. All transformed and co-transformed *E. coli* strains used within this thesis were generated by heat shock transformation method or by electrophoresis. For plasmid transformation, 1-2 µL (50-100 ng) of plasmid DNA was added to 50 µL of competent cells, which were aseptically aliquoted into 1.5 mL microfuge tubes. For cloning purposes, 15 µL of ligation reaction mix was added to 50 µL competent *E. coli* DH5α cells. Mixture of DNA and competent cells was incubated on ice

for 20 minutes and then heat shocked for 90 seconds at 42 °C in water bath. After the heat shock treatment, the centrifuge tubes were returned to ice for 10 minutes. 500 mL of fresh LB was added to each of the tubes and incubated at 37 °C for 1 hour in a shaking incubator at 200 rpm. Following incubation 100 µL of the culture was aseptically transferred and spread onto LB plates (1.25% (w/v) agar) (section *2.1.3*).

2.1.9 Biofilm production

Following a protocol similar to Harrison *et al*., 2010, biofilms where grown from cryogenic stock stored at -80ºC, a 200 µL pipette tip was used to collect the different bacterial strains (Table 2.0) and inoculate 7 sterile 22.0 mL glass test tubes filled with 7.0 mL of M9 or LB media (6 tubes for the mutants and one for wildtype cultures). The test tubes were grown overnight for 24 hours at 37ºC and 150 rpm. Following the overnight growth of the preculture, colonies were resuspended into fresh M9 media or LB media and matched to 1.0 McFarland standard. Next, the cultures were then poured into reagent reservoirs and using a multichannel micropipette, 180 µL of the bacterial cultures were aliquoted into each well from rows B-G, columns 2-12 of a sterile 96 well microtiter plate. Wells in rows A and H acted as negative controls, which contained 180 µL sterile 0.9% saline, while column one's rows B-G contained 180 µL of bacterial culture without an antimicrobial challenge (Growth Control). Both wildtype and mutant *E. coli* biofilms cells had 3 technical replicates when subjugated to the metal exposure-response experiment and subsequent crystal violet assay. The 96 well microtiter plate layout is depicted in Figure 2.0 and 2.1. Using a multichannel micropipette, 180 µL of the concentrated metal challenges (tables) were transferred into column 2 wells of rows B-G (The site of highest antimicrobial challenge during testing). The contents of the wells were thoroughly mixed by pipetting the solution up and down several times. After mixing, transfer 180 µL from the wells in column 2 to the corresponding wells in column 3. Mix the contents of column 3 and transfer 180 µL from each well into the corresponding wells of column 4. The Serially mix and transfer process was continued down the length of the microtiter plate until the last column (12) was reached. Once the final column is met, discard 180 µL of the mixed contents to create equal volumes of wells for the entire microtiter plate. After the wells received the proper inoculum volumes, a Calgary Biofilm Device (CBD) was aseptically transferred to cover the 96 well microtiter plate. The CBD lid contains 96 equivalent polystyrene pegs, which serve as a solid surface for planktonic bacterium to adhere to in order to undergo physiological changes

associated with biofilm production. The plates were then onto a gyrorotary shaker set to 150 rpm and incubated for 24 hours at 37ºC.

2.1.10 Primers

Table 2.4 lists all the different primers generated and used throughout the experiments of this thesis.

Table 2.2: Primers utilized throughout this thesis.

Gene Knockout Primer	Sequence (Homology extensions)	GC%	Tm (ºC)	Template homology
Knockout primers				
rodZ KO	cgg atg ttt cgc ggt gtg g	63.0	61.0	K-12 MG1655
rodZ RC	gtt acc cgt ctg tta ctg cg	55.0	60.5	K-12 MG1655
mreB KO	cgc tgc tgc gtg tgg ttg gta aag taa gcg	57.0	65.7	K-12 MG1655
mreB RC	ctg cct gca tcc gat tac tct tcg ctg aac	53.0	64.4	K-12 MG1655
minC KO	cat gcc tta tag tct tcg gaa cat cat c	43.0	58.0	K-12 MG1655
minC RC	cgg ttg aac ggt caa agc g	58.0	59.0	K-12 MG1655
damX KO	ccg ctt atc aag cgg tct att agc	50.0	59.0	K-12 MG1655
damX RC	gat cgg cct gta cct gac g	63.0	59.0	K-12 MG1655
ispG KO	ccc tca atg ccg aac aat c	53.0	57.5	K-12 MG1655
ispG RC	ctt ccc tca atg ttt cgg g	53.0	57.5	K-12 MG1655
P1* (added to forward primer)	gtg tag gct gga gct tc	59.0	62.5	pKD13 OR pKD32
P4* (added to reverse complement primer)	att ccg ggg atc cgt cga cc	65.9	64.6	pKD13 OR pKD32
Confirmation Primers for λ Red-recombinase				
rodZ F confirmation primer (OS)	gtg cgt ttt tgc tga ctt taa g	41.0	58.4	K-12 MG1655
rodZ RC confirmation primer (OAS)	gat ttg att gac cgt tgc ttc	43.0	57.5	K-12 MG1655
mreB F confirmation primer (OS)	gcg gtt gca aac agg cga g	63.0	61.5	K-12 MG1655
mreB RC confirmation primer (OAS)	gta gaa agg act gac ggc gg	60.0	62.5	K-12 MG1655

minC F confirmation primer (OS)	cac aac cca taa tca ggt cga gat tac g	46.0	59.9	K-12 MG1655
minC RC confirmation primer (OAS)	aga tgc tgt cac gat tag ggt gc	52.0	57.1	K-12 MG1655
damX F confirmation primer (OS)	gcc gtt taa tat cat caa gca ggg	46.0	63.6	K-12 MG1655
damX RC confirmation primer (OAS)	gcg ctt aat tct tcc gtt ggc	52.0	61.2	K-12 MG1655
ispG F confirmation primer (OS)	cag tac aga tcc agt atc aag g	45.0	60.1	K-12 MG1655
ispG RC confirmation primer (OAS)	tgc cgc gaa tgg ctt gaa tg	55.0	60.5	K-12 MG1655
sanA F confirmation primer (OS)	ctc tcg gct gtc aca gta tc	55	56.0	BW25113
sanA RC confirmation primer (OAS)	Ccg aag ccg ata tat gcc ac	55	59.0	BW25113
ybhO F confirmation primer (OS)	cgg act gga tga gat ttt tac c	45	55.0	BW25113
ybhO RC confirmation primer (OAS)	gca gccc gta aat cag ata gct g	50	58.0	BW25113
tolB F confirmation primer (OS)	tcc cga aaa cca ccgc cag	60	60.0	BW25113
tolB RC confirmation primer (OAS)	ccg ccg ttc gca tcc ata c	63	61.0	BW25113
Complementation Primers		**Antibiotic resistance**	**Gene of interest**	**Restriction Enzyme site**
pMS199EHA::*rodZ*	**Forward**: includes start (ATG) codon ATATTCTAGAAGGAGAAATAATATG AATACTGAAGCCACGCACGA **Reverse**: includes stop (ATT) codon ATATAAGCTTTTACTGCGCCGGTGATTGTTCG	*Amp*	*rodZ*	XbaI:TCTAGA HindIII:AAGCTT
pTZ57R/T::*rodZ*	**Forward**: atattctagaaggagaaataatatg aatactgaagccacgcacga **Reverse**: atataagcttttactgcgccggtgattgttcg	-	*rodZ*	XbaI:TCTAGA HindIII:AAGCTT

*__KO__= Knockout forward primer, **RC**= Reverse complement Primer. *The combination of both primers **KO+P1** and **RC+P4** sequences from Table 2.0, generated the complete knockout primer that is utilized to facilitate the insertion of the template plasmids antibiotic cassette in place of gene of interest. Further, it is not necessary to include the 5' homology extensions in the calculation of melting TM. ***F**= Forward primer, **RC**= Reverse complement Primer, **OS** =outside sense, **OAS**= outside antisense. TCTAGA= XbaI restriction enzyme cut site, AAGCTT=HindIII restriction enzyme cut site. ATG=start codon, TTA= stop codon.

2.2 λ Red-recombinase mediated gene replacement

The process of λ Red-recombinase mediated gene replacement contains three key molecular tools. The first being a plasmid with a temperature sensitive replicon and an inducible operon that expresses the lambda (λ) phage genes *gam, bet,* and *exo.* Second, a plasmid that serves as a template for generating the gene replacements. This plasmid cannot replicate in desired *E. coli* strain (strain that is used for the targeted gene deletion) and must have an antibiotic cassette that is flanked by Flp-recombination targets (FRT) sites. Finally, a helper plasmid with a temperature sensitive replicon that transiently expresses the yeast (*Saccharomyces cerevisiae*) recombinase Flp (Datsenko and Wanner, 2000).

The process of generating a gene replacement allele utilizing the Red-recombinase molecular tool is accomplished through polymerase chain reaction (PCR). Primers are used to amplify the template plasmid (pKD13 or pKD32) antibiotic cassette, which are flanked by FRT sites. The primers used to amplify this cassette are created with a 5' flanking homology extension that are 18-26 nucleotides in length. These homology extensions precisely match upstream and downstream nucleotide sequences in the *E. coli* chromosome of the targeted loci for deletion. This PCR product is transformed into electrocompetent *E. coli* (K-12 MG1655) cells that contain the temperature sensitive helper plasmid (pKD46) that expresses the Red-recombinase genes (*gam, bet,* and *exo*) through induction with arabinose. The Gam protein prevents the endogenous RecBCD nucleases from digesting linear DNA introduced into the *E. coli*. Exo protein is a 5'→3' dsDNA-dependent exonuclease and will degrade linear dsDNA starting from the 5' end. The Beta protein protects the ssDNA created by Exo and promotes its annealing to a complementary ssDNA target in the cell. The recombinase then mediates the site-specific insertions of the antibiotic cassette (FRT -Ab^R-FRT) through a double crossover event between the 5' homology extensions and their complementary gene sequences on the *E. coli*

chromosome. This helper plasmid can be further cured from the cells during antibiotic selection for insertions by growing at non-permissible temperatures of >30 °C. After selection, mutant *E. coli* cells can have the antibiotic cassette removed from the chromosome with the insertion of another temperature sensitive plasmid (pCP20) that transiently expresses the yeast recombinase, Flp. Following transformation and selection, the helper plasmid can be cured from the cell with growth at a non-permissive temperature (>30 °C). The then unmarked deletion mutants can be identified through their inability to grow on media supplemented with antibiotics (Datsenko and Wanner, 2000).

2.3 Complementation

Following the successful generation of the deletion mutant K-12 MG1655Δ*rodZ*, plasmid-based complementation of K-12 MG1655Δ*rodZ* was conducted through cloning methods utilizing restriction enzymes and T4 ligase. The *Amp*- resistant expression vector pMS119EH$_A$ generated by Beketskaia *et al*., 2014, was selected as the expression system for complementation because the vector has previously demonstrated to be a low copy number plasmid with about 20-30 copies per cell and also having low levels of expression ("leaky expression") from the PtacI promoter in the absence of induction by IPTG (Bay and Turner, 2009). This expression type has proven to be advantageous for the current study to obtain low non-toxic levels of RodZ protein as previous literature has reported that over-expression of membrane proteins can have detrimental effects in the host cells (Jensen *et al*., 2017). Further, the selection of the pMS119EH$_A$ vector was further chosen for its previous success complementing genes for membrane proteins by the Turner Research Group (Turner *et al*., 2017; Beketskaia *et al*., 2014). In this experiment, because we are cloning the ORF of *rodZ* and inserting (through ligation) the ORF into an expression vector, we include the start codon (ATG) and the stop codon (TGA). The forward primer was designed with a 18-21 bp homology sequence (refer to Table 2.2), which would bind and amplify the target ORF. Additionally, the forward primer was generated to have an XbaI restriction site (TCTAGA) added to the 5' end of the primer. Finally, the forward primer consisted of the addition of 3-6 bp upstream of the inserted cut site XbaI, in order to improve cutting efficiency. The reverse primer has similar design; however, the reverse complement was constructed utilizing OligoCalc: Oligonucleotide Properties Calculator software. Similarly, 18-21 bp with homology to the ORF were used to generate the primer with the addition of the HindIII restriction site (AAGCTT) on the 5' end.

Following the restriction site 4 bp were added to improve restriction enzyme digestion. The full protocol for generating a plasmid-based complementation can be found in the appendix section A of this thesis.

2.4 Culture density analysis

2.4.1 Bacterial growth curves

A bacterial growth curve is a graph illustrating the changes in size of a bacterial population over time. The bacteria are cultured in a sterile nutrient medium and incubated at the optimal temperature for growth. Aliquoted samples are removed at intervals and the concentration of bacteria is evaluated. A logarithmic growth curve is plotted, which shows various phases of growth. In the *lag* (or *latent)* phase there is only small increases in numbers as the bacteria imbibe water, and synthesize ribosomal RNA and subsequent enzymes, in adjusting to their new environmental conditions (Navarro *et al.,* 2010; Rolfe *et al*., 2012) Different bacteria reproduce at different rates. The time it takes the population to double is called the generation time. As this generation time of the cells decreases, they enter the *log* (or *exponential*) *phase*, in which the cells reach a maximum rate of reproduction and the number of bacteria increases directly with time, giving a straight slope on a logarithmic scale. With time, as the population grows, it enters the *stationary phase*, where the nutrients and electron acceptors are depleted, and the pH drops as carbon dioxide and other waste poisons accumulate (Navarro *et al.,* 2010). Eventually the cell's energy storage begins to deplete resulting in cultures having a drastic decrease in the rate of cell divisions. Finally, the *death* (or *final*) *phase* occurs when the rate at which the bacteria die exceeds the rate at which they are produced; the population declines as the levels of nutrients fall and toxin levels increase.

For this experiment, it was imperative to measure the different growth capabilities of the different cell envelope mutant *E. coli* strains to investigate whether they had similar growth patterns, which would allow for the determination of the appropriate exposure times for metal exposure-response experimentations. The different mutant and wildtype strains tested, are displayed in Table 2.0.

2.4.2 Inoculation and growth

Bacteria from cryogenic DMSO stocks at -80^{o}C (section *2.1.1*). Utilizing a 200 µL pipet tip frozen cryogenic stock cultures were inoculated into minimal salts media (M9) and incubated

overnight at 37ºC and shaking at 250 rpm. Following the O/N growth, 100 µL of culture were then aliquoted onto LB (1.25% (w/v) agar plates and incubated at 37ºC overnight. A single colony was then selected from the O/N growth and inoculated into 12 sterile 22.0 mL glass test tubes containing 5.0 mL of M9 media and placed into a 37ºC incubator and shaken at 125 rpm. The 12 test tubes represent the different time intervals at which 1.0 mL of sample was extracted and placed into 2.0 mL cuvette and their turbidity was measured through a SpectraMax Plus 384 Microplate Reader. The optical density (OD) for each culture was recorded for 1, 2, 4, 6, 8, 10, 12, 16, 18, 20, 24, and 48-hour time intervals for BW25113 wildtype and mutant cells. The resulting OD_{600} values were recorded in biological triplicates with 3 technical trials for each wildtype and mutant cell to *E. coli* cell to ensure accuracy of the results.

2.5 Evaluation of different metal exposure-responses of BW25113 *E. coli* cells

2.5.1 *Metal exposure-response curves*

The metal exposure-response experiment was conducted to visualize the dose and exposure-response relationship between mutant and wildtype MG1655 and BW25113 *E. coli* cells against three different metal challenges: silver nitrate ($AgNO_3$), silver sulfadiazine (AgSD), and Copper (II) sulfate ($CuSO_4$)1This experiment aims to describe the phenotypic changes in *E. coli* caused by differing levels of exposure to an antimicrobial stressor after a certain exposure time. The end result will produce a dose-response curve, which is a simple X-Y graph relating to the magnitude of a stressor (concentration of the antimicrobial in µM) to the response of the receptor (the respective OD or viable cell counts of an organism).

2.5.2 Generating the metal exposure-response toxicity curve

In order to generate a metal exposure-response curve a spectrophotometer was used to analysis the OD_{600} antimicrobial challenge plate samples. The spectrophotometer method measures culture turbidity directly and allows for the analysis of culture concentration of bacteria relative to antimicrobial challenge in the suspension. The plates were removed from the incubator and taken to analyzed by a SpectraMax Plus 384 Microplate. The machine was switched on and the SoftMax® Pro optical density reading software was initialized. The program was constructed with the correct format that highlights the proper controls and bacterial culture samples that are illustrated in Figures 2.0 and 2.1.

2.5.3 Growing subcultures, inoculum preparation and preparation of antimicrobial challenge plate

Utilizing methods similar to Lemire *et al.*, 2015, cryogenic stock stored at -80^{o}C (Section *2.1.1*), a 200 µL pipette tip was used to collect the different bacterial strains (Table 2.0) and inoculate 7 sterile 22.0 mL test tubes filled with 7.0 mL of M9 media. The test tubes were grown O/N for 16-hours at 37^{o}C and 150 rpm. During this incubation time the antimicrobial metal challenges were prepared. The challenges were stored in a cold room at 4^{o}C until needed for the metal exposure-response inoculum preparation. The 10 different bacterial suspensions were then prepared to equal turbidity of 1.0 McFarland standard (~1.0 x 10^{8} colony forming units (CFU) mL^{-1}) inside a BioSafety Cabinet (BSC). This was achieved by aliquoting 1.0 mL of each bacterial culture into 7.0 mL of fresh M9 media. The cultures were then poured into reagent reservoirs and using a multichannel micropipette, 180 µL of the sterile bacterial cultures were aliquoted into each well from rows B-G, columns 2-12 of a sterile 96 well microtiter plate. Rows A and H acted as negative controls containing 180 µL sterile 0.9% saline (Sterility growth Control, SC), while column one's rows B-G contained 180 µL of bacterial culture without an antimicrobial challenge (Growth Control = GC). This determination of having these two rows act as negative control wells is because of published literature confirming increased evaporation rate of these exterior wells of a 96 well microtiter plate (Harrison *et al*., 2010). Both wildtype and mutant *E. coli* cells had 3 technical replicates when subjugated to the metal exposure-response experiment. The 96 well microtiter plate layout is depicted in Figures 2.0 & 2.1. Using a multichannel micropipette, 180µL of the concentrated metal challenge was transferred into column 2 wells of rows B-G (The site of highest antimicrobial challenge during testing, 50 or 256 µM). The contents of the wells were thoroughly mixed by pipetting the solution up and down several times. After mixing, 180 µL was transferred from wells in column 2 to the corresponding wells in column 3. The contents were Mixed and 180 µL was again transferred from each well into the corresponding wells of column 4. The Serially mix and transfer process was continued down the length of the microtiter plate until the wells of the last column (12) was reached. Once the final column is met, 180 µL of mixed bacteria and metal solution was discarded to create equal volumes of wells for the entire microtiter plate. The 96 well microtiter plate was then aseptically covered, and the lid and base of the plate was sealed and wrapped with paraffin wax to aid in decreased evaporation rates. The plates were placed onto a gyrorotary shaker set to 150 rpm and incubated overnight at 37^{o}C. Plates were removed from the incubator

and their turbidity was determined using a SpectraMax Plus 384 Microplate described in section *2.1.7*.

	1	2	3	4	5	6	7	8	9	10	11	12
A	SC	SC	SC	SC	SC	SC	SC	SC	SC	SC	SC	SC
B	GC	50.0	25.0	12.5	6.25	3.125	1.56	0.781	0.390	0.195	0.097	0.048
C	GC	50.0	25.0	12.5	6.25	3.125	1.56	0.781	0.390	0.195	0.097	0.048
D	GC	50.0	25.0	12.5	6.25	3.125	1.56	0.781	0.390	0.195	0.097	0.048
E	GC	50.0	25.0	12.5	6.25	3.125	1.56	0.781	0.390	0.195	0.097	0.048
F	GC	50.0	25.0	12.5	6.25	3.125	1.56	0.781	0.390	0.195	0.097	0.048
G	GC	50.0	25.0	12.5	6.25	3.125	1.56	0.781	0.390	0.195	0.097	0.048
H	SC	SC	SC	SC	SC	SC	SC	SC	SC	SC	SC	SC

Figure 2.0: preparation of the antimicrobial challenge plate with highest metal challenge concentration being 50 µM. Using a sterile 96 well microtiter plate, the following steps described in section (*2.5.4*) illustrate how to aseptically prepare the challenge plate for metal toxin exposure-response analysis. The above microtiter plate represents a serial two-fold dilution gradient of a single antimicrobial challenge plate. This plate outline is kept the same for all three metal challenges. Rows B-D consisted of three technical replicates of one *E. coli* strain, while rows E-G consisted of another strain. In total there were 4 antimicrobial challenge plates for each of the metal challenges $AgNO_3$, AgSD, and CuSO4. SC= sterility growth control (0.9% Saline), **GC**= Growth control of one *E. coli* strain. **GC**=Growth control of one *E. coli* strain.

	1	2	3	4	5	6	7	8	9	10	11	12
A	SC	SC	SC	SC	SC	SC	SC	SC	SC	SC	SC	SC
B	GC	256	128	64.0	32.0	16.0	8.00	4.00	2.00	1.00	0.50	0.25
C	GC	256	128	64.0	32.0	16.0	8.00	4.00	2.00	1.00	0.50	0.25
D	GC	256	128	64.0	32.0	16.0	8.00	4.00	2.00	1.00	0.50	0.25
E	GC	256	128	64.0	32.0	16.0	8.00	4.00	2.00	1.00	0.50	0.25
F	GC	256	128	64.0	32.0	16.0	8.00	4.00	2.00	1.00	0.50	0.25
G	GC	256	128	64.0	32.0	16.0	8.00	4.00	2.00	1.00	0.50	0.25
H	SC	SC	SC	SC	SC	SC	SC	SC	SC	SC	SC	SC

Figure 2.1: preparation of the antimicrobial challenge plate with highest metal challenge concentration being 256 µM. Rows B-D consisted of three technical replicates of one *E. coli* strain, while rows E-G consisted of another strain. The above microtiter plate represents a serial two-fold dilution gradient of a single antimicrobial challenge plate. In total there were 4 antimicrobial challenge plates for each of the metal challenges $AgNO_3$, AgSD, and $CuSO_4$. SC= sterility growth control (0.9% Saline), GC= Growth control**.** **GC**= Growth control of one *E. coli* strain. **GC**=Growth control of one *E. coli* strain.

2.5.4 Viable cell counts

Viable cell counts are a method used in microbiology to evaluate the number of cells capable of growing/dividing within a culture. The method which viable cell counts can be represented is through the plate count method. Microliter volumes of bacterial culture are aseptically pipetted onto the solid surface of an agar plate. The plates are incubated, and the resulting cultures are counted and the corresponding colony forming units per mL (CFU/mL) are generated through the formula:

$$\text{(CFU/mL)} = \frac{\text{(number of colonies) x (dilution factor)}}{\text{Volume of culture plate}}$$

The resulting values are used to graph the cell counts as a function to the metal concentration they were challenged with as a logarithmic unit. From these graphs the respective minimal bactericidal concentration (MBC) and minimal biofilm eradication concentration (MBEC) can be determined.

2.5.5 Preparation of antimicrobial challenge plate and manual counts of (CFU/ mL) for viable cell counts

The methodology for preparing viable cell counts for planktonic and biofilm cells from an antimicrobial challenge plate (Figure 2.1) is the exact same to that of the optical density procedure highlighted in section *2.5.3*. However, following the O/N growth (24 hours) the antimicrobial challenge plates were removed from the incubator and placed on the lab bench till ready. New 96 well microtiter plates were prepared containing 180 µL of sterile 0.9% saline. Column 1 of the 96 well microtiter plates contained an addition of 20.0 µL of universal neutralizer (0.5 g l^{-1} histidine (Sigma, St Louis, MO, USA), 0.5 g l^{-1} cysteine (Sigma) and 0.1 g l^{-1} reduced glutathione (Sigma) in ddH_2O) (used to bind free metal ions). To determine the CFU/mL of the distributed planktonic and biofilm cells (after sonication) bacterial populations, 11 dilutions with a dilution factor of 10 were performed. This was accomplished using a multichannel micropipette to transfer 20.0 µL of culture from wells of column 1, which were

mixed by pipetting up and down and transferred to the corresponding wells in column 2. The Serially mix and transfer process was continued down the length of the microtiter plate until the last column (12) was reached. Using a p20 pipette, 20µL of the samples were then plated onto LB agar to determine the colony forming units and subsequently incubated overnight at 37ºC.

2.5.7 Crystal violet assay

This Assay can be used for the indirect quantification of total biomass to determine differences in biofilm adherence to polystyrene pegs upon challenge with a metal antimicrobial agent (O'Toole, 2011). This method relies on the staining of attached cells with crystal violet dye, which binds to proteins and DNA. The difference in optical densities between treated and untreated mutant and wildtype biofilms will be quantified utilizing a spectrophotometer giving qualitative data on the differences in biofilm production and adherence of the different mutant strains biofilms (Table 2.0), when subjected to the three different metal antimicrobial challenges.

2.5.8 Crystal violet dye exposure and biofilm cultivation

Following the biofilm formation, outlined in section *2.1.9*, and utilizing a similar crystal violet staining procedure to O'Toole, 2011, the 96 well microtiter plates containing wildtype and the 6-cell envelope BW25113 mutant *E. coli* strains (Table 2.0), which were exposed to a two-fold 50 µM concentration gradient of the three metal antimicrobial challenges had dye plates prepared. The dye plates consisted of new sterile 96 well microtiter plates, which contained 150 µL of 0.5 % crystal violet staining solution administered to each well of the microtiter plate. 12 dye plates were created for each of the corresponding CBD lids of the challenged wildtype and mutant *E. coli* biofilms. The CBD lids were placed into the dye plates and incubated at RT for 20 minutes on a bench rocker with a frequency of 20 oscillations per minute. The CBD lids were then inverted and placed on filter paper and tapped gently to remove any remaining liquid from the pegs. The CBD lids were then allowed to air-dry for 30 minutes at RT. The CBD lids were then placed into new 96 well microtiter plates containing 200 µL of 30% (v/v) acetic acid (Biofilm's biomass cultivation plates). The lids were incubated in solution for 20 minutes at RT on a bench rocker with a frequency of 20 oscillations per minute. These plates were than taken to have their OD_{570} read by SpectraMax Plus 384 Microplate reader. Following the plate reading,

the average OD_{570} of the wells without cells was subtracted from the OD_{570} of each well on the plate to eliminate background fluorescence picked up by the plate reader.

2.6. Microscopy

Three different microscopy techniques (CLSM, TEM, and SEM) were utilized to visualize differences in planktonic and surface biofilm morphology when in the presence and absence of $AgNO_3$.

2.6.1 Confocal laser scanning microscopy

The confocal laser scanning microscope (CLSM) is an optical imaging technique that captures multiple two-dimensional images at different depths in a sample, which enables for the reconstruction of three-dimensional structures within an object (Pawley, 2006). Given that microbes frequently live in multi or single species solid surface biofilms, which consist of architectural features important for population heterogeneity and emergent cell function (Harrison *et al.*, 2006). This CLSM technique offers an important insight into the understanding of biofilm morphology and the changes associated when an antimicrobial challenge is introduced (Harrison *et al.*, 2006). Bacterial biofilms have been widely studied and have been shown to modulate their architecture to changes in external and internal process when exposed to antimicrobial agents. Here in this experiment, the main goal was to visualize the morphological changes associated with each *E. coli* strain's biofilm when grown in the presence of a Ag^+.

2.6.2 Microscopy biofilm production

Utilizing similar protocol to Harrison *et al*., 2006, cryogenic stock stored at -80^{o}C (Section *2.1.1*), of the different bacterial strains (Table 2.0) was collected by a 200 µL pipette tip and was inoculated 7 sterile 22.0 mL test tubes filled with 7.0 mL of M9 or LB media. The test tubes were incubated overnight for 16 hours at 37^{o}C and 150 rpm. Following the O/N growth the cultures were sub-cultured under the same conditions. Following sub-culturing, 1.0 mL of culture was resuspended into fresh 7.0 mL M9 media and matched to 1.0 McFarland standard. Next, the cultures were then poured into reagent reservoirs and using a multichannel

micropipette, 180 µL of the bacterial cultures were aliquoted into the wells of column 2, rows B-G, column 3 row B-2, column 4 rows B-G, and column 5, row B-4 of a sterile 96 well microtiter plate. The wells in column 4 rows B-G, and column 5, row B-4 acted at growth controls (GC) and were not subjected to any metal challenge. Furthermore, the remaining unused wells of the plate were aliquoted with 180 µL of 0.9% saline, which acted as the sterile control (-). Using a multichannel micropipette, 180 µL of concentrated 50 µM $AgNO_3$ metal challenge was transferred into the wells of column 2 rows B-G and column 3 row B-2. The contents of the wells were thoroughly mixed by pipetting the solution up and down several times. After the wells received the proper inoculum volumes, a CBD lid was aseptically transferred to cover the 96 well microtiter plate. The plates were then placed onto a gyrorotary shaker set to 150 rpm and incubated for 24 hours at 37^{o}C.

2.6.3 Conducting confocal laser scanning microscopy

The overnight growth plates (section *2.6.2*) were removed from the incubator and were placed onto the lab bench. The CBD lid was removed and the corresponding polystyrene pegs with the different *E. coli* strains biofilms were aseptically broken off with alcohol flamed pliers. The pegs were then transferred to a new sterile 96 well microtiter plate. The pegs were rinsed in 200 µL 0.9% saline twice and then placed into 200 µL of 5.0% of glutaraldehyde PBS buffer and incubated at 37^{o}C for 30 min. During the time of incubation, 0.1% acridine orange dye was prepared by adding 0.05 g of acridine orange in 50 mL of PBS buffer. The pegs were removed from the incubator and placed in 150 µL of 0.1% acridine orange dye. The pegs were incubated for 15 min and wrapped in tinfoil as the stain is light sensitive. Once the incubation was finished, the pegs were washed again one more time in 200 µL 0.9% saline. Following the last wash, the pegs were transferred to microscope slides using tweezers and a drop of ddH_2O was placed onto the pegs. The biofilms of the challenged and unchallenged pegs were then examined through Bitplane: Imaris© x 64 Microscopy image analysis software.

2.6.4 Transmission electron microscopy

The transmission electron microscope (TEM) is a powerful tool utilized in microbiology to investigate microorganisms through which electrons can pass through specimens and generate a projection image. Traditionally, TEM has been the “gold standard” for imaging dividing

microbial cells (Hazelton and Gelferblom, 2003). This microscopy method offers detailed information about *E. coli* cells ultrastructure.

2.6.5 Whole cell transmission electron microscopy preparation

Utilizing the cryogenic stocks of the different *E. coli* strains (Table 2.0) stored at -80^{o}C (section *2.1.1*), a 200 µL pipette tip was used to collect the different bacterial strains and inoculate 7 sterile 22.0 mL test tubes filled with 5.0 mL of M9 media. These test tubes were placed in an incubator set to 37^{o}C and shaking at 150 rpm and incubated for 24-hours. After the incubation, 1.0 mL of the 5.0 mL cultures was removed and added into fresh 4.0 mL of M9 media. These test tubes served as the challenged cells samples (treated with $AgNO_3$). The remaining 4.0 mL of the overnight culture is kept and utilized as the negative control sample. The 4.0 mL was centrifuged at >10,000 x g for 2 minutes to produce a cell pellet and was stored at -20^{o}C. The challenged test tubes received 25.0 µL of 10mM $AgNO_3$ stock solution to generate a final antimicrobial challenge of 50 µM. These tubes were then allowed to incubate overnight for 16-24 hours at 37^{o}C and 150 rpm. Following the incubation period and 30 minutes prior to imaging, the *E. coli* cells were spun down >10,000 x g for 2 minutes to obtain a cell pellet. Both control and challenge cell pellets were then resuspended in 5.0 mL of sterile ddH_2O. A 1/10 dilution was then performed, which required 100 µL of the resuspended cultures being transferred to a 1.5 mL microcentrifuge tube containing 900 µL of sterile ddH_2O. subsequently, 5.0-10 µL of each sample was placed onto the carbon side of the carbon-copper coated TEM grids. 5.0 µL of 1.0% phosphotungstic acid contrasting agent (used to improve image visibility) was added onto each sample, which were then left to air-dry for 10 minutes. Each carbon-copper grid was loaded into the TEM and imaged utilizing Gatan Digital Micrograph© and FEI microscope interface© at 80-100 -keV.

2.6.6 Scanning electron microscopy

The scanning electron microscope (SEM) uses a focused beam of high-energy electrons to generate a reflected image/signal at the surface of solid specimens. The signals that derive from electron-sample interactions reveal information about the sample particularly external morphology. This technique was utilized to observe the changes in physical characteristics of the *E. coli* biofilms when challenged by Ag^{+}.

2.6.7 Sputter deposition/coating and fixing of E. coli biofilms for SEM imaging

Biofilm formation for SEM imaging followed the same procedural steps as section *2.6.*2. The overnight growth plates were removed from the incubator are placed onto the lab bench. The CBD lid was removed and the corresponding polystyrene pegs with the different *E. coli* strains biofilms were aseptically broken off with alcohol flamed pliers. The pegs were then transferred to a new sterile 1.5 mL microcentrifuge tubes and placed in a BSC to air-dry for 24 hrs. The pegs were then transferred to microscope slides, which were placed into the coater glass chamber of a Hummer Sputter Coater. The voltage and the main power to the machine was turned on allowing for the creation of a vacuum system within the glass gas chamber. Once the vacuum's gage reached 50 millitorr (takes roughly 30 minutes), the valve for argon gas was opened until the pressure inside the chamber was 400 millitorr. The argon valve was then closed, and the glass chamber was again pumped to create another vacuum with a pressure of 50 millitorr. At this time, the high voltage control knob was set to 9 and turned on. The argon valve was reopened, and the gas flow was adjusted until the amp meter read 10 milliamperes. When a pinkish purple glow of argon plasma begins to emit from the top of the glass chamber, a timer of four minutes was set. At this time physical vapor deposition (PVD) is taking place, whereby atoms are ejected from a target or source material (platinum) that is to be deposited on a substrate (polystyrene pegs) (Bouzakis and Michailidis, 2014). Once the four-minute timer is reached, the samples are well coated in the platinum source material. The glass gas chamber is re-pressurized, and the samples are removed. The pegs are then transferred onto double sided carbon tape (improves imaging), which is placed on the sample stand inside the SEM chamber and were visualized using Phillips and Scandium© software at 120 -keV.

2.7 High throughput metal resistance profiling:

2.7.1 Disk diffusion assay

The purpose of the disk diffusion susceptibility test is to determine the sensitivity or resistance of aerobic bacteria to various antimicrobial compounds. 6-mm filter paper disk are impregnated with a known concentration of an antimicrobial compound and placed onto spread agar plates containing the different bacterial inoculum. immediately water is absorbed into the disk from the agar and the antimicrobial begins to diffuse into the surrounding agar. The rate of diffusion through the agar is not as rapid as the rate of extraction of the antimicrobial out of the disk, therefore the concentration of antimicrobial is highest closest to the disk and a logarithmic reduction in concentration occurs as the distance from the disk increases (Jorgensen and Turnidge, 2008). The rate of diffusion of the antimicrobial through the agar is dependent on the diffusion and solubility properties of the antimicrobial compound in the agar and its molecular weight (Bauer *et al.*, 1966). Larger molecules will diffuse at a slower rate than lower molecular weight compounds. These factors, in combination, result in each antimicrobial having a unique breakpoint zone (zone of inhibition) size, which indicates the susceptibility of a bacterial culture to that antimicrobial compound.

2.7.2 Preparation of Inoculum and placement of antimicrobial disks

Utilizing cryogenic stock stored at -80ºC, a 200 µL pipette tip was used to collect the different bacterial strains (Table 2.0) and inoculate 7 sterile 22.0 mL test tubes filled with 7.0 mL of M9 media. The test tubes were incubated overnight for 16 hours at 37ºC and 150 rpm. Following the O/N growth of the pre-culture, the colonies were suspended in 0.9% NaCl to match the density of a 1.0 McFarland standard. Subsequently, 250 µL of each mutant bacterial strain and wildtype strain were aliquoted onto fresh LB agar plates and spread evenly with an ethanol flamed glass spreader. Sterile antimicrobial disks, presoaked in each metal stock solution found in section *2.1.4* for 2 hours, were placed on the LB agar plates and incubated for 16 hours at 37ºC. The region of bacterial susceptibility (zone of inhibition) was measured with a ruler from edge to edge across the zone of inhibition and recorded as a diameter value in millimeters.

Chapter Three: Results

3.1 Choice of cell envelope associated genes

Gene choice was based off the chemical genetic screen conducted by Dr. Lemire (unpublished results), which related mutant colony size to fitness and enabled identification of quantitative genetic interactions from high-throughput, genome-scale screen. The genetic screen evaluated 3985 single gene deletions of all non-essential gene mutants of the Keio collection, resulting in the discovery of 225 mutants to be sensitive to the exposure of the 100μM $AgNO_3$ challenge and 177 mutants to display a resistant phenotype. The Sensitive ('sicker') or resistant ('healthier') mutants were selected based on a difference of 2 standard deviations of colony size from the normal, which was determined through photographed images that were processed using software that measures colony areas in terms of pixels. Of the total mutants, 20 sensitive and 4 resistant mutants were found to be involved in cell envelope homeostasis. The genes were then analyzed through bioinformatic and literature analysis, which evaluated their cellular function and involvement in cell envelope homeostasis. From these analysis of the 24 genes, one resistant (*damX*) and five sensitive mutants (*rodZ, minC, sanA, ybhO, and tolB)* where chosen to evaluate their collective phenotype in the presence of Ag^+ (Table 2.0).

3.2 Chromosomal disruptions

As a comparable biological analysis, mutations of genes *rodZ, ispG, mreB, damX, minC, sanA, ybhO,* and *tolB* in the genomic background of *E. coli* K-12 MG1655 were attempted in order to evaluate the discrepancy in Ag^+ toxin response phenotypes when compared to the same mutants in Keio collection BW25113 strain.

3.2.1 MG1655ΔrodZ knockout mutant and Ag^+ exposure-response

Utilizing λ Red-recombinase mediated gene replacement (section 2.2), and a standard protocol and methodology similar to Datsenko *et al.*, (2000), the Δ*rodZ* chromosomal deletion was generated by using several pairs of 56-to70-nt-long primers that included 18-to50-nt homology extensions and 20-nt priming sequences for helper plasmids pKD13 or pKD32 as template for amplification of their respective antibiotic cassettes (Table 2.1). Figure 3.0 demonstrates the respective ~1.29-kbp PCR product/replacement allele (gel lane: 6-10), which

represented successful annealing of the knockout primers (Table 2.2) to the Cm^R cassette from the template plasmid pKD32, which was further purified and transformed into a *E. coli* MG1655 cell already carrying pKD46, which is a low copy number easily curable plasmid encoding the Red-recombinase. This plasmid facilitated homologous recombination through a double cross-over event with the ORF of the gene of interest (*rodZ*) and the replacement allele (Figure 3.0) effectively replacing the gene of interest with the FRT-Cm^R-FRT. Once transformed, successful recombinants with targeted chromosomal disruptions can be selected for by being plated on LB agar containing the appropriate selection marker; 1.25% (w/v) LB agar + 10 μg/ml chloramphenicol. The Red recombinase plasmid pKD46 contains a temperature-sensitive origin of replication and is cured at growth at the non-permissive temperature of 37^{o}C. The resulting transformants were then transformed with the temperature sensitive helper plasmid (pCP20) that transiently expressed the yeast recombinase, Flp. The successful removal of the antibiotic cassette facilitated by the flipase enzyme, is illustrated in Figure 3.1. MG1655Δ*rodZ* cells were confirmed via PCR, using the OS and OAS confirmation primers (Table 2.2). mutants produced a band at approximately ~412bp (180 OS and ORF + 146 OAS and ORF). Unsuccessful deletion mutants generated a banding pattern equal to about 1014bp – about the size of the undeleted *rodZ* gene or the intact Cm^R antibiotic resistance cassette (1293bp). The mutants were further validated through Sanger sequencing.

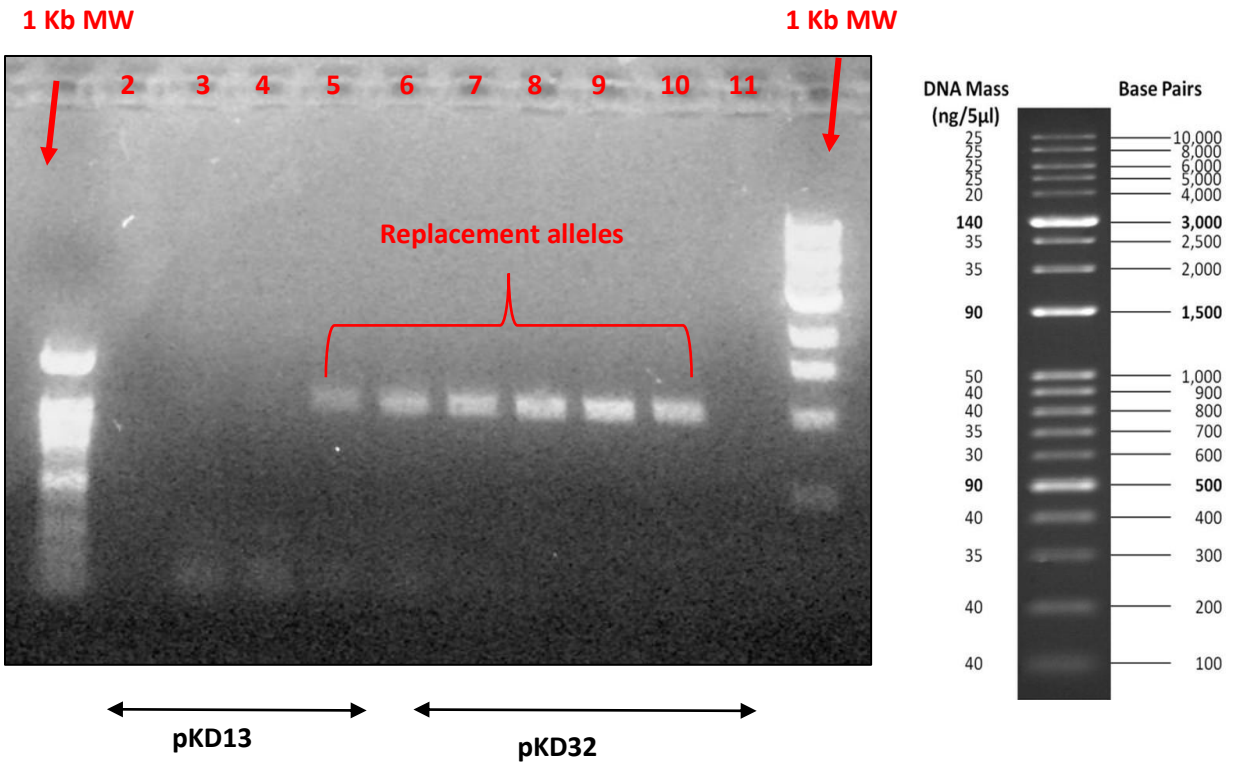

Figure 3.0: Agarose gel to confirm amplification of the gene replacement allele using the template plasmids pKD13 and pKD32 and *rodZ* KO and RC primers (Table 2.2). The primers have 5' 18-50 nt-homology extension, which recognize *E. coli* K-12 MG1655 chromosome, as well having 3' primers with sequence homology that matches the template plasmid. Successful reactions (Lanes:6-10) produce a single clean PCR product that is ~1.29 (Cm^R) or ~1.4 kbp (Kn^R) (lane 5) in size relative to the antibiotic cassette from the template plasmids.

Figure 3.1: Confirmation of Flp-mediate excision of the FRT-flanked *Cm*^{R} antibiotic resistance cassette. MG1655 Δ*rodZ*:: FRT-*Cm*^{R}-*FRT* insertion mutants were subjected to Flp-mediated excision of the antibiotic resistance cassette by electroporating pCP20 into the positive insertion mutants. Flp excision of the antibiotic resistance (*Cm*^{R}) cassette was accomplished by incubating the transformants at 30°C overnight and then at 43°C following antibiotic selection. The deletion mutants were confirmed via PCR using the OS and OAS primers (Table 2.2). Clean mutants should produce a band at approximately 412bp (180 OS and ORF + 146 OAS and ORF). Unsuccessful deletion mutants will have a banding pattern equal to about 1113bp – about the size of the undeleted gene or the intact antibiotic resistance cassette (1293bp).

Following the creation of MG1655Δ*rodZ* mutant *E. coli* cells, a comparative biological analysis of Δ*rodZ* mutants in the Keio collection strain background and the newly created MG1655Δ*rodZ* was conducted to evaluate differences in pre-exposure-response (grown in the presence) to three metal challenges. The optical density at 600nm was utilized to evaluate differences in culture turbidity and cell morphology (Section 2.5.1). From Table 3.0, it is evident that Δ*rodZ* mutant cells were more susceptible to the three metal challenges compared to the wildtype of each strain based of its respective minimum inhibitory concentration (MIC). Moreover, the Δ*rodZ* mutant in the K-12 MG1655 strain was a full dilution more sensitive to $AgNO_3$ compared to the Δ*rodZ* Keio collection counterpart.

Table 3.0: Minimal Bactericidal Concentrations (MBC) and Minimal Inhibitory Concentrations (MIC)

	Metal Challenge					
***E. coli* Strain** **Keio Collection** **BW25113**	**$AgNO_3$ (µM/µL) MBC**	**$AgNO_3$ (µM/µL) MIC**	**AgSD (µM/µL) MBC**	**AgSD (µM/µL) MIC**	**$CuSO_4$ (µM/µL) MBC**	**$CuSO_4$ (µM/µL) MIC**
BW25113	50.0	6.25	>50.0	6.25	>50.0	12.5
BW25113Δ*rodZ*	25.0	6.25	>50.0	6.25	>50.0	12.5
MG1655	25.0	12.5	>50.0	3.13	>50.0	3.13
MG1655Δ*rodZ*	**12.5**	**6.25**	50.0	3.13	>50.0	3.13

*These values are averages calculated from three biological trials containing three technical replicates.

Regrettably, with the unsuccessful chromosomal disruptions of both *ispG* and *mreB,* resulted in a change of coarse for analyzing the collective phenotype of the selected genes. Reformulating the original comparative biology question that aimed to evaluate the changes exposure-response to metal challenges in different genomic backgrounds, I instead focused on characterizing the 6 Ag-responsive Keio collection mutants (Table 2.0) and their phenotypic responses to three metal antimicrobials.

3.2.2 MG1655ΔispG knockout mutant

Following the same protocol, which generated the MG1655Δ*rodZ* cells, *ispG* the downstream gene in the same operon as *rodZ* was targeted for chromosomal disruption. This gene was targeted to give insight into whether the exposure response phenotype of was a MG1655Δ*rodZ* cells direct response from the chromosomal deletion or the from alteration in expression of downstream genetic elements. However, transformation and targeted replacement of *ispG,* resulted in unsuccessful generations of MG1655Δ*ispG* transformants. Probing the

literature, it was suggested that *ispG* is an 'essential' gene that produces a [4Fe–4S] cluster-containing protein that is involved in isoprenoid synthesis in *E. coli* (Loiseau *et al*., 2007). Thus, when comparing the validation that *ispG* is 'essential' under other experimental conditions, our experimental methods too suggested that in our growth conditions resulted in *ispG* being unable to be deleted from the chromosome.

3.2.3 MG1655ΔmreB knockout mutant

Utilizing the same Red recombinase protocol for *rodZ* and *ispG*, the gene, *mreB*, an associated genetic factor whose protein product functions in close association to RodZ was targeted. However, transformation and targeted replacement of *mreB*, resulted in unsuccessful generations of MG1655Δ*mreB* transformants. Investigating literature, *mreB* is described as a quasi-essential (meaning can be removed is substituted nutrient is provided) gene in (Baba *et al*., 2006) and is crucial in determining cell shape in rod-shaped bacteria (Bacilli) (Curtis, 2016). In comparison here it was suggested, that in under our experimental conditions it too was concluded *mreB* was unable to be deleted from the *E. coli* chromosome.

3.3 Plasmid based complementation and comparative analysis

Following the successful generation of the chromosomal gene disruption mutant K-12 MG1655Δ*rodZ*, plasmid based complementation of K-12 MG1655Δ*rodZ*::pMS119EH$_A$::*rodZ* was conducted through the use of restriction enzymes and T4 ligase (sub-cloning). This method aimed to restore the original wildtype phenotype in response to metal challenges. Utilizing molecular cloning primers (Table 2.2) *rodZ* was successfully amplified from genomic DNA and ligated into the Amp-resistant expression vector pMS119EH$_A$ generated by Beketskaia *et al*., 2014, through the use of restriction digestions, T4 Ligase, and antibiotic selection plates.

Following successful plasmid based complementation, the pMS199EH$_A$::*rodZ* plasmid was transformed into K-12 MG1655*ΔrodZ* cells and subjected to metal exposure-response assay aimed to generate a comparative analysis between wildtype, Δ*rodZ*, and pMS199EH$_A$::*rodZ* complemented cells when grown in the presence of $AgNO_3$, AgSD, and $CuSO_4$. When analysing the resulting phenotypes, it was determined from Figure 3.3, that in the presence of $AgNO_3$ challenge, both Δ*rodZ* mutant and complemented strain were more susceptible to $AgNO_3$ by two dilutions. Evaluating the phenotypic response of each strain to the AgSD metal antimicrobial, all

three strains recorded similar optical densities, however, the complemented MG1655Δ*rod*Z::pMS119EH$_A$::*rodZ* cells achieved similar turbidity to that of the wildtype strain when compared to the mutant MG1655*Δrod*Z. Finally, assessing the $CuSO_4$ toxin response curves, which served as a comparison antimicrobial metal, resulted in all three cultures achieving similar optical densities at 600nm. Furthermore, at the experimental conditions implemented during the metal exposure-response assay, it appears that at the given antimicrobial 2-fold concentration gradient, $CuSO_4$ reduced culture density of the three *E. coli* cultures the least as evident from the evaluated turbidity of the samples.

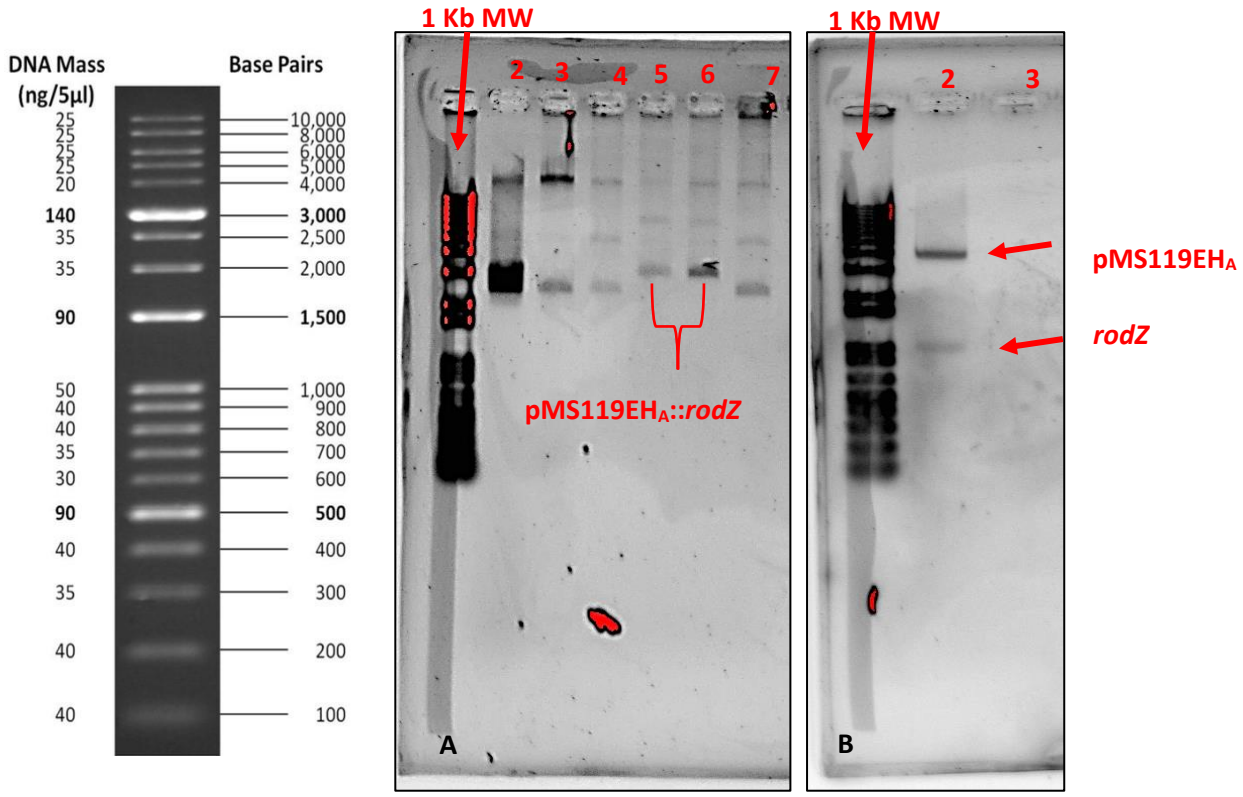

Figure 3.2: Showing agarose gel containing the products of the ligation reaction of *rodZ* insert (1,014 bp) into the low copy number Amp-resistant expression vector pMS119EH$_A$ (3,967bp). Successful ligation (A) produced a product band roughly ~4,981 bp (3,967bp pMS119EH$_A$ + 1,014 bp *rodZ*) in size (lane 5 and 6). The subsequent digestion of the successful ligation products in lanes 5 and 6 in the top gel can be visualized in the (B) gels lane 2. After digestion from restriction enzymes HindIII and XbaI, two bands representing pMS119EH$_A$ (3,967bp) and **(**1,014 bp) *rodZ* are present.

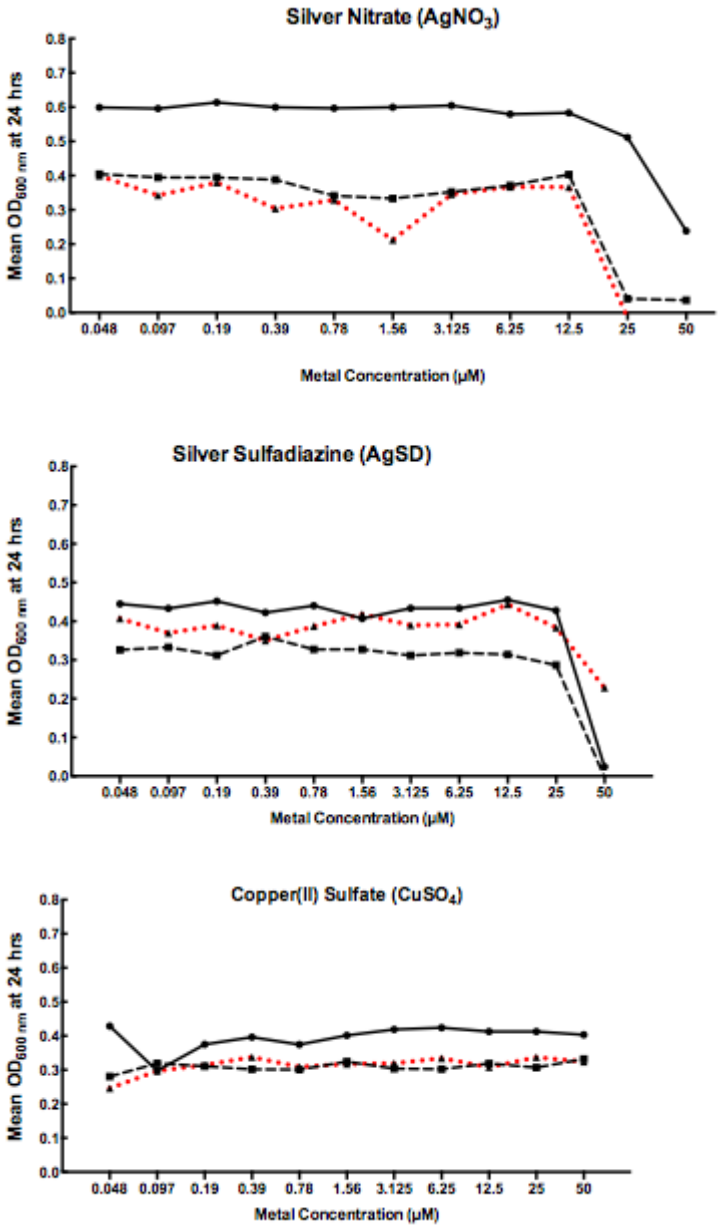

Figure 3.3: Metal exposure-response curves of the gene deletion mutant K-12 MG1655*ΔrodZ*, the plasmid based complementation transformant MG1655Δ*rodZ::*pMS119EH$_A$::*rodZ*, and wildtype K-12 MG1655 *E. coli* cells. The three bacterial strains were subjected to 16-hour growth in the presences of three different metals antimicrobial challenges $AgNO_3$, AgSD, and $CuSO_4$ (Table 2.2). The average OD_{600} of three biological trials each containing three technical replicates was recorded utilizing a SpectraMax Plus 384 Microplate Reader. The solid black line represents K-12 MG1655 cultures, the dotted black line represents K-12 MG1655*ΔrodZ*, and dotted red line represents MG1655*ΔrodZ::*pMS119EH$_A$::*rodZ*.

3.4 Bacterial growth curves

As detailed in section 3.2.1, with the unsuccessful chromosomal deletions of *ispG* and *mreB* in the genomic background of K-12 MG1655, I reformed my approach and aimed to characterize the Ag^{+} phenotypic responses of the targeted 6 cellular envelope associated genes in the genomic background of the Keio collection, BW25113 strain. Before conducting metal exposure-response analysis of the Keio collection cellular envelope associated Ag-responsive genes towards three chosen metal antimicrobials growth curves for the individual K-12 BW25113 mutant strains (Δ*rodZ*, Δ*damX*, Δ*minC*, Δ*sanA*, Δ*ybhO*, Δ*tolB*) (Table 2.0) and wildtype *E. coli* cells was conducted. The 7 strains were inoculated into sterile M9 media and subjected to optical density readings by SpectraMax Plus 384 Microplate Reader (section *2.1.7*) at 1, 2, 4, 6, 8, 10, 12, 16, 18, 20, 24, and 48-hour time intervals. Each strain was subjugated to three biological trials, having three technical triplicates when recording their changes in cellular density over time. This methodology aimed to reduce discrepancy and increase accuracy of the culture turbidity readings at each designated time interval. Figure 3.4 illustrates the average OD_{600} of 3 technical trials and 3 biological replicates of each of the 7 K-12 BW25113 strains. From the analysis of the growth curve in Figure 3.4, it was inferred that all strains reached mid *log* (*or exponential) phase* at around the 12-hour mark with all cultures transitioning into *stationary phase* around 16 hours of growth. However, one striking observation that was made from all the mutant growth curve cultures during the assay, was each had a prolonged *lag phase* when compared to the wildtype culture. Thus, it was suggested that with deletion in genes associated with cell envelope homeostasis, that mutant cells have a considerably more challenging time synthesizing the enzymes and factors needed to facilitate cell division and population growth resulting in prolonged *lag phase*. Figure 3.5, further illustrates a comparative analysis of two mutant strains (Δ*damX* and Δ*rodZ*) growth curves being compared to wildtype cells, which both displayed similar cellular density at each time interval, except at the 6-hour mark. With each mutant strain generating similar cultural turbidity through out the assay, the remaining growth curves can be found in the appendix B section.

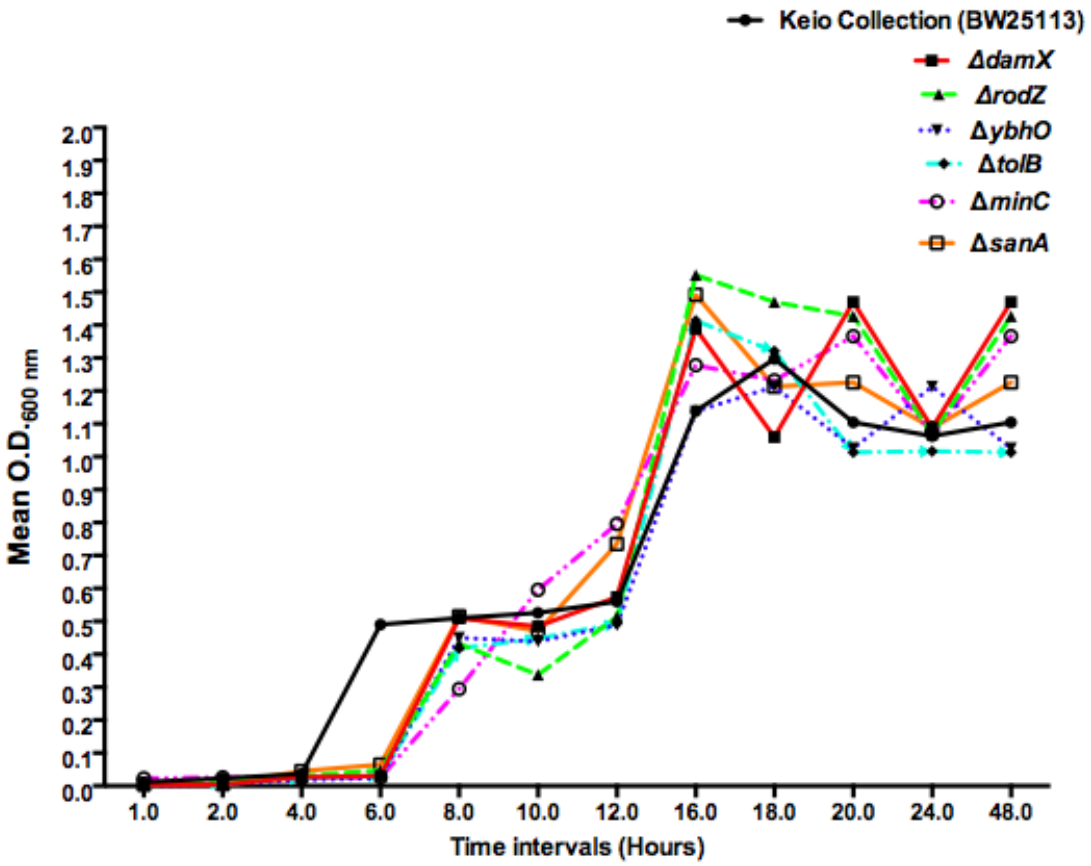

Figure 3.4: Growth curve average of 3 biological trials each containing 3 technical trails, which measured the OD_{600} by SpectraMax Plus 384 Microplate Reader of the 7 different K-12 BW25113 *E. coli* strains (Table 2.0).

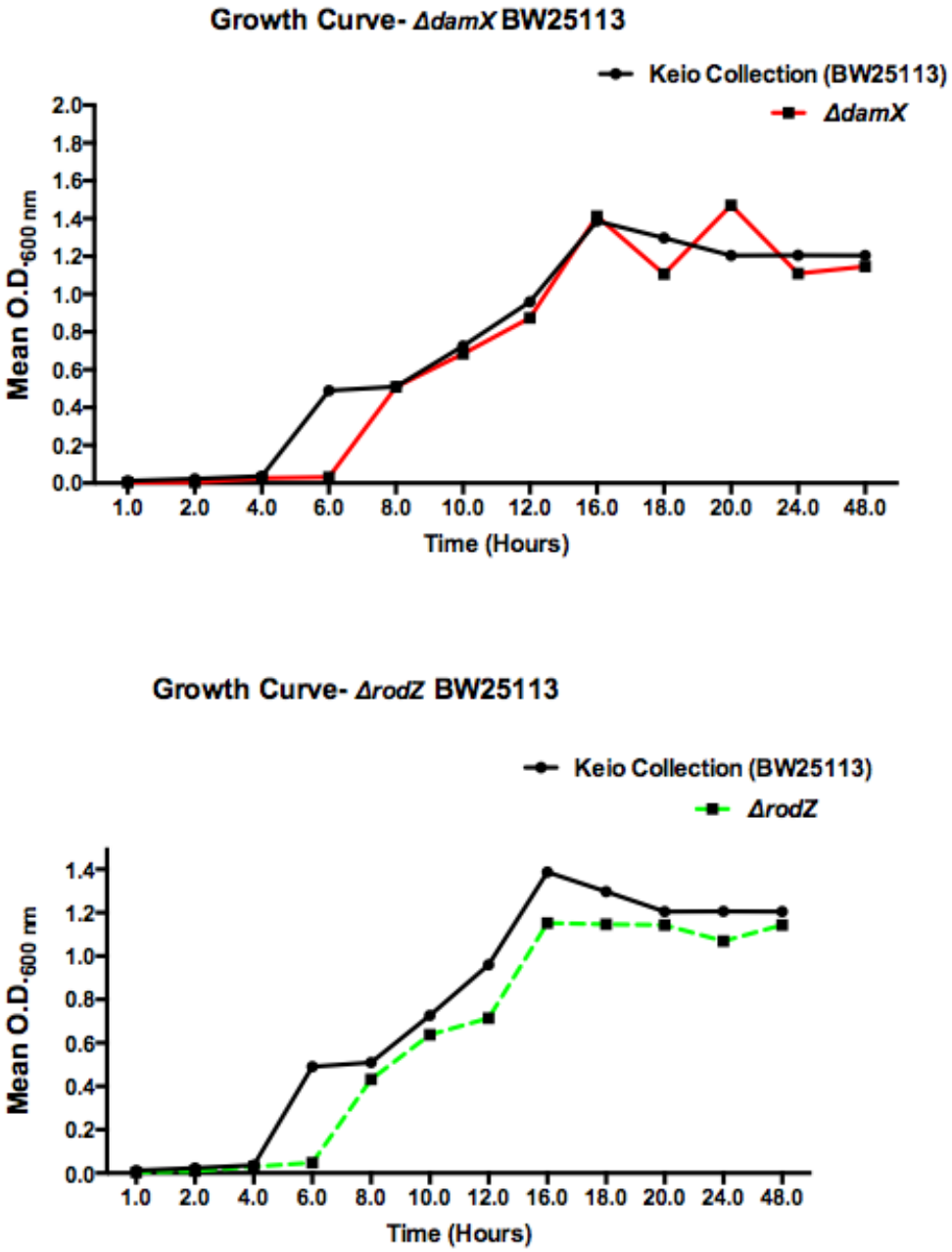

Figure 3.5: Growth curve of the average of 3 biological trials each containing 3 technical trails, which measured OD_{600} readings of BW25113Δ*rodZ* and BW25113Δ*damX* being compared to wildtype BW25113 cells. The results confirmed that all strains achieved a similar growth pattern, however, mutants appeared to have a prolonged *lag phase*.

3.5 Cell viability Assay (CFU/mL) for planktonic *E. coli* cells

In order to determine planktonic *E. coli* cell viability of the 6 cell envelope associated mutants and wildtype cells after growing in the presence to the three metal antimicrobials in M9 media, viable cell counts were conducted on 1.25% (w/v) LB agar. Utilizing the formula in section 2.5.4, colony forming units (CFU) per mL of bacterial culture was evaluated for three separate biological trails and expressed in logarithmic notation (Log-kill CFU/mL) (Figure 3.6). These CFU/mL calculations accurately depict the number of viable cells in each culture suspension and precisely determined the metal concentrations required to prevent planktonic growth (Minimal Bactericidal Concentration, MBC) of the respective *E. coli* cells. Moreover, the resulting colonies sizes were also analyzed for discrepancies between the mutants and wildtype cells, which resulted in all 7 strains having comparable colony size (appendix D). Examining the planktonic cell viability results, $AgNO_3$ proves again to be the most efficacious metal antimicrobial resulting in cellular death at much lower concentrations then the other two comparable metals. Examining the silver resistant phenotypes in the presence of $AgNO_3$, Δ*damX*, Δ*sanA,* and Δ*ybhO* were found to be a full dilution more resistant to the Ag^+ challenge when compared to the wildtype cells. The remaining 3 mutants, had similar MBC values to that of the wildtype cells, which were only permitted to grow at $AgNO_3$ concentrations less than 16.0 µM. When evaluating the CFU's/mL for the AgSD challenge, it was shown that BW25113 Δ*damX* was 3 full dilutions more resistant to the AgSD antimicrobial challenge in comparison to the wildtype culture. At a dose concentration of 256.0 µM, Δ*damX* mutant BW25113 *E. coli* cells were still viable, which far exceeded the MBC value of any other Ag-responsive mutant strain. All the other mutants, however, displayed a resistant phenotype compared to the wildtype cells in the presences of AgSD, except for Δ*ybhO,* which had the same MBC as the wildtype cells, which were unable to grow at concentrations of 64.0 µM and higher. Lastly, evaluating the CFU's/mL produced in the presence of $CuSO_4$, Δ*rodZ*, Δ*minC*, and Δ*ybhO* produced the same MBC phenotype as the wildtype cells, being unable to grow at concentrations of Cu^{2+} higher than 128.0 µM. The other mutants Δ*damX* and Δ*sanA* produced a resistant phenotype, while Δ*tolB* was a full dilution more susceptible to the toxicity of Cu^{2+} when compared to the wildtype cells. Table 3.1, highlights the metal concentrations of each antimicrobial required to prevent planktonic growth of each strain of *E. coli*. Furthermore, Figure 3.6, demonstrates a generated log-kill CFU/mL challenge curve from metal exposure-response assay for the *damX* mutant and

the wildtype BW25113 cells. The remaining cell viability curves for each mutant can be found in the appendix D section, along with photographs of one of the three biological trails for $AgNO_3$ treatment spot plated onto 1.25% (w/v) LB agar.

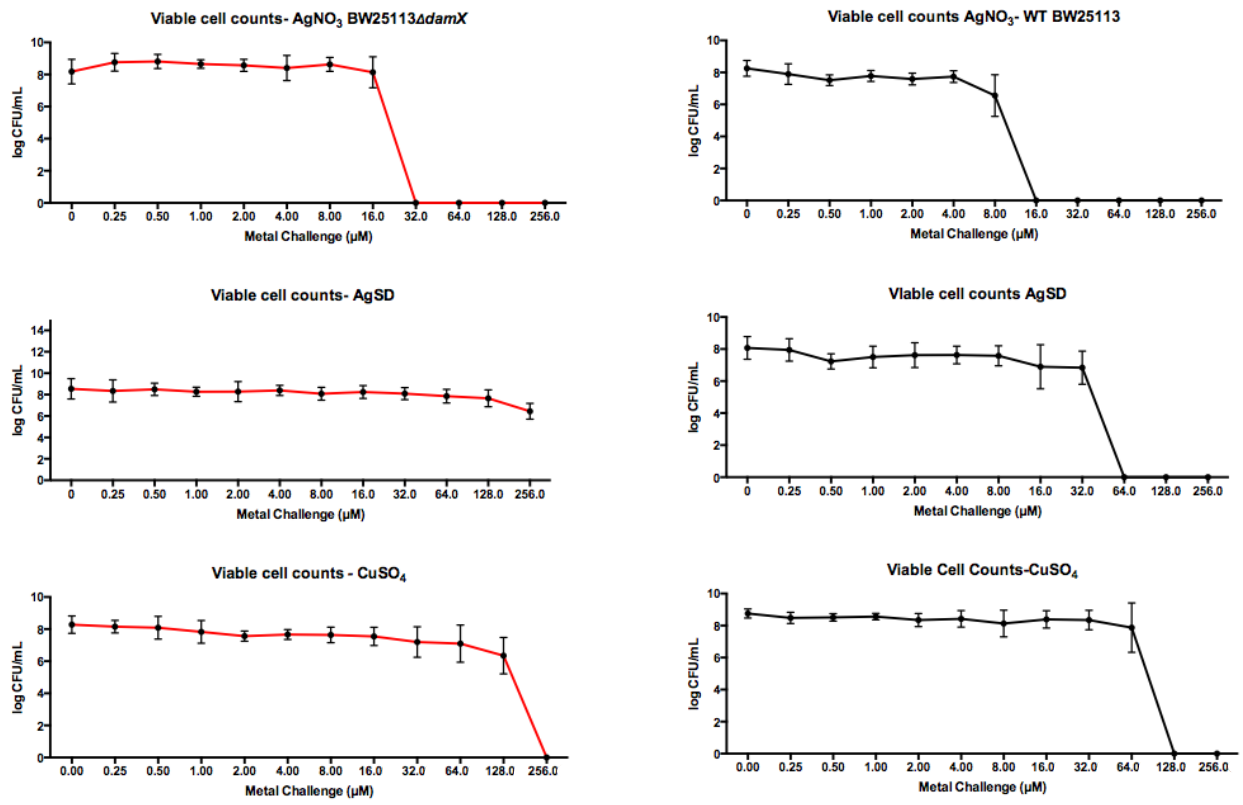

Figure 3.6: log-kill CFU/mL generated for K-12 BW25113Δ*damX* and wildtype *E. coli* planktonic cells exposed to three antimicrobial metals $AgNO_3$, AgSD, and $CuSO_4$. The Δ*damX* cells were exposed to a 256 µM two-fold antimicrobial gradient (Figure 2.0) for a 24-hour period. These cultures were then diluted in dilution plates and 20 µL of culture was aliquoted onto 1.25% (w/v) LB agar plates. CFU/mL was calculated by multiplying the number of viable bacteria colonies by its respective dilution factor, divided by the total volume of the culture (180 µL). The CFU/mL was then expressed using logarithmic notation.

3.5.1 Cell viability (CFU/mL) for E. coli biofilms

To determine *E. coli* biofilm viability of the 6 cell envelope associated mutants and wildtype biofilm grown in Lysogeny broth media after post-growth exposure to the three metal antimicrobials, viable cell counts were conducted on 1.25% (w/v) LB agar. Utilizing the formula in section 2.5.4, colony forming units (CFU) per mL of bacterial biofilm was evaluated for three separate biological trails. These CFU/mL calculations accurately depict the number of viable cells in each culture suspension and precisely determined the metal concentrations required to prevent Biofilm growth (Minimal Biofilm Eradication Concentration, MBEC) of the respective *E. coli* cells. The biofilms were grown in accordance to section 2.1.9. and sonicated of the polystyrene pegs of the CBD lid in to determine the CFU/mL. From the biofilm viability results, $AgNO_3$ was demonstrated to be the most efficacious of the three metal challenges. The resistant determinant, Δ*damX*, biofilm was a full dilution more resistant to the $AgNO_3$ challenge, while sensitive mutants, Δ*rodZ* and Δ*tolB*, were one dilution more susceptible when compared to the wildtypes biofilm cells viability. The remaining mutants had similar MBEC values to that of the wildtype culture. Analyzing the MBEC values for the AgSD challenge, Δ*damx*, Δ*minC*, Δ*sanA*, and Δ*ybhO* were more resistant to the metal challenge when compared to the wildtype. Δ*tolB* was found to be more sensitive to the AgSD challenge compared to the wildtype, while Δ*rodZ*, had a similar MBEC value. Finally, analysing the comparator metal $CuSO_4$, only Δ*tolB* was found to be more susceptible to the metal challenge in comparison to all other metals and wildtype biofilms. Table 3.1 shows the respective MBEC values generated from the biofilm viability assay, which display similar MBEC values to that of publish literature (Lemire *et al.,* 2017). These MBEC end-point values were utilized for generating a challenge concentration, which was utilized for the different microscopy techniques throughout this thesis.

Table 3.1: Minimal Biocidal Concentrations (MBC) and Minimal Biofilm Eradication Concentrations (MBEC)

	Metal Challenge					
***E. coli* Strain** **Keio Collection** **BW25113**	**$AgNO_3$ (µM/µL) MBC**	**$AgNO_3$ (µM/µL) MBEC**	**AgSD (µM/µL) MBC**	**AgSD (µM/µL) MBEC**	**$CuSO_4$ (µM/µL) MBC**	**$CuSO_4$ (µM/µL) MBEC**
wildtype	16.0	64.0	64.0	64.0	128.0	256.0
Δ*damX*	**32.0**	**128**	**>256.0**	**256.0**	**256.0**	256.0
Δ*rodZ*	16.0	**32.0**	**128.0**	64.0	128.0	256.0
Δ*minC*	16.0	64.0	64.0	**128.0**	128.0	256.0
Δ*sanA*	**32.0**	64.0	**256.0**	**256.0**	**256.0**	256.0
Δ*ybhO*	**32.0**	64.0	**256.0**	**128.0**	**256.0**	256.0
Δ*tolB*	16.0	**32.0**	**128.0**	**32.0**	**64.0**	**128.0**

*There was no variability between end-point values (MBC and MBEC) for each mutant and wildtype planktonic and biofilm cells with the established experimental conditions.

3.6 Microscopy

Utilizing three different microscopy techniques (CLSM, TEM, and SEM), planktonic and surface biofilm physiology in the presence and absence of a 50 μM metal antimicrobial challenge ($AgNO_3$) were characterized. 50 μM was chosen based of the representative MBEC and MBC values found from the cell viability assay. However, complication arising from both SEM and CLSM experimental procedures generated inconclusive results

3.6.1 Transmission electron microscopy analysis of treated and untreated *E. coli* biofilms

TEM analysis of 50 μM pre-treated 1.0% phosphotungstic acid stained *E. coli* bacteria showed the external planktonic morphological features of the cell envelope associated mutant BW25113 strains, wildtype BW25113 and MG1655 cells, and the recombinase generated MG1655Δ*rodZ* cells. Images were processed and captured with Gatan Digital Micrograph© and FEI microscope interface© (section 2.6.5) at 80-100 keV. The untreated BW25113 and MG1655 *E. coli* cells of wildtype and mutant strains retained their bacillus morphology and appeared normal in solution. However, MG1655Δ*rodZ* mutants, commonly displayed elongated bacillus morphology, which contrasted the wildtype MG1655 cells. However, this change in cell morphology present in TEM imaging of MG1655Δ*rodZ* cultures did not influence optical density measurements.

All the *E. coli* strains treated with the 50 μM $AgNO_3$ challenge appeared to have cells in culture undergo lysis, resulting in the release of cellular contents into the surrounding environment. It was common to find electron-dense particles (Figure 3.7) or precipitates surrounding damaged cells, which were electron translucent in comparison to undamaged cells. When examining the cellular envelope of the treated and untreated *E. coli* strains, significant morphology changes were observed. Untreated cells, seemed to have normal phenotypical characteristics. The internal structures appeared to be normal, with some displaying their multilayered cell envelope consisting of the outer membrane a peptidoglycan layer in the periplasmic space, and the inner cytoplasmic membrane (Figure 3.8). On the contrary, it was routinely observed that treated cells had a compromised cellular envelope (Figures 3.7 and 3.8, Images B and D). Treated cells displayed either localized or complete separation of the cell membrane from the cell wall. Furthermore, plumes of cellular debris with accompanied electron-translucent cytoplasm and cellular disruption was observed in treated cells. Even the Ag^+

resistant determinant, Δ*damX*, could not withstand the given Ag^{+} ion toxicity in solution and had similar planktonic morphologies as to that of all the other genes and wildtype treated cells (Figure 3.7). During TEM analysis, it was also noted that mutant *E. coli* strains had a drastic reduction in cellular density, making imaging of full populations of cells difficult to achieve. Even with centrifugation steps aimed to increased cell density, resulted in low planktonic cell concentrations. More TEM photos at different magnifications are present in the appendix E section of this thesis.

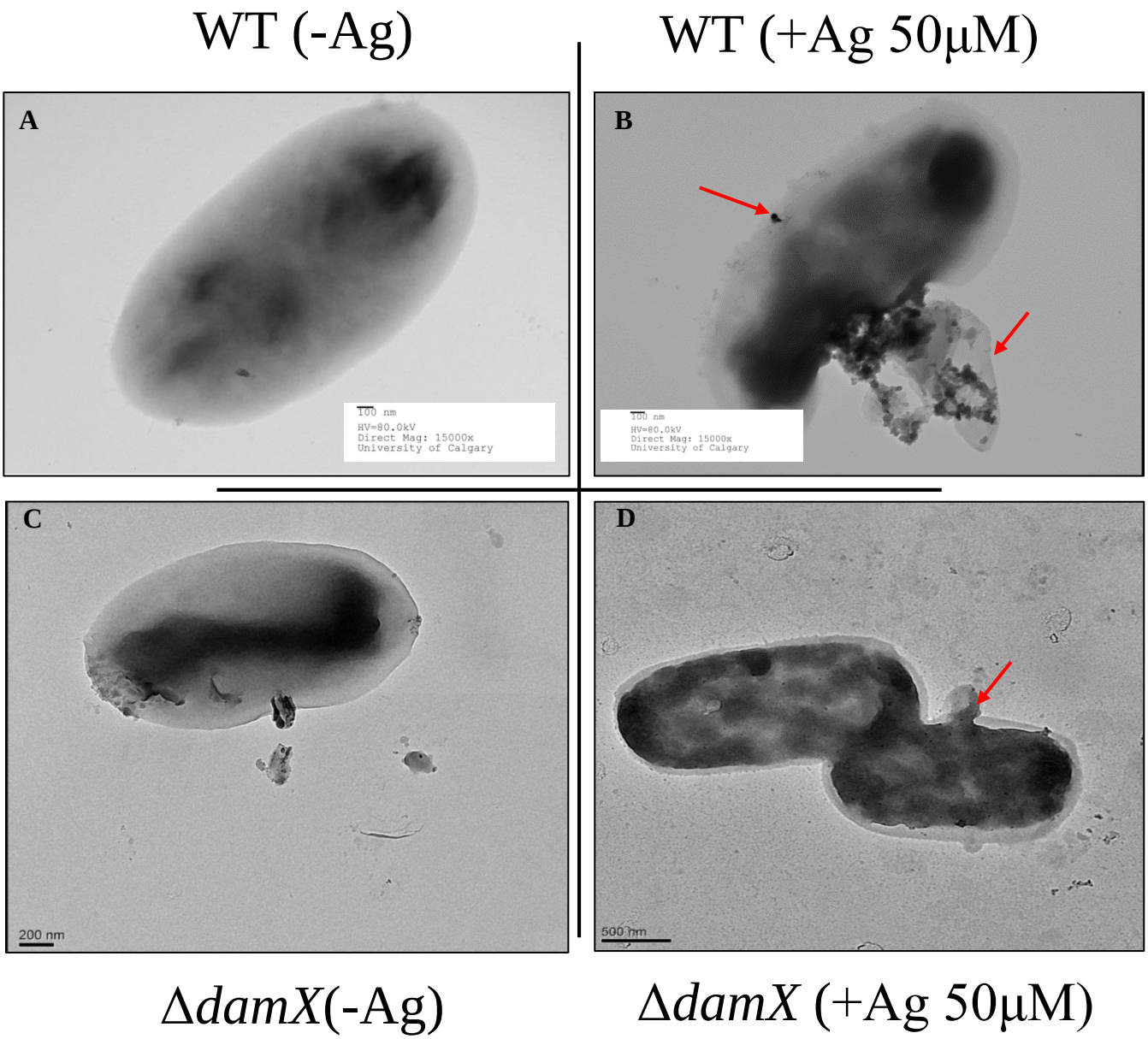

Figure 3.7: External cell morphologies of 1.0% phosphotungstic acid stained wildtype and BW25113Δ*damX* *E. coli* planktonic cells untreated (A and C) and pre-treated with 50 µM $AgNO_3$ treated (B and D) observed by transmission electron microscopy. Images A and B, are wildtype cells imaged at 15000x mag, and images C and C, were BW25113Δ*damX* cells taken at 9600 x magnification. Red arrows indicated electron-dense particles that were commonly found in treated TEM samples and areas of cell membrane separation. Some treated cells displayed either localized or complete separation of the cell membrane from the cell wall. plumes of cellular debris were also witnessed with accompanied electron-translucent cytoplasm and cellular disruption.

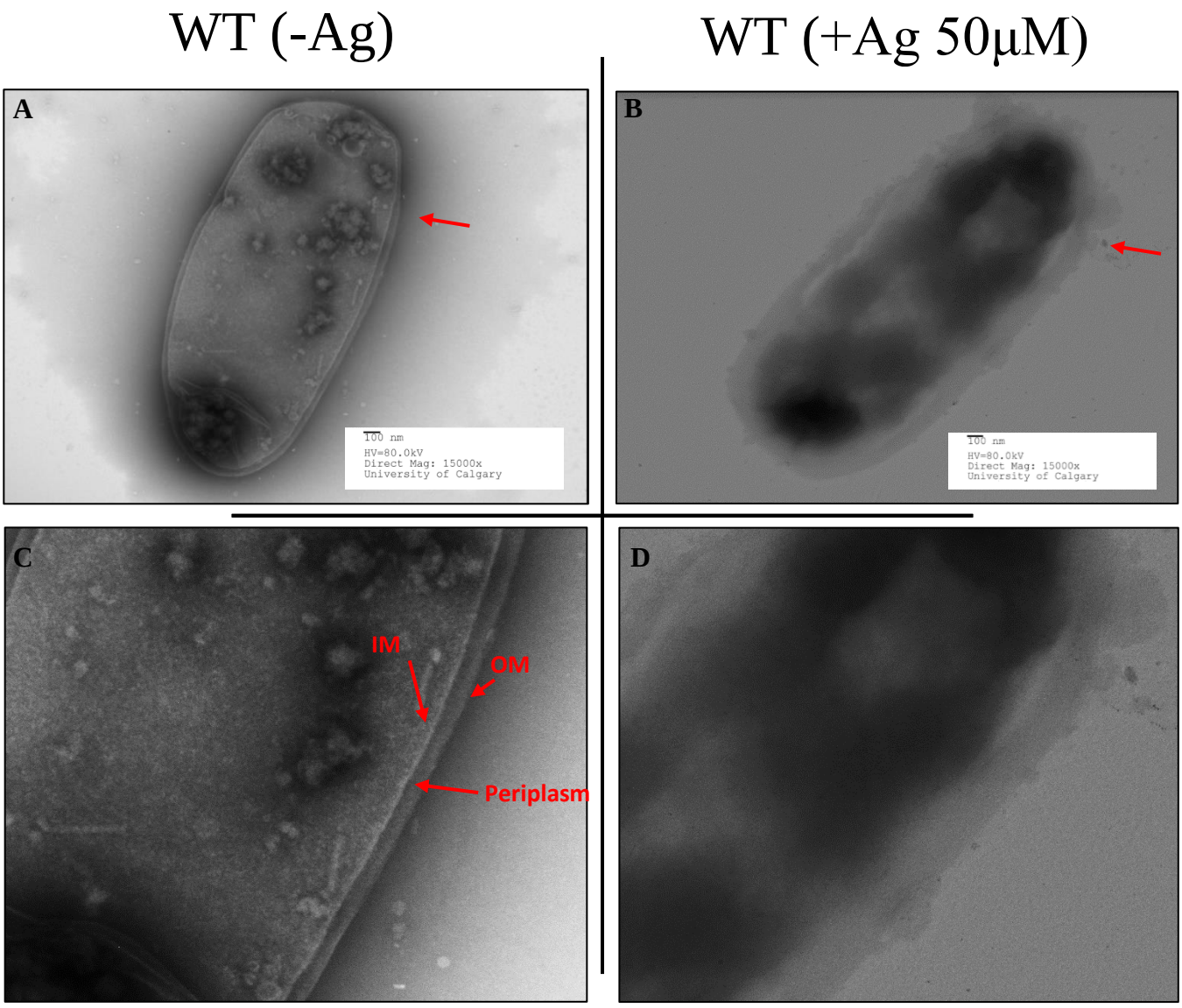

Figure 3.8: Internal cell envelope structures of planktonic of 1.0% phosphotungstic acid stained wildtype and BW25113 *E. coli* cells untreated (A and C) and pre-treated with 50 µM $AgNO_3$ (B and D) observed by Transmission electron microscopy.

3.6.2 Silver nanomaterial structure

In Figure 3.9, it is observable that a wildtype BW25113 and MG1655Δ*rodZ* treated cells have synthesized electron-dense nanomaterials in the form of a pyramid or nanoprism (1-100 nm) in close proximity to its cellular envelope. In conjunction to these observations, Raheem *et al*., (2011), also reported on finding similar Ag (I) nano structures when exposing the *E. coli* strain (ATCC 8739) to (1% v/v) of aqueous $AgNO_3$ in Luria and Burrous broth solution. Furthermore, other types of silver nanomaterials including spheres, cubes, and nanorods were also observed throughout TEM imaging of the treated *E. coli* cells (Appendix E). It appears that under the imposed procedural conditions, that the *E. coli* cells synthesize triangular silver nanoparticles by chemical reduction method through the reduction of silver nitrate in the presence of a reducing agent.

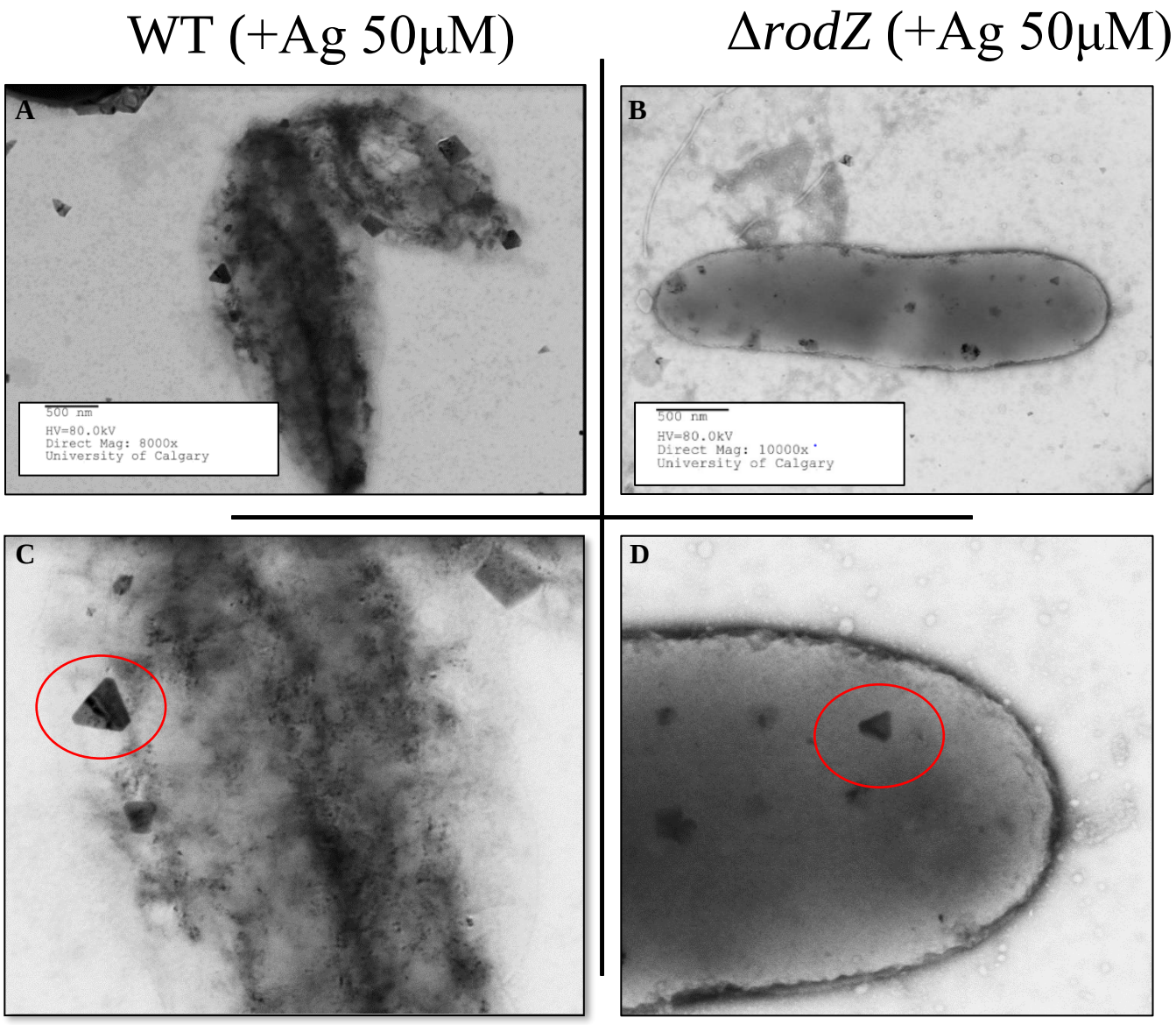

Figure 3.9: Wildtype and MG1655Δ*rodZ* cells with an electron-dense nanoparticle in the shape of a pyramid or nanoprism associating with its cellular envelope.

3.7 Disk diffusion assay

In order to provide a comparison to the susceptibility of each cell envelope mutant of *E. coli* to other metal antimicrobials, a disk susceptibility test was conducted. Initial experimental concerns expressed included the formation of metal complexes with the components of the agar media resulting in limited diffusion, nullifying the potential for this simple assay. We confirmed that all metals diffuse through the media agar producing growth inhibition zones, by measuring the resulting translucent areas without noticeable bacterial growth surrounding the antimicrobial infused disks. In the thesis research, we observed that all the bacterial strains were susceptible to the metal-salts in the tested concentrations (section *2.1.4*). Figures of one of two biological trials, which were utilized for the measurement of growth inhibition zones (where growth was inhibited by dissociation of metal-salt into its respective antimicrobial ion) can be found in the appendix F section of this thesis. These measurements were averaged in millimeters (mm) and used for comparison between wildtype and mutant strains. Several metals, such as; Zn^{2+}, Ni^{2+}, and Cu^{2+}, appeared to be the most efficacious antimicrobials at the tested concentrations, indicative of the larger zones of growth inhibitions (Table 3.2). BW25113Δ*damX* was less susceptible to Ag^{+}, Zn^{2+}, and Ni^{2+} toxicity when compared to wildtype cells, but generally had the same susceptibility to all other metals tested. Moreover, BW25113Δ*rodZ* was found to be more susceptible to Ni^{2+} and Zn^{2+} exposure when compared to all other strains.

Table 3.2: Detection of metal toxicity by use of disk diffusion susceptibility test illustrating displaying the zones of inhibition

Challenges

Strains	NaCl	$NaNO_3$	$NaSO_4$	$Ga(NO_3)_3 \cdot H2O$	$ZnSO_4 \cdot 7H_2O$	AgNO3	$NiSO_4 \cdot 6H_2O$	$Al_2(SO_4)_3 \cdot H2O$	$CuSO_4$
BW25113	0	0	0	11.5	24.0	11.0	23.8	15.0	19.1
BW25113ΔdamX	0	0	0	12.00	**22.8±0.8**	**9.60±0.1**	**21.5±0.3**	15.0	18.5
BW25113*ΔrodZ*	0	0	0	12.2	**26.0±0.2**	11.2	**26.6±0.4**	16.0	20.3
BW2511*3ΔminC*	0	0	7.00	**13.4±0.8**	**21.5±0.3**	11.0	23.3	14.5	19.8
BW25113*ΔsanA*	0	0	0	11.50	23.0	10.2	23.3	15.3	18.0
BW25113*ΔybhO*	0	0	0	**13.0±0.1**	23.4	10.4	23.1	15.2	18.5
BW25113ΔtolB	0	0	0	**15.0±0.2**	25.0	10.5	23.8	15.5	20.6

* Values are represented as the mean ± the SD and if no change in SD ± 0.00, n=2,. † Diameter (mm) of the zone of growth inhibition.

Chapter Four: Discussion

4.1 Metal exposure-response of the respective cellular envelope associated genes.

Silver has been known for its antimicrobial properties throughout antiquity (Akram *et al*., 2016; Jung *et al*., 2008; Lemire *et al*., 2013). However, the mechanism by which Ag^+ imposes its toxicity is still not fully understood (Clement and Jarret, 1994). Recent literature has demonstrated that *E. coli* and *S. aureus* microorganisms treated with Ag^+ ions, display a severely compromised cell envelope resulting in cell lysis and separation of the cell membrane from the cell wall (Jung *et al*., 2008). Investigating this uncharacterized toxicity mechanism, data was collected from Dr. Lemire's chemical genetic screen (unpublished), which provided genetic analysis of the Keio collections ordered mutant library. This assay presented phenotypic analysis of the libraries non-essential genes in the presence of 100 µM of $AgNO_3$ infused into M9 minimal noble agar media. Analyzing colony size as a proxy for fitness, Dr. Lemire discovered over 225 mutants found to be sensitive to the exposure of the 100 µM $AgNO_3$ challenge, while 177 mutants displayed a resistant phenotype. Of these genetic determinants, 20 sensitive and 4 resistant mutants were found to be involved in cell envelope homeostasis. From these 24 genes, 6 were chosen through further bioinformatic analysis and literary searches for their involvement in cell envelope homeostasis. Of the 6, 1 determinant was resistant in Dr. Lemire's screen, *damX*, the other 5; *rodZ, minC, sanA, ybhO,* and *tolB*, (Figure 4.0) were found to be sensitive.

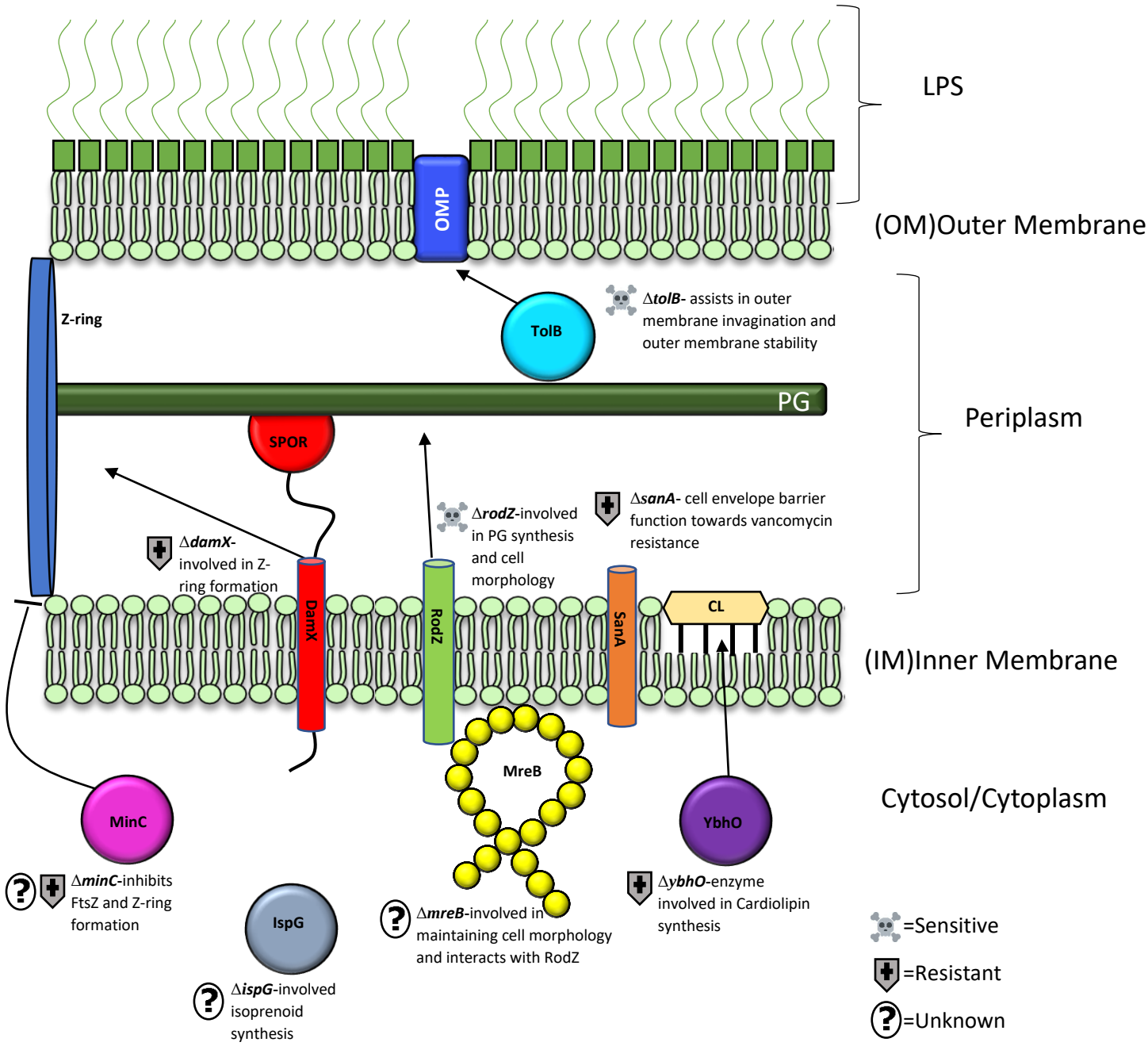

Figure 4.0: The identified silver resistant and sensitive genes protein product and their relative cellular roles within the organism *E. coli*. Contents of the cell are not to scale. Notation defines genes that are silver sensitive or resistant as determined in this study. PG: Peptidoglycan, OMP: Outer membrane porin.

To confirm the respective sensitive and resistant phenotypes of these genetic determinants, I set out to characterize their collective phenotype when subjected to a silver antimicrobial challenge. Utilizing metal-exposure response I aimed to determine the relative minimal bactericidal concentration and minimal biofilm eradication concentration of each of the mutant's planktonic and biofilm cell cultures against three metals. Before conducting this analysis, certain experimental parameters were considered. Despite the abundance of literature committed to examining the anti-microbial activity of metals, less attention has been paid to determining the susceptibility of bacteria to metals within a defined set of conditions (Gugala *et al*., 2017). Although the minimal inhibitory concentration, minimal bactericidal concentration and minimal biofilm eradication concentrations for many metals have been determined (Harrison *et al.,* 2004), the lack of consistency between techniques, conditions and media has resulted in difficulties when comparing the susceptibilities of bacterial strains to metal compounds. Here, M9 minimal media was utilized for the growth curve analysis, metal exposure-response assays and microscopy analysis. The decision to utilize minimal media rather a rich medium like Lysogeny broth, was based of ionic bonding chemistry. With the establishment that antimicrobial activity of Ag (I) based compounds being intrinsically dependent on the formation of the Ag^{+} ions (Walker and Parsons, 2014), there was concern that high NaCl concentration associated with LB media, would cause for the dissociating Cl^{-} ions and cause the precipitation of Ag^{+} as AgCl, as well as complexation of silver in diverse soluble chlorocomplexes and chelation with molecules within the LB. This concern was further validated by investigations into literature, which suggested that high Cl^{-} concentrations in the exposure medium indeed have a pivotal influence on the resulting toxicity of a Ag(I) based antimicrobial, appearing to significantly attenuate toxicity (Gadd *et* al., 1989; Groh *et al*., 2015). However, when trying to accumulate sufficient biomass of the mutant's strains biofilms for examination during the metal exposure-response assay, it was found that M9 media did not support measurable optical density. This determination was also supported by literary sources that described the BW25113 *E. coli* strain to be motility-impaired in minimal media, when compared to the MG1655 strain, due to the differences in the expression of motility loci, *qseB, flhD, fliA, fliC*, and *motA* (Wood *et al*., 2006). Wood *et al*., (2006) found that *qseB* expression, which is responsible for the activation of the flagella regulon, was 139-fold higher in the MG1655 strain than in BW25113 (Sperandio *et al*. 2002; Wood *et al*., 2006). They further suggested that the differentiation in expression has led

to both reduced motility and deficiency of flagellar apparatuses in the BW25113 strain, making them "poor" biofilm producers. Although measurable amounts of biofilm were unachievable through spectroscopy methods, when the biofilms grown in M9 media and were visualized during different microscopy techniques, it was confirmed that each mutant could grow a thin confluent biofilm. This was important finding, for this determination allowed for viable cell counts of BW25113 biofilms to be conducted and respective MBEC values to be determined for each mutant (Table 3.2).

The resulting MBC and MBEC findings from the metal exposure-response assay, suggested that the single gene deletions of Δ*damX*, Δ*sanA*, and Δ*ybhO*, in *E. coli* K-12 BW25113 strain withstood a higher concertation of Ag(I) metal challenge when compared to the wildtype cultures. This finding proposes the idea that *E. coli* cells lacking these genes and their respective transcribed protein products are more resistant to Ag^+ toxicity. To understand why the deletions of these genes conferred relative Ag^+ resistance resulted in analysing their cellular function and possible association with Ag^+ ions. The cell, which showed the highest levels of resistance had a *damX* gene deletion. This gene is predicted to code for a bitopic inner membrane protein, which is involved in cell division; as it contains a C-terminal SPOR domain, which targets the protein to the septal ring (Gerding *et al*., 2009). Utilizing both YFP-DamX and GFP-DamX, Gerding and colleges confirmed that the DamX protein localizes sharply to division sites in wildtype *E. coli* cells. Further, DamX has been shown through a two-hybrid system to interact strongly to essential cell division proteins FtsQ and FtsN, who are required for septum formation and mid-cell localization of the Z-ring (Arends *et al*., 2010). Moreover, that same assay also suggested that DamX has weak interactions with FtsZ, which is responsible for forming the contractile ring Z-ring structure (Arends *et al*., 2010). Investigating into the amino acid composition of the DamX protein resulted in no thiol groups (R-SH) being evident, which have been demonstrated to be favorable binding targets for silver and the energetically favorable bonding of SH-Ag has been shown to result in protein deactivation (Klueh *et al*., 2000; Rai *et al*., 2012). However, the DamX protein contains 22 charged amino acid residues of arginine (R). Recent literature has suggested that of all the amino acids, arginine has the highest affinity towards silver ions (Shoeib *et al*., 2002), and binds silver via chelation and complexation mechanisms (Agnihotri *et al*., 2015). A study supporting this finding conducted by Agnihotri *et* al., 2015, demonstrated that ZnO nanorods served as nano-reactors for *in situ* synthesis of silver

nanoparticles concurrently providing a template for their subsequent immobilization using arginine as a linker (Agnihotri *et al*., 2015). Thus, from evidence proposed in the literature it is suggested here that the presence of the arginine in the DamX protein could be immobilizing free Ag^+ onto its surface, which could inhibit DamX's role in cellular division leading to silver sensitivity in cells containing the Δ*damX* gene deletion.

With the findings from two-hybrid protein interactions in literature, it is suggested that DamX could also directly link the peptidoglycan layer to the Z-ring. If confirmed, and if Ag^+ can be shown to be sequestered and immobilized on the DamX protein by its arginine residues, then silver ions could impose their toxicity on the Z-ring and the formation of the septum in dividing cells. The Z-ring is essential step required for cellular division, with any interruption of its formation process leading to the interruption of cellular growth (Hwang and Lim, 2015). Consequently, *E. coli* cells that have the chromosomal deletion Δ*damX*, have their cellular division and growth less effected by Ag^+ binding to DamX, making them more tolerant to the silver challenge than the wildtype *E. coli* cells.

The DamX amino acid sequence was further subjected for analysis utilizing Phyre2 (Protein Homology/AnalogY Recognition Engine) a web-based service for protein structure prediction (Kelley *et al*., 2015). The resulting 3-D model was generated based of techniques that utilize homology modeling, resulted in the SPOR domain being identified with 99.9% confidence and 97% identity. The model further provided secondary structures of the predicated biotic inner membrane protein, that hypothesized the presence of arginine residues being present in both the cytosol and periplasmic space. Thus, adding more speculation to DamX possibly having silver ions immobilized on its periplasmic surface by arginine residues.

The other two resistant determinants validated by MBC and MBEC values, Δ*sanA* and Δ*ybhO*, were found to be more resistant to the exposure of the silver-based antimicrobials when compared to the wildtype cultures. These findings contradict the initial Ag-sensitive phenotype that was observed from the chemical genetic screen. Possible explanations for this discrepancy in phenotype, could have resulted from the difference in the growth mediums utilized. The chemical screen was conducted on solid M9 minimal noble agar infused with 100 µM of $AgNO_3$, where as the metal exposure-response experiments in this thesis were carried out in M9 liquid broth medium, present in 96 well plates with cultures grown in the presence of 256 µM of silver

metal challenge, then subsequently plated on to LB agar plates for colony viability analysis. Expositions from literature, have suggested that the rate of diffusion of silver ions in agar gel is much slower than that of liquid broth medium (Kant, 1962). Thus, the agar infused $AgNO_3$ plates could have different Ag^+ saturation throughout the plate, complexation, Ag^+ dissociation and diffusion rates, that resulted in the reporting of a sensitive MBC for cells containg the gene deletions Δ*sanA* and Δ*ybhO*, when grown on the solid media in comparison to liquid or aqueous mediums. Similar susceptibility findings have been reported in literature where discrepancy between concentration of metals in media can lead to different susceptibility phenotypes. Kumar *et al.,* (2013), reported that the Gram negative rod-shaped *S. marcescens* organisms displayed higher MIC values to transition metals on solid Mueller-Hinton agar then in comparison to liquid medium. Therefore, the possible unequal distribution of Ag^+ throughout the M9 noble Agar could be the contributing factor for the different Ag- phenotypic responses observed.

Nonetheless, the gene *sanA* has been identified to code for the sole member of the vancomycin-sensitivity protein family in the Transporter Classification Database (Saier *et al*., 2016). SanA is predicated to be a bitopic inner membrane transport protein, roughly 239 amino acids in size. Unlike DamX, SanA does contain cysteine amino acid residues within its protein sequence, which have been demonstrated empirically through the Hard-soft acid base theory, that soft acids like Ag(I) have electron-sharing affinities that can result in the energetically favourable formation of covalent bonds between soft bases, such as the sulphhydryl groups present on the amino acid, cysteine (Gordon *et al*., 2010; Harrison *et* al., 2007; Leung *et al*., 2013). Thus, Ag^+ ions could be binding to the sulphhydryl groups present within the SanA protein inhibiting its function. Another observation from literature that could possibly support this associated Ag-resistant phenotype in Δ*sanA E. coli* cells, was the determination that silver enhances the antimicrobial efficacy of the antibiotic, vancomycin (Esmaeillou *et al*., 2017; QingShan *et al*., 2006). QinShan and colleagues investigated vacomycin-capped silver nanoparticles and examined their antibacterial activities *in vitro* against *E. coli*. They reported from microscopy TEM images, that single bacteria treated with the vacomycin-capped silver nanoparticles, had plenty of aggregates in the cell wall of the *E. coli* organism (QingShan *et al*., 2006). QinShan *et al*., (2006) proposed that a possible antibacterial mechanism of the silver nanoparticles was to destroy or destabilize the membrane, allowing for vancomycin to easily bind to the terminal d-Ala-d-Ala dipeptide inhibiting peptidoglycan biosynthesis (Ge *et al*.,

1999). In addition to this proposed mechanism, other work conducted by Mitchell *et al.*, (2017) predicted that SanA is involved in OM permeability to sodium dodecyl sulfate (SDS) in carbon-limited cells. Thus, it is proposed if Ag^+ can bind and inhibit SanA function, there would be subsequent changes in membrane permeability. This would account for Δ*sanA* mutants having different membrane properties that could account for relative resistance to the Ag^+ challenge in respect to the wildtype cells.

The other resistant genetic determinant, *ybhO*, codes for an enzyme involved in cardiolipin synthesis. Cardiolipin is a unique phospholipid which was historically identified as a major lipid in the inner mitochondrial membrane of cardiac muscle cells (Paradies *et al.*, 2014). Considerable progress has recently been made in understanding the role of cardiolipin in mitochondrial function and bioenergetics (Paradies *et al.*, 2014). It has been shown that cardiolipin is associated with membranes designed to generate an electrochemical gradient that is used to produce ATP, such as bacterial plasma membranes and inner mitochondrial membrane (Schlame *et al*., 2000). Literary inferences have suggested that cardiolipin seems to participate in the structural organization and stabilization of the respiratory chain complexes (Electron transport chain, ETC or oxidative phosphorylation) in high order structure of functional importance and play a significant role in the formation of the membrane curvature (Pfeiffe*r et al*., 2003; Schägger, 2002). Its role in ETC functionality, however, has been shown to have deleterious effects if in the presences of reactive oxygen species (ROS)-induced oxidation. Interestingly, this determination that ROS induces the depletion of cardiolipin in the membrane, relates to Ag^+ induced toxicity. With the establishment that Ag^+ ions have the ability to disrupt iron-sulfur clusters [4Fe-4S] in proteins (Xu *et al*., 2009; Xu and Imlay, 2012) by binding to the sulphhydryl groups, it has been suggested that this binding induces the release of Fe^{2+} from these proteins. It has thus been suggested that this release of Fe^{2+} might account for observations that the Fenton-inactive Ag, could generate ROS within a bacterial cell (Park *et* al., 2009; Xu *et al*., 2009). Therefore, if Ag^+ ions are causing the generation of ROS within *E. coli* cells, then cardiolipin would be subjected to its toxicity, resulting in deleterious effects upon the ETC. Thus, cells that have the chromosomal deletion Δ*ybhO*, could have a reduction in cardiolipin synthesis, possibly causing the resistant phenotype in comparison to wildtype cells, for the ROS has less of a lethal effect on the Δ*ybhO E. coli* cells for their membrane physiology has changed and their ETC are not being directly targeted.

In contrast to the to the Ag-resistant determinants, the gene deletions of *rodZ* and *tolB*, resulted in BW25113 *E. coli* cells to become more susceptible to the silver and copper metal antimicrobial challenges. Thus, suggesting that the protein products of these genes aid in generating relative tolerance to the toxicity of the metal challenges in the wildtype cells. The *rodZ* gene codes for a bitopic inner membrane protein that has been identified to be involved in cell wall synthesis and retaining cellular morphology (Morgenstein *et al*., 2015). Bacterial cell shape is structurally determined by the rigid peptidoglycan built outside the cytoplasmic membrane by a series of cell wall assembling enzymes (Typas *et al*., 2012). In many bacillus, or rod-shaped species, the enzymes have been showing to be coordinated by an actin-like protein, MreB (Morgenstein *et al*., 2015), with its polymeric nature being identified as the key determinant in retaining the rod shape. However, it has remained difficult to explain the mechanistic link between cell wall growth and MreB located in the cytosol of the bacteria cell. Morgenstein and colleagues however, provided substantial evidence through functional GFP-RodZ fusion, demonstrating that RodZ and MreB are colocalized within *E. coli* cells and located together around the cells circumferences. They further inferred that RodZ has a periplasmic tail that is important for cell shape and could interact with penicillin binding proteins and a cytoplasmic tail that directly interacts with MreB, thus linking the MreB to protein(s) in the periplasm (Bendezú *et al*.,2009; Morgenstein *et al*., 2015; van den Ent *et al*., 2010). Therefore, it is suggested that cells having the Δ*rodZ* gene deletion have a reduction in cell wall biosynthesis and stabilization. Without RodZ linking MreB to the periplasm, proteins could be assembling in a non-orderly manner resulting in decreased cell wall integrity. With compromised structural integrity of the cell wall, it is thought that these Δ*rodZ E. coli* cells would have a lower MBC and MBEC values than wildtype cells, which was confirmed from the metal exposure-responses experiments within this thesis.

The other Ag-sensitive genetic determinant, *tolB*, codes for a periplasmic protein, which participates in the trimeric porin assembly of OmpF, OmpC, PhoE, and LamB (Rigal *et al*., 1997) and is involved in outer membrane stability (Lazzaroni *et al*., 1999). The interaction between TolB proteins and outer membrane stability and porin assembly may be the direct cause for the resulting Ag^+ sensitive phenotype. Recent literature, conducted by Randall *et al*., 2015, demonstrated that in *E. coli* endogenous resistance arose to silver as a consequence of two-point mutations in *ompR* and *cusS* resulting in loss of the OmpC/F porins. Thus, confirming that silver

resistance in *E. coli* can be associated with the depressed expression of the OmpC/F outer membrane porins (Randall *et al*., 2015). This silver resistance phenotype was also reported by Radzig *et al*., 2009, who demonstrated that *E. coli* MC4100 strain cells with chromosomal deletions for the genes encoding OmpF and OmpC, were found to be three to four times more resistant to silver ions than the wild-type strain. Radzig and colleagues further suggested, that their data indicates that these porins may be involved directly or indirectly with the movement of silver ions into the cell. Furthermore, literary insight provided by Lazzaroni *et al*., (1999) has also described that *tolB* mutants in *E. coli* cells demonstrated an increase in OmpC porins (Lazdunksi *et al*., 1998; Lazzaroni *et al*.,1999; Misra and Reeves, 1987). Thus, it is suggested here that increased number of OmpC porins from the gene deletion of Δ*tolB*, could increase the amount of intracellular Ag^{+} accumulation, resulting in the sensitive phenotype that was observed throughout the metal exposure-response experiments in this thesis. Moreover, this explanation provides further insight into the increased susceptibility of BW25113Δ*tolB* to the Cu^{2+} antimicrobial challenge. According to Elger *et al.*, (2005), who investigated the pathways of copper uptake by *E. coli* cells, they have suggested that intracellular accumulation of Cu^{2+} is facilitated through the OmpC and OmpF porins. They further showed that increased expression of OmpC can lead to increased intracellular concentration of metals. Therefore, it is suggested that Δ*tolB* genetic deletions generate *E. coli* cells that are both more susceptible to copper and silver antimicrobials as a result of the amplified OmpC porin protein production and through destabilizing of the OM causing 'leakiness' of Ag^{+} through the OM.

The last genetic determinant, *minC*, is involved in ensuring the correct placement of the septum during cell division, suppressing formation of the septa in aberrant loci within the cell (Pichoff and Lutkenhaus, 2001). Evaluating the resulting MBC and MBEC values for the BW25113Δ*minC* cells, saw only the biofilm cells being more resistant to the AgSD challenges when compared to the wildtype. Furthermore, BW25113Δ*minC* cells achieved similar MBC and MBEC values to that of the wildtype cells for the other two metal antimicrobials. One potential cause for the resulting resistant phenotype, was the presence of cysteine residues within the MinC protein. As discussed, Ag^{+} ions have been shown to bind sulphhydryl groups with in proteins, resulting in their inactivation (Xu *et al*., 2009; Xu and Imlay, 2012).

Comparing the toxicity of Ag^+ ions to the planktonic and biofilm cells of each mutant strain, it is evident that biofilms offered cells increased tolerance to the Ag^+ and Cu^{2+} challenges. Bacterial biofilms are sessile microbial communities frequently imbedded in a EPS matrix (Garret *et al*., 2008). These robust structures offer bacterial cells protection from persistent environmental pollutants (Teitzel and Parsek, 2003). Teitzel and Parsek (2003), demonstrated that when *P. aeruginosa* (PAO1) strain cells were assayed with heavy metals, free-swimming planktonic cells were more susceptible to the metal challenge in comparison to biofilms cells. This similar trend was found in this thesis, where generated planktonic cells MBC values for each mutant, were lower then the compared biofilms cells MBEC values. Moreover, the MBC and MBEC values were similar to values found in the literature, where Harrison *et al.,* (2004) assayed *E. coli* JM109 strain cells against silver ions in Lysogeny broth medium, generating a MBC and MBEC values of 0.09±0.04 and 0.07±0.02 mM respectively.

4.2 Effects of Ag^+ on *E. coli* planktonic cell morphology

Although the mechanisms underlying the antibacterial actions of silver are still not fully understood, several previous inferences from the literature (McDonnell and Russell, 1999; Pal *et al*., 2007) have suggested that the interaction between silver ions and the constituents of the bacterial cell envelope caused structural changes, damage to the membranes and intracellular metabolic activity which might be the cause or consequence of cell death. Thus, suggesting that genetic determinants involved in cell envelope homeostasis could be direct or indirect targets involved in Ag^+ ions-imposed toxicity mechanism. Investigating the morphological changes of the mutant BW25113 planktonic cells in the presence of a 50 μM $AgNO_3$ challenge, was observed through the utilization of TEM. Each of the *E. coli* strains resulted in similar phenotypes with the unchallenged cells conforming to normal bacillus cellular morphology, while treated cells had aberrant cellular morphology and extensive cell envelope damage and apparent cell lysis. It was also observed that untreated cells had visible intact internal structures with both the IM, periplasm, and OM visible through the use of TEM (Figure 3.18). This observation too has been made in the literature where both Jung *et al.,* (2008) and Yamanaka *et al*., (2005) both reported that intracellular structures of *E. coli* were observable utilizing TEM. Jung *et al.,* (2008) further showed that both *E. coli* and *S. aureus* cells treated with 0.2 ppm Ag^+

solution displayed either localized or complete separation of the cell membrane from the cell wall. Jung *et al*., (2008), further concluded that electron-dense particles or precipitates were also observed around damaged bacterial cells, which were also observed in the TEM treated cells within this thesis. Anlysisng the TEM images, however, concluded that there was no difference in phenotype of treated cells in both wildtype and mutant cells. Thus, suggesting that other genetic determinants or cellular mechanisms must be involved in Ag^{+} cell envelope toxicity mechanism.

The TEM images from my study here further lead to the observations of the BW25113 and MG1655 *E. coli* cells synthesizing Ag nanoparticles (AgNP) in the shape of spheres, pyramids or nanoprisms. Comparable observations have also been recorded in the literature where Shanshoury *et al*., (2011) observed *E. coli* strain ATCC 8739 cells, treated with aqueous $AgNO_3$ in nutrient broth could biosynthesize Ag-nanoparticles that appeared spherical in shape and appeared to be reasonably monodispersed. Shanshoury *et al*., (2011), further concluded that the nanoparticles ranged in size of 5-25 nm in diameter. These findings have important implications for possible 'biosynthesis' of Ag nanoparticles, which has been actively pursued in recent years as an alternative, efficient, inexpensive, and environmentally safe method for producing nanoparticles with specified properties. Currently, physical and chemical processes are widely used to synthesize metal nanoparticles, which allow one to obtain particles with the desired characteristics (Okitsu *et al*., 2007). However, these production methods are usually expensive, labor-intensive, and are potentially hazardous to the environment and living organisms (Narayanan and Skthivel, 2010). Thus, investigations into "Green" nanoparticle development that is environment friendly, cost effective and easily scalable is becoming highly sought after. Thus, the mutants and strains of *E. coli* evaluated here may turn out to be excellent biofactories to produce AgNPs. Optimization of culturing and exposure conditions could lead to control over nanomaterial shapes and characteristics.

4.3 Conclusion

MDR bacterial pathogens have become a serious challenge for healthcare professionals (Bartlett et al., 2013). With the reduction in new investment, focused on developing new novel antibiotic medicines, the subsequent 'drying up' of the development pipeline for new antibiotics, has begun to exacerbate the problem of MDR bacteria (Bartlett *et al*., 2013). Research scientists

must now begin to investigate the efficacy of alternative antimicrobial compounds to be considered as methods of treatment or to be used synergistically alongside other antibacterial medicines in the treatment of these MDR infections (Allen *et al*., 2014). These new investigations are now focusing on uncovering the complex toxicity mechanisms by which these alternative antimicrobial agents function.

This thesis utilized data from a chemical genetic screen, which was utilized to investigate genetic determinants, to provide an extensive genomic analysis of possible cellular targets by which silver imposes its toxicity onto *E. coli* cells. It was demonstrated that the growth of planktonic and biofilm cells of both BW25113 and MG1655 *E. coli* strains were affected when grown in the presence of Ag^{+} and Cu^{2+}, with cells being susceptible to silver toxicity at micro molar concentrations. The exposure to Ag^{+} resulted in morphological changes in planktonic cells, causing extensive cell envelope damage. Biofilm morphology could not be characterized due to the presence of artifacts and complication arising from both SEM and CLSM experimental procedures generated inconclusive results.

Many different mechanisms of Ag(I) toxicity have been suggested in the literature, from its ability to induce oxidative stress through the generation of reactive oxygen species and causes damage to cellular components including DNA damage, activation of antioxidant enzymes, depletion of antioxidant molecules (i.e., glutathione), and binding and disabling of proteins (McShan *et al*., 2014). Moreover, it is also apparent from many observations from the literature and here from this thesis work, that Ag^{+} ions cause extensive damage to the cellular envelope of Gram-negative bacteria. We see that functions around the cell wall and transport across the cell membranes have roles in both silver resistance and sensitivity (summarized in Figure 4.0). This data provides support to the idea that silver appears to be a multi-target antimicrobial by imposing its toxicity on multiple biochemical pathways such as those involved in cell wall homeostasis within the *E. coli* organism.

References

Afessa, B. Shorr. A. Anzueto, A. Craven, D. Schinner, R. Kollef, M. (2010). Association between a silver-coated endotracheal tube and reduced mortality in patients with ventilator-associated pneumonia. *Chest* .137(5):1015–1021.

Agnihotri, S. Bajaj, G. Mukherji, S. Mukherji, S. (2015). Arginine-assisted immobilization of silver nanoparticles on ZnO nanorods: an enhanced and reusable antibacterial substrate without human cell cytotoxicity. *Nanoscale*. 7:7415-7429.

Akram, F. El-Tayeb, T. Abou-Aisha, K. El-Azizi, M. (2016). A combination of silver nanoparticles and visible blue light enhances the antibacterial efficacy of ineffective antibiotics against methicillin-resistant Staphylococcus aureus (MRSA). *Annals of Clinical Microbiology and Antimicrobials*.15:48.

Alanis, A. (2005). Resistance to Antibiotics: Are We in the Post-Antibiotic Era?. *Archives of Medical Research*. 36(6):697-705.

Alekshun, M. Levy, S. (2007). Molecular mechanisms of antibacterial multidrug resistance. *Cell*.128:1037-50.

Alexander, J. (2009). History of the Medical use of Silver. *Surgical infections*. 10(3):289-292

Allison, D. Lambert, P. (2015). Modes of Action of Antibacterial Agents. *Molecular Medical Microbiology*.1:583-598.

Alle, H. Trachsel, J. Looft, T. Casey, T. (2014). Finding alternatives to antibiotics. *Annals of the New York Academy of Sciences*. 1323(1):91-100

Aminov, R. I. (2010). A Brief History of the Antibiotic Era: Lessons Learned and Challenges for the Future. *Frontiers in Microbiology*.1:134.

Ansari, M. Khan, H. Khan, A. Ahmad, M. Mahdi, A. Pal, R. Cameotra, S. (2013). Interaction of silver nanoparticles with *Escherichia coli* and their cell envelope biomolecules. *Journal of Basic Microbiology*.53:1-11.

Ansari, M. Khan, M. Khan, H. Mahdi, A. Cameotra, S. Pal, R. (2013). Antibiofilm efficacy of silver nanoparticles against biofilm of extended spectrum β-lactamase isolates of *Escherichia coli* and *Klebsiella pneumoniae*. *Applied Nanoscience*.4(7):859-868.

Arends, S. Williams, K. Scott, R. Rolong, S. Popham, D. Weiss, D. (2010). Discovery and Characterization of Three New *Escherichia coli* Septal Ring Proteins That Contain a SPOR Domain: DamX, DedD, and RlpA. *Journal of Bacteriology*.192(1):242–255.

Baba, T. Ara, T. Hasegawa, M. Takai, Y. Okumura, Y. Baba, M. Mori, H. (2006). Construction of *Escherichia coli* K-12 in-frame, single-gene knockout mutants: the Keio collection. *Molecular Systems Biology*. *2*:2006-0008.

Bachmann, B. (1972). Pedigrees of some mutant strains of *Escherichia coli* K-12. *Bacteriological Reviews*. 36: 525–557.

Bachmann, B. (1996). Derivations and genotypes of some mutant derivatives of *Escherichia coli* K-12. In *Escherichia coli* and *Salmonella typhimurium* Cellular and Molecular Biology, Neidhardt FC, Curtiss III R, Ingraham JL, Lin ECC, Low Jr KB, Magasanik B, Reznikoff WS, Riley M, Schaechter M, Umbarger HE (eds), 2 edn, pp 2460–2488. Washington, DC: ASM Press

Bassett, E. Keith, M. Armelagos. G, Martin, D. Villanueva, A. (1980). Tetracycline-labeled human bone from ancient Sudanese Nubia (A.D.350). *Science*. 209:1532–1534.

Bartlett. J, Gilbert, D. Spellberg, B. (2013). Seven ways to preserve the miracle of antibiotics. *Clinical Infectious Diseases*. 56(10):1445–1450.

Baryshnikova, A. Costanzo, M. Dixon, S. Vizeacoumar, F. Myers, C. Andrews, B. Boone, C. (2010). Synthetic Genetic Array (SGA) Analysis in Saccharomyces cerevisiae and Schizosaccharomyces pombe. *Methods in Enzymology*.470:145-179.

Bauer, A. Kirby, W. Sherris, J. Turck, M. (1966). Antibiotic susceptibility testing by a standardized single disk method. *American Journal of Clinical Pathology*.45(4):493-6.

Béahdy, J. (1874). Recent Developments of Antibiotic Research and Classification of Antibiotics According to Chemical Structure. *Advances in Applied Microbiology*. 18: 309-406.

Beketskaia, M. Bay, D. Turner, R. (2014). Outer membrane protein OmpW participates with small multidrug resistance protein member EmrE in quaternary cationic compound efflux. *Journal of Bacteriology.* 196: 1908–1914.

Belly, R. Kydd, G. (1982). Silver resistance in microorganisms. *Developments in Industrial Microbiology.* 23:567-577.

Belvins, S. Bronze, M. (2009). Robert Koch and the 'golden age' of bacteriology. *International Journal of Infectious Disease*s. 14(9):e744-e751.

Bennett, P. (2008). Plasmid encoded antibiotic resistance: acquisition and transfer of antibiotic resistance genes in bacteria. *British Journal of Pharmacology*.153(Suppl 1), S347–S357.

Bendezú, F. Hale, C. Bernhardt, T. de Boer, P. (2009). RodZ (YfgA) is required for proper assembly of the MreB actin cytoskeleton and cell shape in E. coli. *The EMBO Journal.* 28(3):193–204

Bessey, P. (2007). Wound care. *Total Burn Care.* 3:127-135.

Beveridge, T. (1999). Structures of Gram-Negative Cell Walls and Their Derived Membrane Vesicles. *Journal of Bacteriology*. 181(16):4725-4733.

Bononi, I. Balatti, V. Gaeta, S. Tognon, M. (2008). Gram-Negative Bacterial Lipopolysaccharide Retention by a Positively Charged New-Generation Filter. *American Society for Microbiology*.74(20):6470-6472.

Bouzakis, K. Michailidis, N. (2014). Physical Vapor Deposition (PVD). In: The International Academy for Production Engineering, Laperrière L., Reinhart G. (eds) CIRP Encyclopedia of Production Engineering. Springer, Berlin, Heidelberg.

Bragg, P. Rainnie, J. (1974). The effect of silver ions on the respiratory chain of *Escherichia coli*. *Canadian Journal of Microbiology*. 20:883-889.

Braun, V. Rehn, K. (1969). Chemical Characterization, Spatial Distribution and Function of a Lipoprotein (Murein-Lipoprotein) of the *E. coli* Cell Wall. *European Journal of Biochemistry*.10: 426–438.

Chan, W. Verma, C. Lane, D. Gan, S. (2013). A comparison and optimization of methods and factors affecting the transformation of *Escherichia coli*. *Bioscience Reports*. 33(6). e00086.

Cherepanov, P. Wackernagel, W. (1995). Gene disruption in *Escherichia coli*: TcR and KmR cassettes with the option of Flp-catalyzed excision of the antibiotic-resistance determinant. *Gene*.158: 9–14.

Chopra, I. Roberts, M. (2001) Tetracycline antibiotics: mode of action, applications. Molecular biology, and epidemiology of bacterial resistance. *Microbiology and Molecular Biology Reviews*.65:232-260.

Clardy, J. Fischbach, M. Currie, C. (2009). The natural history of antibiotics. *Current Biology: CB*, 19(11): R437–R441.

Clement, J. Jarrett, P. (1994). Antibacterial Silver. *Metal-Based Drugs*. 1(5-6):467–482.

Cooper, GM. The Cell: A Molecular Approach. 2nd edition. Sunderland (MA): Sinauer Associates; (2000). Structure of the Plasma Membrane. Available from: https://www.ncbi.nlm.nih.gov/books/NBK9898/

Costerton, J. Ingram, J. Cheng, K.(1974). Structure and Function of the Cell Envelope of Gram Negtaive Bacteria. *American Society for Microbiology. 38*(1): 87-110.

Cowan, S. Schirmer, T. Rummel, G. Steiert, M. Ghosh, R. Pauptit, RA. Jansonius, J. Rosenbusch, J. (1992). Crystal structures explain functional properties of two E. coliporins. *Nature*. 358: 727–733.

Cumming, G. Fidler, F. Vaux, D. (2007). Error bars in experimental biology. *Journal of Cell Biology*.177 (1):7-11.

Curtis, P. (2016). Essential Genes Predicted in the Genome of Rubrivivax gelatinosus. *Journal of Bacteriology*.198(16):2244-2250.

Davies, J. Wright, G. (1997). Bacterial resistance to aminoglycoside antibiotics. *Trends in Microbiology*. 5:234–240.

Dakal, T. Kumar, A. Majumdar, R. Yadav, V. (2016). Mechanistic Basis of Antimicrobial Actions of Silver Nanoparticles. *Frontiers in Microbiology*. *7*:1831.

Darzynkiewicz, Z, Juan G, Srour, E. (2004). Differential staining of DNA and RNA. *Current Protocols in Cytometry*. Chapter 7: Unit 7.3.

Datsenko, K. Wanner, B. (2000). One-step inactivation of chromosomal genes in *Escherichia coli* K-12 using PCR products. *Proceedings of the National Academy of Sciences of the United States of America*. 97(12):6640–6645.

De Duve, C. Wattiaux, R. (1966). Functions of lysosomes. *Annual Review of Physiology*.28: 435–492.

Dobson, A. Carper, E. (1996). Infectious Diseases and Human Population History. *BioScience.* 46(2):115-126.

Domínguez, C. Rosa, M. Borobio, V. (2001). Application of a spectrophotometric method for the determination of post-antibiotic effect and comparison with viable counts in agar. *Journal of Antimicrobial Chemotherapy*. 47(4):391–398

Drlica, K. Zhao, X. (1997). DNA gyrase, topoisomerase IV, and the 4-quinolones. *Microbiology and Molecular Biology Reviews* 61: 377-392

Economou, V. Gousia, P. (2015). Agriculture and food animals as a source of antimicrobial-resistant bacteria. *Infection and Drug Resistance*. 8:49–61.

Ehrlich, P. Bertheim, A. (1912). Über. das salzsaure 3.3´-Diamino-4.4´ -dioxy-arsenobenzol und seine nächsten Verwandten. Ber. Dtsch. Chem. Ges. 45, 756–766 (in German).

Egler, M. Grosse, C. Grass, G. Nies, D. (2005). Role of the Extracytoplasmic Function Protein Family Sigma Factor RpoE in Metal Resistance of *Escherichia coli*. *Journal of Bacteriology*:187(7):2297–2307.

Esmaeillou, M. Zarrini, G. Rezaee, M. Mojarrad, J. Bahadori, A.(2017). Vancomycin Capped with Silver Nanoparticles as an Antibacterial Agent against Multi-Drug Resistance Bacteria. *Advanced Pharmaceutical Bulletin*7(3):479-483

Erhman, M. (2007). The periplasm. ASM Press, Washington, D.C.

Finley, P. Norton, R. Austin, C. Mitchell, A. Zank, S. Durham, P. (2015). Unprecedented Silver Resistance in Clinically Isolated Enterobacteriaceae: Major Implications for Burn and Wound Management. Antimicrobial Agents and Chemotherapy.59(8):4734-4741.

Finney, L. O'Halloran, T. (2003). Transition metal speciation in the cell: insights from the chemistry of metal ion receptors. *Science*. 300: 931–936.

Furr, J. Russell, A. Turner, T. Andrews, A. (1994). Antibacterial activity of Actisorb Plus, Actisorb and silver nitrate. *Journal of Hospital Infection*. 27:201-208.

Gadd, G. Laurence, O. Briscoe, D. Trevors, J. (1989). Silver accumulation inPseudomonas stutzeri AG259. *BiolMetals*.2:168-173.

Garret, T. Bhakoo, M. Zhang, Z. (2008). Bacterial adhesion and biofilms on surfaces. *Progress in Natural Science*. 18(9):1049-1056.

Ge, M. Zhong, C. Russell, H. Onishi, Kohler, J. Silver, L. Kerns, R. Fukuzawa, S. Thompson, C. Kahne, D. (1999). Vancomycin Derivatives That Inhibit Peptidoglycan Biosynthesis Without Binding d-Ala-d-Ala. *Science*. 284(5413):507-511

Gerding, M. Liu, B. Bendezú, F. Hale, C. Bernhardt, T. de Boer, P. (2009). Self-Enhanced Accumulation of FtsN at Division Sites and Roles for Other Proteins with a SPOR Domain (DamX, DedD, and RlpA) in *Escherichia coli* Cell Constriction. *Journal of Bacteriology*.191(24):7383–7401.

Goldstein, J. (2003). Scanning Electron Microscopy and X-Ray Microanalysis. Springer. ISBN 978-0-306-47292-3. Retrieved December 31, 2017.

Gooch, J. (2011) Germ Theory of Disease. In: Gooch J.W. (eds) Encyclopedic Dictionary of Polymers. Springer, New York, NY

Gordon, O. Slenters, T. Brunetto, P. Villaruz, A. Sturdevant, D. Otto, M. Landmann, R. Fromm, K. (2010). Silver coordination polymers for prevention of implant infection: thiol interaction, impact on respiratory chain enzymes, and hydroxyl radical induction. *Antimicrobial Agents and Chemotherapy*. 54:4208–4218.

Gould, I. Bal A. (2013). New antibiotic agents in the pipeline and how they can overcome microbial resistance. *Virulence*. 4(2):185–191.

Greenwood, D. Irving, W. (2012). Antimicrbial agents. *Medical Microbiology*. 8:54-68

Grenier, F. Matteau, D. Baby, V. Rodrigue, S. (2014). Complete Genome Sequence of *Escherichia coli* BW25113. *Genome Announcements*. *2*(5):e01038–14.

Groh, K. Dalkvist, T. Piccapietra, F. Behra, R. Sulter, M. Schirmer, K.(2015). Critical influence of chloride ions on silver ion-mediated acute toxicity of silver nanoparticles to zebrafish embryos. *Nanotoxicology*. 9(1):81-91.

Guardabassi, L. Courvalin, P. (2006). Modes of Antimicrobial Action and Mechanisms of Bacterial Resistance, p 1-18. In Aarestrup F (ed), Antimicrobial Resistance in Bacteria of Animal Origin. ASM Press, Washington, DC.

Gugala, N. Lemire, J. Turner, R. (2017). The efficacy of different anti-microbial metals at preventing the formation of, and eradicating bacterial biofilms of pathogenic indicator strains. *The Journal of Antibiotics* (*Tokyo*). 70(6):775-780.

Gupta, S. Nayak, R. (2014). Dry antibiotic pipeline: Regulatory bottlenecks and regulatory reforms. *Journal of Pharmacology & Pharmacotherapeutics*. *5*(1): 4–7.

Gutsafson, R. Bpowen, R. (1997). Antibiotic use in animal agriculture. *Journal of Appplied microbiology*. 83:531-541.

Harrison, R. (1964). Animal Machines: the new factory farming industry. London, Vincent Stuart.

Harrison, J. Ceri, H. Yerly, J. Stremick, C. Hu, Y. Martinuzzi, R. Turner, R. (2006). The use of microscopy and three-dimensional visualization to evaluate the structure of microbial biofilms cultivated in the Calgary Biofilm Device. *Biological Procedures Online*. *8*:194–215.

Harrison, J. Ceri, H. Stremick, C. Turner, R. (2004). Biofilm susceptibility to metal toxicity. *Applied and Environmental Microbiology*. 6:1220–1227.

Harrison, J. Rabiei, M. Turner, R. Badry, E. Sproule, K. Ceri, H. (2006). Metal resistance in *Candida* biofilms. *FEMS Microbiology Ecology*. 55: 479–491.

Harrison, J. Turner, R. Joo, D. Stan, M. Chan, C. Allan, N. Vrionis, H. Olson, M. Ceri, H. (2008). Copper and quaternary ammonium cations exert synergistic bactericidal and anti-biofilm activity against Pseudomonas aeruginosa. *Antimicrobial Agents and Chemotherapy*. 52: 2870–2881.

Harrison, J. Trearoli, V. Chan, C. Vacchi-Suzzi, C. Heyne, B. Parsek, M. Ceri, H. Turner, R. (2009). Chromosomal antioxidant genes have metal ion-specific roles as determinants of bacterial metal tolerance. *Applied and Environmental Microbiology*. 11:2491–2509.

Harrison, J. Ceri, H. Stremick, C. Turner, R. (2010). Microtiter susceptibility testing of microbes growing on peg lids: a miniaturized biofilm model for high-throughput screening. *Nature Protocols*. 5:1236-1254.

Hartmann, M Berditch, M. Hawecker, J. Ardakani, M Gerthsen. D. Ulrich, A. (2010). Damage of the Bacterial Cell Envelope by Antimicrobial Peptides Gramicidin S and PGLa as Revealed by Transmission and Scanning Electron Microscopy. *Antimicrobial Agents and Chemotherapy*. 54 (8): 3132-3142.

Hayashi, K. Morooka, N. Yamamoto, Y. Fujita, K. Isono, K. Choi, S. Horiuchi, T. (2006). Highly accurate genome sequences of *Escherichia coli* K-12 strains MG1655 and W3110. *Molecular Systems Biology*. *2*: 2006.0007.

Hazan, R. Que, Y. Maura, D. Rahme, L. (2012). A method for high throughput determination of viable bacteria cell counts in 96-well plates. *BMC Microbiology*. 12: 259.

Hazelton, P. Gelderblom, H. (2003). Electron microscopy for rapid diagnosis of infectious agents in emergent situations. *Emerging Infectious Diseases*. 9(3):294-303.

Henk, M. (2004). Method for Collecting Air-Water Interface Microbes Suitable for Subsequent Microscopy and Molecular Analysis in both Research and Teaching Laboratories. *Appl. Applied and Environmental Microbiology*. 70(4):2486-2493.

Hobman, J. Crossman, L. (2014). Bacterial antimicrobial metal ion resistance. *Journal of Medical Microbiology*. 64:471-497.

Hooper, D. (1999). Mechanisms of fluoroquinolone resistance. *Drug Resistance Updates.*2:38–55.

Horinouchi, T. Suzuki, S. Hirasawa, T. Ono, N. Yomo, T. Shimizu, H. Furusawa, C. (2015). Phenotypic convergence in bacterial adaptive evolution to ethanol stress. *BMC Evolutionary Biology*.15180.

Hsu, Y. VanNieuwenhze, M. (2016). Methods for visualization of peptidoglycan biosynthesis. *Methods in Microbiology*. 43:3-48.

Hwang, S. Gumbart, J. (2017). Engineering the Cell Envelope of Gram-Negative Bacteria. *Biophysical Journal*. 112(3):P309a.

Jensen, H. Eng, T. Chubukov, V. Herbert, R. Mukhopadhyay, A. (2017). Improving membrane protein expression and function using genomic edits. *Scientific Reports*.7:13030.

Jeppson, J. Laurell, C. Franzen, B. (1979). "Agarose gel electrophoresis". *Clinical Chemistry*. 25(4): 629–638. PMID 313856.

Jordan, S. Hutchings, M. Mascher, T. (2008), Cell envelope stress response in Gram-positive bacteria. *FEMS Microbiology Reviews*. 32: 107–146.

Jorgensen, J. Turnidge, J. (2015). Susceptibility Test Methods: Dilution and Disk Diffusion Methods*, p 1253-1273. In Jorgensen, James H. and Pfaller, Michael A. and Carroll, Karen

C. and Funke, Guido and Landry, Marie Louise and Richter, Sandra S. and Warnock, David W.(ed), Manual of Clinical Microbiology, Eleventh Edition.

Jung, W. Koo, H. Kim, K. Shin. S. Kim, S. Park, Y. (2008). Antibacterial Activity and Mechanism of Action of the Silver Ion in Staphylococcus aureus and *Escherichia coli*. *Applied and Environmental Microbiology*. 74(7):2171-2178.

Kalan, L. Pepin, D. Ul-Haq, I. Miller, S. Hay, M. Precht, R. (2016). Targeting biofilms of multidrug-resistant bacteria with silver oxynitrate. *International Journal of Antimicrobial Agents*.49(6):719-726.

Kant, K. (1963). Effect of the rate of diffusion of ions on the periodic precipitation of silver chromate. *Colloid and Polymer Science*. 190(1):43-44.

Kamio, Y. Nikaido, H. (1976). Outer membrane of Salmonella typhimurium: accessibility of phospholipid head groups to phospholipase c and cyanogen bromide activated dextran in the external medium. *Biochemistry*. 15(12):2561-70.

Kaneko, Y. Theondel, M. Olakanmi, O. Britigan, B. Singh, P. (2007). The transition metal gallium disrupts Pseudomonas aeruginosa iron metabolism and has antimicrobial and antibiofilm activity. *Journal of Clinical Investigation*. 117:877–888.

Kelley, L. Mezulis, S. Yates, C. Wass, M. Sternberg, M. (2015). The Phyre2 web portal for protein modeling, prediction and analysis. *Nature protocals*.10:845-858.

Kelly, R. Kydd, C. (1982). Silver resistance in microorganisms. Developments in Industrial Microbiology. 23:567–578.

Klasen, H. (2000). Historical review of the use of silver in the treatment of burns. I. Early uses. *Burns*. 26:117-130.

Klueh, U. Wagner, V. Kelly, S. Johnson, A. Bryers, J. (2000). Efficacy of silver-coated fabric to prevent bacterial colonization and subsequent device-based biofilm formation. *Journal of Biomedical Materials Research*.53(6):621-31.

Kollef, M. H. Afessa, B. Anzueto, A. Veremakis, C. Kerr, K. Margolis, B. Craven, D. Roberts, P. Arroliga, A. Hubmayr, R. Restrepo, M. Auger, W. Schinner, R. (2008). Silver-coated endotracheal tubes and incidence of ventilator-associated pneumonia: the NASCENT randomized trial. *JAMA*. 300:805–813.

Kumar, R. Nongkhlaw, M. Acharya, C. Joshi, S. (2013). Growth media composition and heavy metal tolerance behavior of bacteria characterized from the sub-surface oil of uranium rich ore bearing site of Domiasiat in Meghalaya. *Indian Journal of Biotechnology*.12:115-119.

Lazdunski, C. Bouveret, E. Rigal, A. Journet, L. Lloubès, R. Bènèdetti, H. (1998) Colicin import into *Escherichia coli* cells. *Journal of Bacteriology*. 180:4993-5002.

Lazzaroni, J. Germon, P. Ray, M. Vianney, A. (1999). The Tol proteins of *Escherichia coli* and their involvement in the uptake of biomolecules and outer membrane stability. *FEMS Microbiology*.177:191-197.

Lederberg, J. Shope, R. Oaks SC Jr, eds. Microbial threats to health in the United States. Washington, DC: National Academy Press, 1992.

Lemire, J. Kalan, L. Gugala, N. Bradu, A. Turner, R. (2017). Silver oxynitrate- an efficacious compound for the prevention and eradication of dual species biofilms. *Biofouling*. 33(6):460-469.

Lemire, J. Kalan, L. Bradu, A. Turner, T. (2015). Silver oxynitrate: An Unexplored Silver Compound with Antimicrobial and Antibiofilm Activity. *Antimicrobial Agents and Chemotherapy*. 59(7):4031-4039.

Leung, B. Jalilehvand, F. Mah, V. Parvez, M. Wu, Q. (2013). Silver(I) Complex formation with Cysteine, Penicillamine and Glutathione. *Inorganic Chemistry*. 52(8):4593-4602

Li, W. Xie, X. Shi, Q. Zeng, H. Yang, Y. Chen, Y. (2009). Antibacterial activity and mechanism of silver nanoparticles on *Escherichia coli*. *Applied Microbiology and Biotechnology*. 85:1115-1122.

Liu, P. Müller, M. Derendorf, H. (2002). Rational dosing of antibiotics: the use of plasma concentrations versus tissue concentrations. *International Journal of Antimicrobial Agents*. 19(4): 285-290.

Loiseau, L. Gerez, C. Bekker, M. Ollagnier-de Choudens, S. Py, B. Sanakis, Y. Teixeira de Mattos, J. Fontecave, M. Barras, F. (2007). ErpA, an iron–sulfur (Fe–S) protein of the A-type essential for respiratory metabolism in *Escherichia coli*. *Proceedings of the National Academy of Sciences of the United States of America*.104 (34):13626-13631

Lok, C. Ho, C. Chen, R. He, Q. Yu, W. Sun, H. Tam, P. Chiu, J. Che, C. (2006). Proteomic analysis of the mode of antibacterial action of silver nanoparticles. *Journal of Proteome Research.* 5: 916–924.

Lorenz, T. (2012). Polymerase Chain Reaction: Basic Protocol Plus Troubleshooting and Optimization Strategies. *Journal of Visualized Experiments: JoVE*, (63):3998. Advance online publication.

O'Toole, G. (2011). Microtiter Dish Biofilm Formation Assay. *Journal of Visualized Experiments*: *JoVE*. (47):2437. Advance online publication.

Macomber, L. Elsey, S. Hausinger, R. (2011) Fructose-1,6-bisphosphate aldolase (class II) is the primary site of nickel toxicity in *Escherichia coli*. *Molecular Microbiology*. 82:1291–1300

Macomber, L. Imlay, J. (2009). The iron-sulfur clusters of dehydratases are primary intracellular targets of copper toxicity. *Proceedings of the National Academy of Sciences of the United States of America*.106:8344–8349.

Macnab, R. (2003). "How bacteria assemble flagella". *Annual Review of Microbiology*. 57: 77–100.

Makarov, V. Love, A. Sinitsyna, O. Makarova, S. Yaminsky, I. Taliansky, M. Kalinina, N. (2014). "Green" Nanotechnologies: Synthesis of Metal Nanoparticles Using Plants. *Acta Naturae*. 6(1):35-44.

Martinez, J. Baquero, F.(2000). Mutation Frequencies and Antibiotic Resistance. *Antimicrobial Agents and Chemotherapy*. 44(7):1771-1777.

McCaustland, K. (2005). Real-Time PCR: An Essential Guide. *Emerging Infectious Diseases*.11(1): 185–186.

McDonnell, G. Russell, A. (1999). Antiseptics and disinfectants: activity, action, and resistance. *Clinical Microbiology Reviews*. 12:147-179.

McShan, D. Ray, P. Yu, H. (2014). Molecular Toxicity mechanism of silver. *Journal of Food and Drug analysis*. 22(1):116-127.

Middaugh, J. Hamel, R. Jean-Baptiste, G. Beriault, R. Chenier, D. Appanna, V. (2005). Aluminum triggers decreased aconitase activity via Fe-S cluster disruption and the overexpression of isocitrate dehydrogenase and isocitrate lyase: a metabolic network mediating cellular survival. *Journal of Biological Chemistry*. 280:3159–3165

Mitchell, A. Wang, W. Silhavy, T. (2017). Novel RpoS-Dependent Mechanisms Strengthen the Envelope Permeability Barrier during Stationary Phase. *Journal of Bacteriology*.199(2): e00708-16

Misra, R. Reeves, P. (1987). Role of micF in the tolC-mediated regulation of OmpF, a major outer membrane protein of Escherichia coli K-12. *Journal of Bacteriology*. 169(10):4722-4730

Morgenstein, R. Bratton, B. Nguyen, J. Ouzounov, N. Shaevitz, J. W. Gitai, Z. (2015). RodZ links MreB to cell wall synthesis to mediate MreB rotation and robust morphogenesis. *Proceedings of the National Academy of Sciences of the United States of America*. 112(40):12510–12515.

Mullineaux, C. Nenninger, A. Ray, N. Robinson, C. (2006). Diffusion of Green Fluorescent Protein in Three Cell Environments in *Escherichia Coli*. *Journal of Bacteriology*.188(10):3442–3448.

Munita, J. Arias, C. (2016). Mechanisms of Antibiotic Resistance. *Microbiology Spectrum*. 4(2): 10.1128/microbiolspec.VMBF–0016–2015.

Nakamura, S. Nakamura, M. Kojima, T. Yoshida, H. (1989). gyrA and gyrB mutations in quinolone-resistant strains of *Escherichia coli*. *Antimicrobial Agents and Chemotherapy*. 33:254–255.

Narayanan. K. Sakthivel, N. (2010). Biological synthesis of metal nanoparticles by microbes. *Advances in Colloid and Interface Science*. 156(1-2):1-13.

Navarro Llorens J, Tormo A, Martínez-GarcíA E. (2010). Stationary phase in gram-negative bacteria. *FEMS Microbiology Reviews*. 34:476–495.

Nelson M. Dinardo A. Hochberg J. Armelagos G. (2010). Brief communication: mass spectroscopic characterization of tetracycline in the skeletal remains of an ancient population from Sudanese Nubia 350–550 CE. *American Journal of Physical Anthropology*. 143:151–154.

Nies, D. (1999) Microbial heavy-metal resistance. *Applied Microbiology and Biotechnology*. 51: 730–750.

Ocampo, P. Lázár, V. Papp, B. Arnoldini, M. Abel zur Wiesch, P. Busa-Fekete, R. Bonhoeffer, S. (2014). Antagonism between Bacteriostatic and Bactericidal Antibiotics Is Prevalent. *Antimicrobial Agents and Chemotherapy*. *58*(8):4573–4582.

Okitsu, K. Mizukoshi, Y. Bandow, H. Maeda, Y. Yamamoto, T. Nagata, Y. (2002).Sonochemical synthesis of gold nanoparticle on chitosan. *Materials Letters*. 61:3429-3431.

Pal, S. Tak, Y. Song, J.(2007). Does the Antibacterial Activity of Silver Nanoparticles Depend on the Shape of the Nanoparticle? A Study of the Gram-Negative Bacterium *Escherichia coli*. *Applied and Environmental Microbiology*. 73(6):1712-1720.

Palmer, L. Skaar, E. (2016). Transition Metals and Virulence in Bacteria. *Annual Review of Genetics*. 50: 67–91.

Pankey, G.. Sabath, L. (2004). Clinical Relevance of Bacteriostatic versus Bactericidal Mechanisms of Action in the Treatment of Gram-Positive Bacterial Infections. *Clinical Infectious Diseases*. 38(6): 864–870.

Paradies, G. Paradies, V. Benedicitis, V. Ruggiero, F. Petrosillo, G.(2014). Functional role of cardiolipin in mitochondrial bioenergetics. *BBA-Bioenergetics*.1837(4):408-417.

Park, H. Kim, J. Kim, J. Lee, J. Hahn, J. Gu, M. Yoon, J. (2009). Silver-ion-mediated reactive oxygen species generation affecting bactericidal activity. *Water Research*. 43, 1027–1032.

Pawley, J. (1995). Handbook of Biological Confocal Microscopy. Boston, MA, Springer.

Pellieux, C. Dewilde, A. Pierlot, C. Aubry, J. (2000). Bactericidal and virucidal activities of singlet oxygen generated by thermolysis of naphthalene endoperoxides. *Methods in Enzymology*. 319:197–207.

Pereira, J. (1836). Materia medica, or pharmacology, and general therapeutics. *Lond. Med. Gaz.* 18: 305–314.

Pichoff, S. Lutkenhaus, J. (2001). *Escherichia coli* Division Inhibitor MinCD Blocks Septation by Preventing Z-Ring Formation. *Journal of Bacteriology*.183(22):6630–6635.

Piddock, L. (2012) The crisis of no new antibiotics—what is the way forward? *The Lancet Infectious Diseases*. 12(3):249–253.

Poehlsgaard,J. Douthwaite, S. (2005). The bacterial ribosome as a target for antibiotics. *Nature Reviews Microbiology*. 3(20): 870-881.

Porcheron, G. Garénaux, A. Proulx, J. Sabri, M. Dozois, C. M. (2013). Iron, copper, zinc, and manganese transport and regulation in pathogenic Enterobacteria: correlations between strains, site of infection and the relative importance of the different metal transport systems for virulence. *Frontiers in Cellular and Infection Microbiology*. 3:90.

Pray, L. (2008) DNA Replication and Causes of Mutation. *Nature Education*. 1(1):214.

Prathyumnan, S. Sellappa, S. Keyan, S. Joseph, S. (2011). Cloning of CRT cDNA from human blood and its over expression in MCF-7 cells. *International Journal of Current Pharmaceutical Review and Research*.1(3):120-124.

QingShan, W. Jian, J. JinHong, F. JiaCong, S. (2006). Norvancomycin-capped silver nanoparticles: Synthesis and antibacterial activities against *E. coli*. *Science in China Series B: Chemsitry*. 50(3):418-424.

Radzig, M. Koksharova. O. Khmel, I. (2009). Antibacterial effects of silver ions: Effect on gram-negative bacteria growth and biofilm formation. *Molecular genetics Microbiology and Virology*. 24(4):194-199.

Raetz, C. Whitfield, C. (2002). Lipopolysaccharide endotoxins. *Annual Review of Biochemistry*. 71:635-700.

Rai, M. DeshmukH, S. Ingle, A. Gade, A. (2102). Review Silver nanoparticles: the powerful nanoweapon against multidrug-resistant bacteria. *Journal of Applied Microbiology*.112(5):841-52.

Randall, C. Gupta, A. Jackson, N. Busse, D. O'Neill, A. (2015). Silver resistance in Gram-negative bacteria: a dissection of endogenous and exogenous mechanisms. *Journal of Antimicrobial Chemotherapy*. (70)4: 1037–1046.

Ratte, H. (1999). Bioaccumulation and toxicity of silver compounds: A review. *Environmental Toxicology and Chemistry*, 18: 89–108.

Reynolds. P, (1989). Structure, biochemistry and mechanism of action of glycopeptide antibiotics. *European Journal of Clinical Microbiology & Infectious Diseases*.8: 943-950

Richmond, P. (1954). American Attitudes Toward the Germ Theory of Disease (1860-1880). *Journal of the History of Medicine and Allied Sciences*. 9(4):428-454. Retrieved from http://www.jstor.org/stable/24619485

Rittié, L. Perbal, B. (2008). Enzymes used in molecular biology: a useful guide. *Journal of Cell Communication and Signaling*. 2(1-2):25–45.

Roberts. R, Hota. B, Ahmad. I, Scott, R. Foster, S. Abbasi, I. Schabowski, S. Kampe, L. Ciavarella, G. Supino,M Naples, J. Cordell, R. Levy, S. Weinstein, R.(2009). Hospital and societal costs of antimicrobial-resistant infections in a Chicago teaching hospital: implications for antibiotic stewardship. *Clinical Infectious Diseases*. 15;49(8):1175-84.

Rosche, W. Foster, P. (2000). Determining Mutation Rates in Bacterial Populations. *Methods (San Diego, Calif)*. 20(1):4–17.

Rolfe, M. Rice, C. Lucchini, S. Pin, C. Thompson, A. Cameron, A. Hinton, J. (2012). Lag Phase Is a Distinct Growth Phase That Prepares Bacteria for Exponential Growth and Involves Transient Metal Accumulation. *Journal of Bacteriology*.194(3): 686–701.

Saene, R. Fairclough, S. Petros, A.(1998). Broad- and narrow-spectrum antibiotics: a different approach. *Clinical Microbiology and Infection*. 4(1):56-57.

Saint, S. Elmore, J. Sullivan, S. Emerson, S. Koepsell, T. (1998). The efficacy of silver alloy-coated urinary catheters in preventing urinary tract infection: a meta-analysis. *The American Journal of Medicine*. 105: 236–241.

Schirmer, T. (1998). "General and specific porins from bacterial outer membranes". *Journal of Structural Biology*. 121 (2): 101–9.

Schlame, M. Rua, D. Greenber, M. (2000). The Biosynthesis and functional role of cardiolipin. *Progress in Lipid Research.* 39:257-288.

Scully, M. (2002). Dominion: the power of man, the suffering of animals, and the call to mercy. St. Martins Griffin, New York (Book).

Shanshoury. A. ElSilk, S. Ebeid, M. (2011). Extracellular Biosynthesis of Silver Nanoparticles Using *Escherichia coli* ATCC 8739, Bacillus subtilis ATCC 6633, and Streptococcus thermophilus ESh1 and Their Antimicrobial Activities. *ISRN Nanotechnology*. 2011: Article ID 385480, 7 pages.

Shoeib, T. Michael, K. Hopkinson, A. (2002). Silver Ion Binding Energies of Amino Acids: Use of the Theory to Assess the Validity of Experimental Silver Ion Basicities Obtained from the Kinetic Method. *Journal of Physical Chemistry A.* 106(25):6121-6128.

Silhavy, T. Kahne, D. Walker, S. (2010). The Bacterial Cell Envelope. *Cold Spring Harbor Perspectives in Biology*. 2(5):a000414.

Silver, S. Phung, L. (1996). Bacterial heavy metal resistance: new surprises. *Annual Review of Microbiology*

Slawson, R. Van Dyke, M. Lee, H. Trevors. J. (1992). Germanium and silver resistance, accumulation, and toxicity in microorganisms. *Plasmid*. 27:72-79.

Spellberg, B. Gilbert, D. (2014). The Future of Antibiotics and Resistance: A Tribute to a Career of Leadership by John Bartlett. *Clinical Infectious Diseases: An Official Publication of the Infectious Diseases Society of America*. *59*(Suppl 2), S71–S75.

Sperandio, V. Torres, A. Kaper, J. (2002). Quorum sensing *Escherichia coli* regulators B and C (QseBC): a novel two-component regulatory system involved in the regulation of flagella and motility by quorum sensing in *E. coli*. *Molecular Microbiology*. 43(3):809-21.

Stiefel, P. Schmidt-Emrich, S. Maniura-Weber, K. Ren, Q. (2015). Critical aspects of using bacterial cell viability assays with the fluorophores SYTO9 and propidium iodide. *BMC Microbiology*. 15:36.

Stocks, S. (2004). Mechanism and use of the commercially available viability stain, BacLight. *Cytometry A*.61(2):189-95.

Strominger, J. Tipper, D. (1965). Bacterial cell wall synthesis and structure in relation to the mechanism of action of penicillins and other antibacterial agents. *The American Journal of Medicine*. 39:708 -721.

Tan, S. Tatsumura, Y. (2015). Alexander Fleming (1881–1955): Discoverer of penicillin. *Singapore Medical Journal*.56(7):366–367.

Teitzel, G. Parsek, M. (2003). Heavy metal resistance of biofilm and planktonic *Pseudomonas aeruginosa*. *Applied and Environmental Microbiology*.69: 2313–2320.

Tenson, T. Lovmar, M. Ehrenberg M. (2003). The mechanism of action of macrolides, lincosamides and streptogramin B reveals the nascent peptide exit path in the ribosome. *Journal of Molecular Biology*. 330(5):1005-14.

The PLOS Medicine Editors. (2016). Antimicrobial Resistance: Is the World UNprepared? *PLoS Medicine*. *13*(9):e1002130.

Tomasz, A. (1979). The mechanism of the irreversible antimicrobial effects of penicillins: how the beta-lactam antibiotics kill and lyse bacteria. *Annual Review of Microbiology*. 33:113–137.

Thomas, C. Nielsen, K. (2005). Mechanisms of, and Barriers to, Horizontal Gene Transfer between Bacteria. *Nature Reviews Microbiology*. 3:711-721.

Turner, R. (2017). Metal-based antimicrobial strategies. *Microbial Biotechnology*. *10*(5):1062–1065.

Turner, R. Weiner, J. Taylor D. (1994). In vivo complementation and site-specific mutagenesis of the tellurite resistance determinant kilAtelAB from IncP alpha plasmid RK2Ter. *Microbiology*. 140 (Pt 6):1319-26.

Typas, A. Banzhaf, M. Gross, C. Vollmer, W. (2012). From the regulation of peptidoglycan synthesis to bacterial growth and morphology. *Nature Reviews Microbiology*. 10(2):123–136.

Van den Ent, F. Johnson, C. Persons, L. de Boer, P. Löwe, J. (2010). Bacterial actin MreB assembles in complex with cell shape protein RodZ. *The EMBO Journal*. 29(6):1081–1090.

Ventola, C. (2015). The Antibiotic Resistance Crisis: Part 1: Causes and Threats. *Pharmacy and Therapeutics*. 40(4):277–283.

Walker M, Parsons D. 2014. The biological fate of silver ions following the use of silver-containing wound care products- a review. *International Wound Journal.*11:496-504.

Waxman, D. Strominger, J. (1983). Pencillin-Binding Proteins and the Mecahnism of Action of β-lactams Antibiotics. *Annual Review of Biochemistry.*52:825-69.

WHO. (2014) WHO's first global report on antibiotic resistance reveals serious, worldwide threat to public health http://www.who.int/mediacentre/news/ releases/2014/amr-report/en/. Accessed [12/19/2017]

Weisblum, B. Davies. J. (1968). Antibiotic inhibitors of the bacterial ribosome. *Bacteriological Reviews.*32:493-528.

Wood, T. González Barrios, A. Herzberg, M. Lee, J. (2006). Motility influences biofilm architecture in *Escherichia coli*. *Applied Microbiology and Biotechnology.* 72(2):361-7.

Woodward, T. (1989). The golden era of microbiology: people and events of the 1880s. *Maryland Medical Journal.*38(4):323-8.

Xu, H. Qu, F. Xu, H. Lai, Wang, A. Aguilar, Z. Wei, H. (2009). Role of reactive oxygen species in the antibacterial mechanism of silver nanoparticles on *Escherichia coli* O157:H7. *BioMetals* 25(1):45–53.

Xu, F. Imlay, J. (2012). Silver(I), Mercury(II), Cadmium(II), and Zinc(II) Target Exposed Enzymic Iron-Sulfur Clusters when They Toxify *Escherichia coli*. *Applied and Environmental Microbiology*. 78(10), 3614–3621.

Yamanaka, M. Hara, K. Kudo, J. (2005). Bactericidal Actions of a Silver Ion Solution on *Escherichia coli*, Studied by Energy-Filtering Transmission Electron Microscopy and Proteomic Analysis. *Applied and Environmental* Microbiology. 71(11):7589-7593.

Zhou, M. Gomez-Sanchez, C. (2000). Universal TA cloning. *Current Issues in Molecular Biology*.2(1):1-7.

Zhu XD, Sadowski PD (1995). "Cleavage-dependent Ligation by the FLP Recombinase". Journal of Biological Chemistry. 270 (39): 23044–54.

Appendix A: Plasmid Based complementation

Includes intermediate steps necessary to carry out plasmid-based complementation of the gene *rodZ*.

A.1 Complementation: genomic DNA isolation, ligation to the InsTAclone cloning vector, and restriction enzyme digestion.

Following the successful generation of the chromosomal gene disruption mutant K-12 MG1655 Δ*rodZ*, plasmid-based complementation was conducted through the use of restriction enzymes and T4 ligase. The first step was to isolate and amplify the *rodZ* gene from *E. coli* k-12 MG1655 genomic DNA with designed PCR primers (Table 2.2). Utilizing gel electrophoresis, the amplified PCR product was identified through size comparison with a 1 Kb molecular DNA ladder. Successful amplification produced a band relative to the size of the *rodZ* gene (1014bp). Figure B-1, illustrates the 0.7% (w/v) agarose gel generated with the respective *rodZ* amplified PCR product in well 3. Well 2 acted as the negative control, containing only the PCR primers and no genomic DNA added to the PCR reaction. Well 3 contained digested pMS199EH$_A$, which was stored at -20 ^oC for later ligation. The *rodZ* PCR product was purified and ligated into the InsTAclone cloning vector, pTZ57R/T. This vector offered one-step cloning of *rodZ* PCR product by exploiting terminal transferase activity of *Taq* DNA polymerase (Zhou, 2000). *Taq* polymerase has non-template dependent activity, which preferentially adds a single adenosine to the 3'-ends of a double stranded DNA molecule, and thus most of the molecules PCR amplified by *Taq* polymerase possess single 3'-A overhangs (Zhou, 2000). The use of a linearized " pTZ57R/T -vector", which has single 3'-T overhangs on both ends allowed for direct, high-efficiency cloning of the *rodZ* PCR product, facilitated by complementarity between the PCR product 3'-A overhangs and vector 3'-T overhangs. The pTZ57R/T vector, also offered for easy quantitative analysis for recognizing successful ligation. Since successful ligation of desired gene fragment with pTZ57R/T lead to the disruption of lacZ gene activity resulting in lack of ability to cleave X-gal and when transformed into DH5α *E. coli* cells and grown on 1.25% (w/v) LB +/- Amp +/- X-gal at 37^oC, 20-50 single white colonies were produced, which were picked and qualitatively examined (Figure B-2) . Figure B-3, demonstrates the successful ligation of the purified *rodZ* PCR product to the pTZ57R/T-vector. The pTZ57R/T::*rodZ* was isolated from transformed DH5α *E. coli* cells and using a 1Kb molecular DNA ladder the PCR product band sizes were visualized. Analyzing the gel in Figure B-3, wells 3, 4, and 5 correspond to the successful ligation between insert (*rodZ*) and the TA vector, which resulted in a band shift relative to the negative control well 2, which only contained the circular pTZ57R/T vector from the Thermo Fischer Scientific kit and no insert. The successful ligation should result in a product

band around ~3,900bp (2,886bp TA vector +1,014bp *rodz* ORF). The PCR products in wells 3,4, and 5 were purified (section *2.1.7*) and subjected to digestion by restriction enzymes XbaI and HindIII . Figure B-4, demonstrates the successful digestion of the pTZ57R/T::*rodZ* resulting in two bands (Well 3) corresponding to the TA vector (2,886bp) and *rodz* (1,014bp) ORF. The negative controls in well 2 and 5 are the circularized TA vector and the undigested pTZ57R/T::*rodZ* respectively. The *rodz* (1014bp) ORF was purified and utilized for ligation into the Amp- resistant expression vector pMS119EH$_A$ generated by Beketskaia *et al*., (2014). The presence of *rodZ* was again confirmed by running the purified 2nd band from well 3 of Figure B-4 on a 0.7% (w/v) agarose gel to ensure *rodZ* ORF was successfully isolated (Figure B-5).

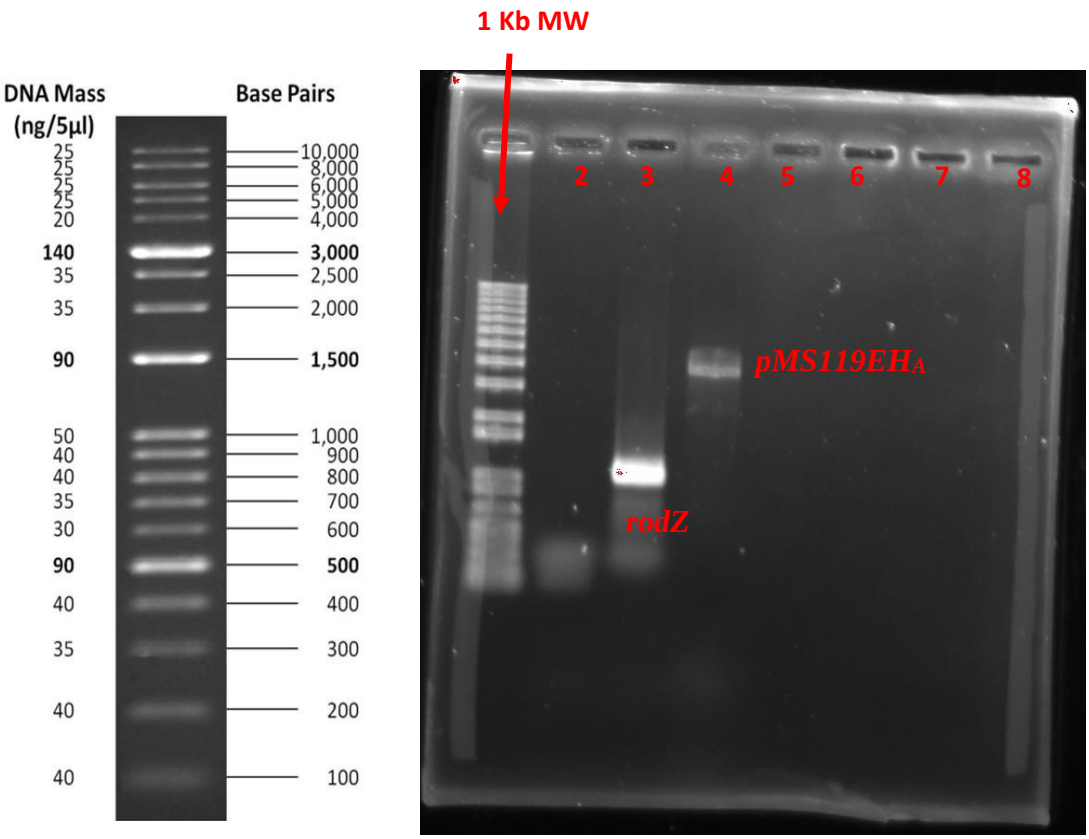

Figure A-1: A agarose gel illustrating the successful amplification of the *rodZ* gene through PCR from the genomic DNA of K-12 MG1655 *E. coli.* Well 2 contains the negative control where no genomic DNA was added to the PCR reaction, while well 3 contains the successful amplified product, which corresponds to the size of the *rodZ* gene (1,014bp). Well 4 contains digested (XbaI and HindIII) Amp- resistant expression vector pMS119EHA, which was utilized for plasmid-based complementation.

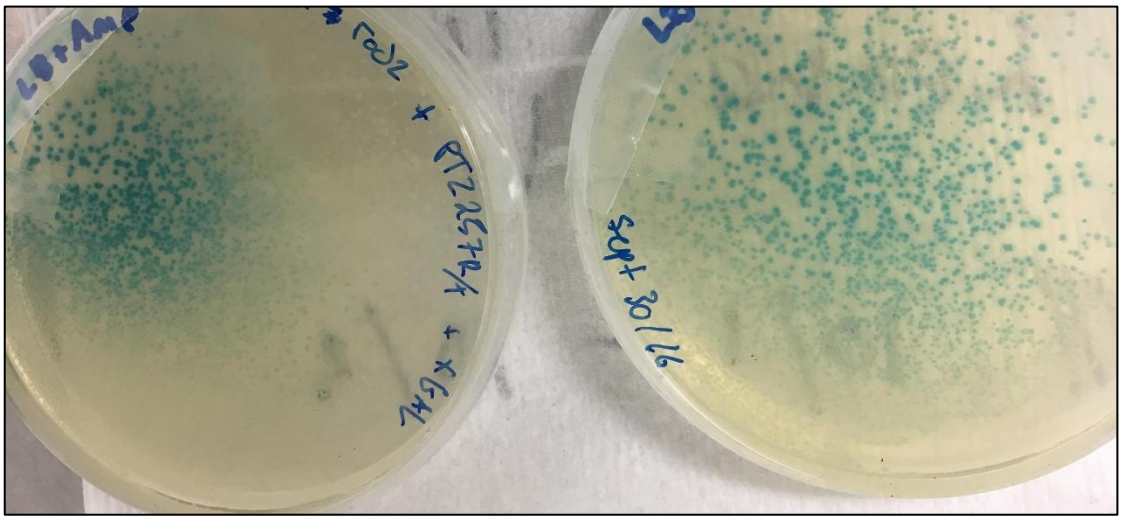

Figure A-2 Illustrates the 1.25% (w/v) LB +/-Amp +/- X-gal plates used for the identification of successful ligation of pTZ57R/T::*rodZ* plasmids, which was transformed into DH5α *E. coli* cells. Plates were grown overnight at 37ºC and plasmids were isolated using commercial kit (section *2.1.8*) These plasmids were then subjected to gel electrophoresis (section *2.1.*9) for qualitatively analysis (Figure B-3).

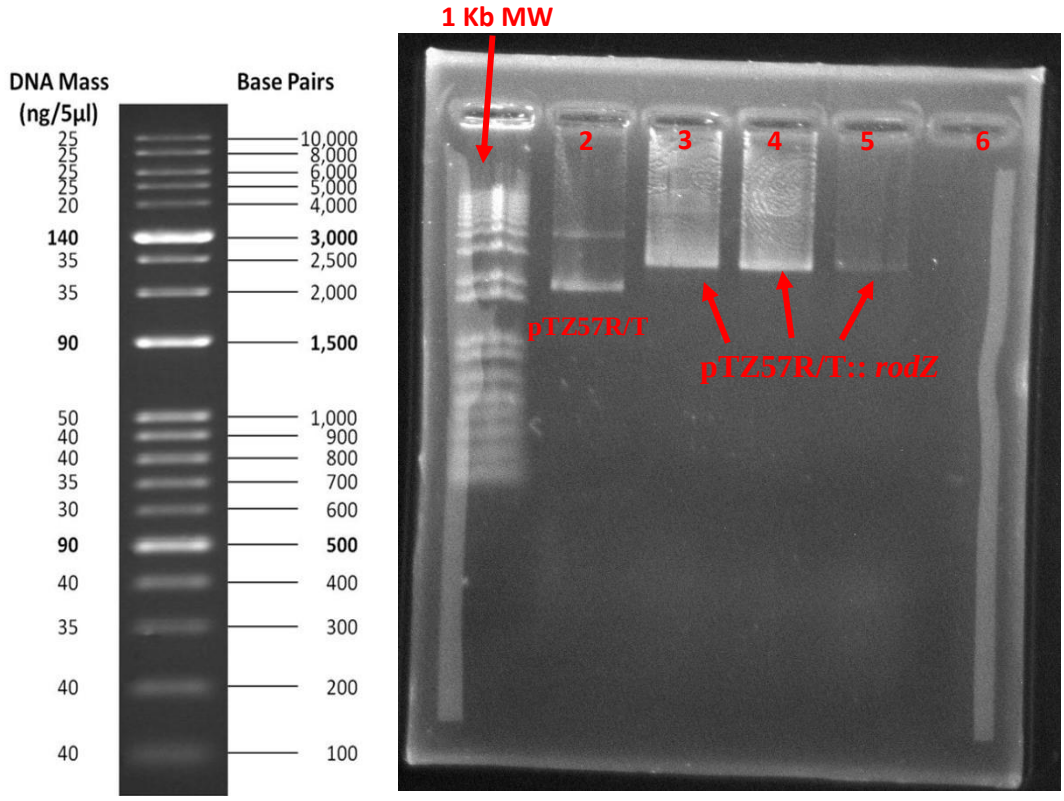

Figure A-3: A agarose gel demonstrating the successful ligation of the *rodZ* insert to the InsTAclone (Thermo Fischer Scientific) cloning vector pTZ57R/T. Well 2 consists of the negative control circularized pTZ57R/T and corresponds to a band size of 2887bp. Wells 3, 4, and 5 represent successful ligation for their corresponding product band is roughly band around ~3,900bp (2,886bp TA vector +1,014bp *rodz* ORF).

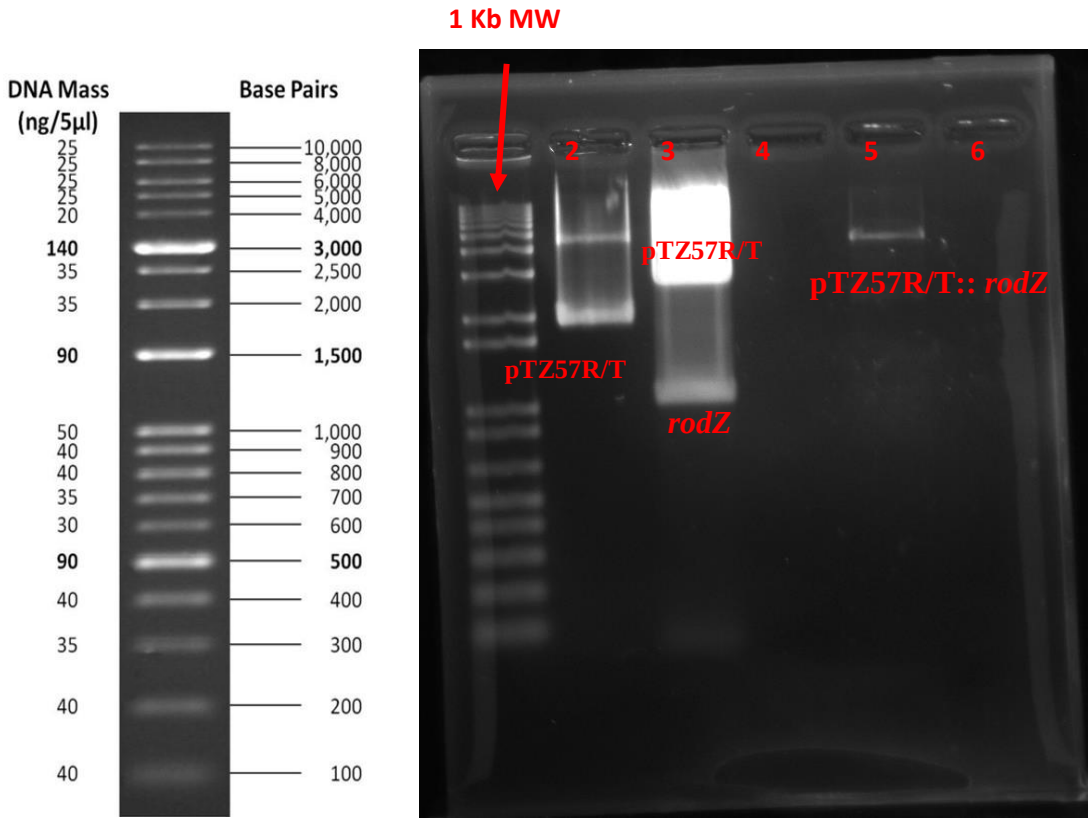

Figure A-4: Demonstrates the digestion of pTZ57R/T::*rodZ* by restriction enzymes XbaI and HindIII. Well three product bands highlight the TA (2,886bp) vector (top band) and the *rodz* (1,014bp) ORF (bottom band). Wells 2 and 5 consist of the negative controls used in the comparison of the digested pTZ57R/T::*rodZ* product.

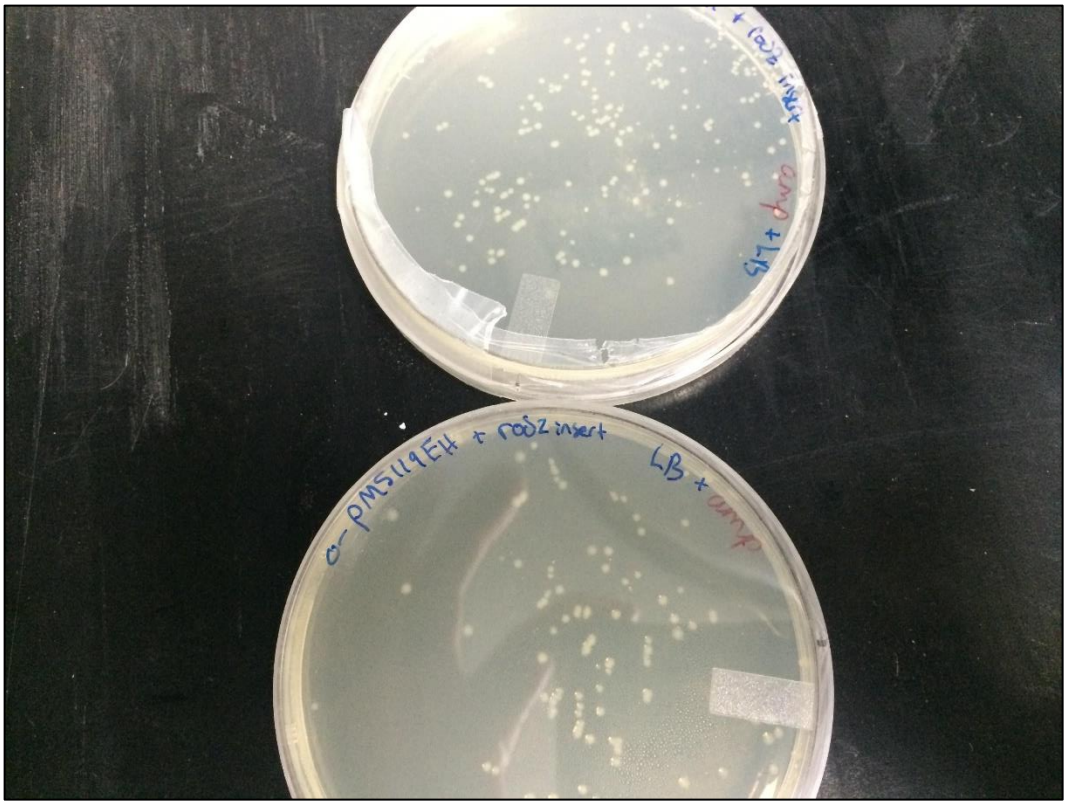

Figure A-5: The successful transformation of pMS119EH$_A$::*rodZ* into K-12 MG1655Δ*rodZ* *E. coli* cells. K-12 MG1655Δ*rodZ* cells are unable to grow in the presence of +100 μg/mL *Amp*, unless having acquired the Amp-resistant expression vector pMS119EH$_A$::*rodZ*. These cells were cultivated and utilized for cryogenic stock, which was stored at -80^{o}C.

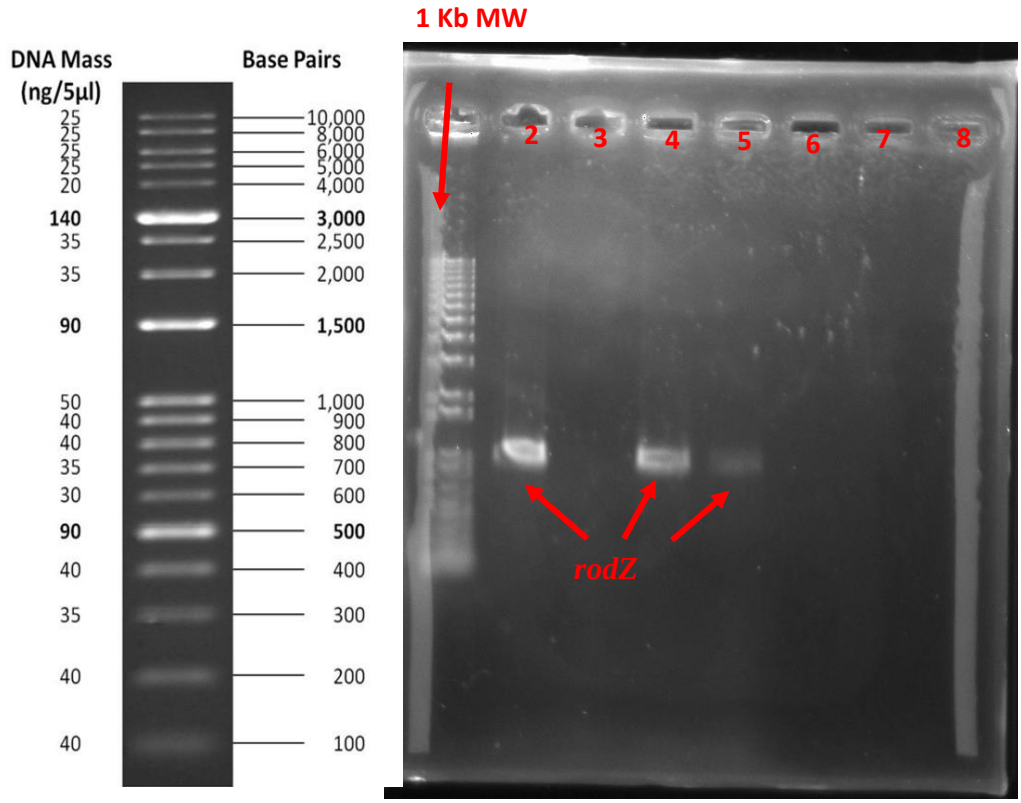

Figure A-6: A agarose gel containing the purified *rodZ* inserts (1014bp) extracted from the digestion reaction of pTZ57R/T::*rodZ* by restriction enzymes XbaI and HindIII. This gel confirmed that infact the lower band corresponded to the *rodZ* ORF and that ligation of the insert into the Amp- resistant expression vector pMS119EH$_A$ could continue.

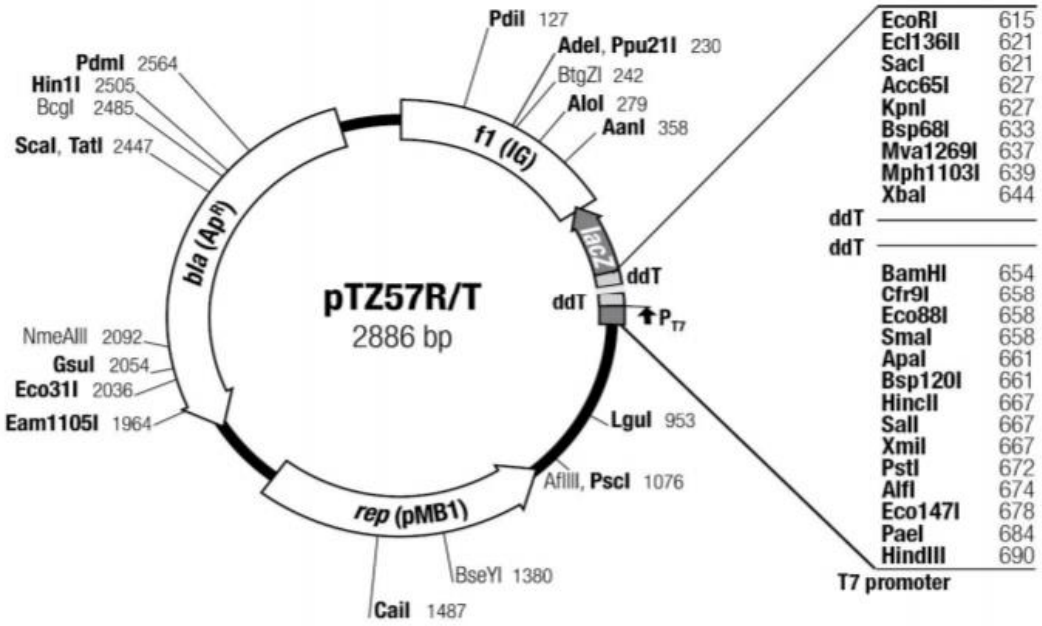

Figure A-7: Plasmid map of the InsTAclone cloning vector pTZ57R/T (from Thermo Fisher Scientific). The pTZ57R/T cloning vector is linearized and ddT tailed for direct use in cloning of PCR products (section *2.3.6*), generated with *Taq*, or other DNA polymerases or polymerase mixtures, which add extra adenines to the ends of PCR products. The map and the MCS region of the vector are presented in Figure 2.1 showing where XbaI and HindIII restriction enzyme sites are located. (Prathyumnan *et al*., 2011).

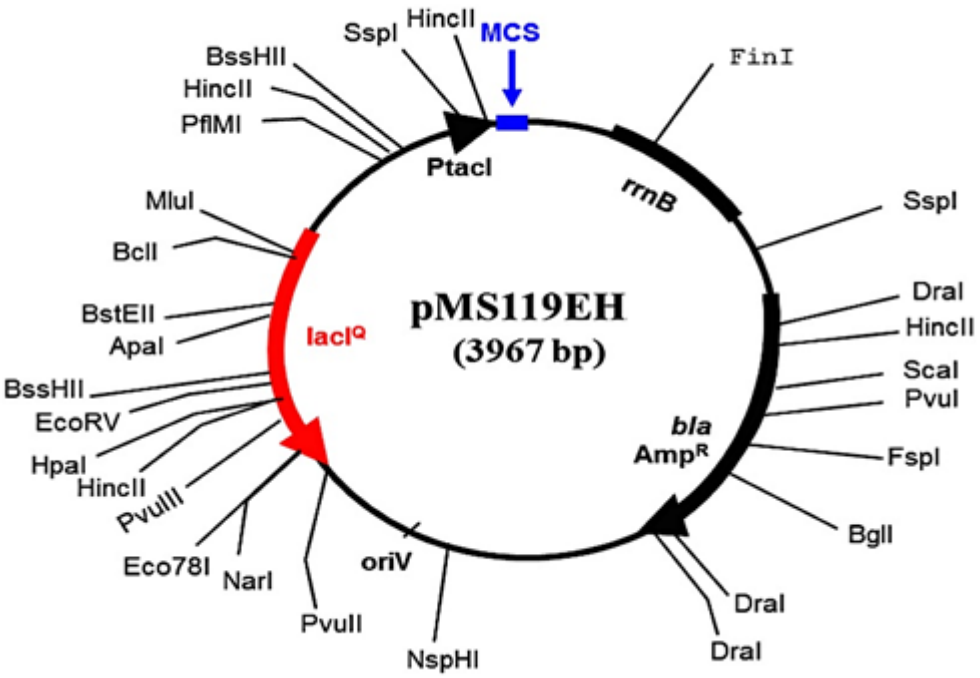

Figure A-8: Plasmid map of *Amp*-resistant expression vector pMS119EH$_A$ (Beketskaia *et al*., 2014) utilized for plasmid complementation analysis.

Appendix B: ΔOD_{600} vs Time

Includes the remaining four *E. coli* BW25113 cell envelope mutant's growth curve analysis.

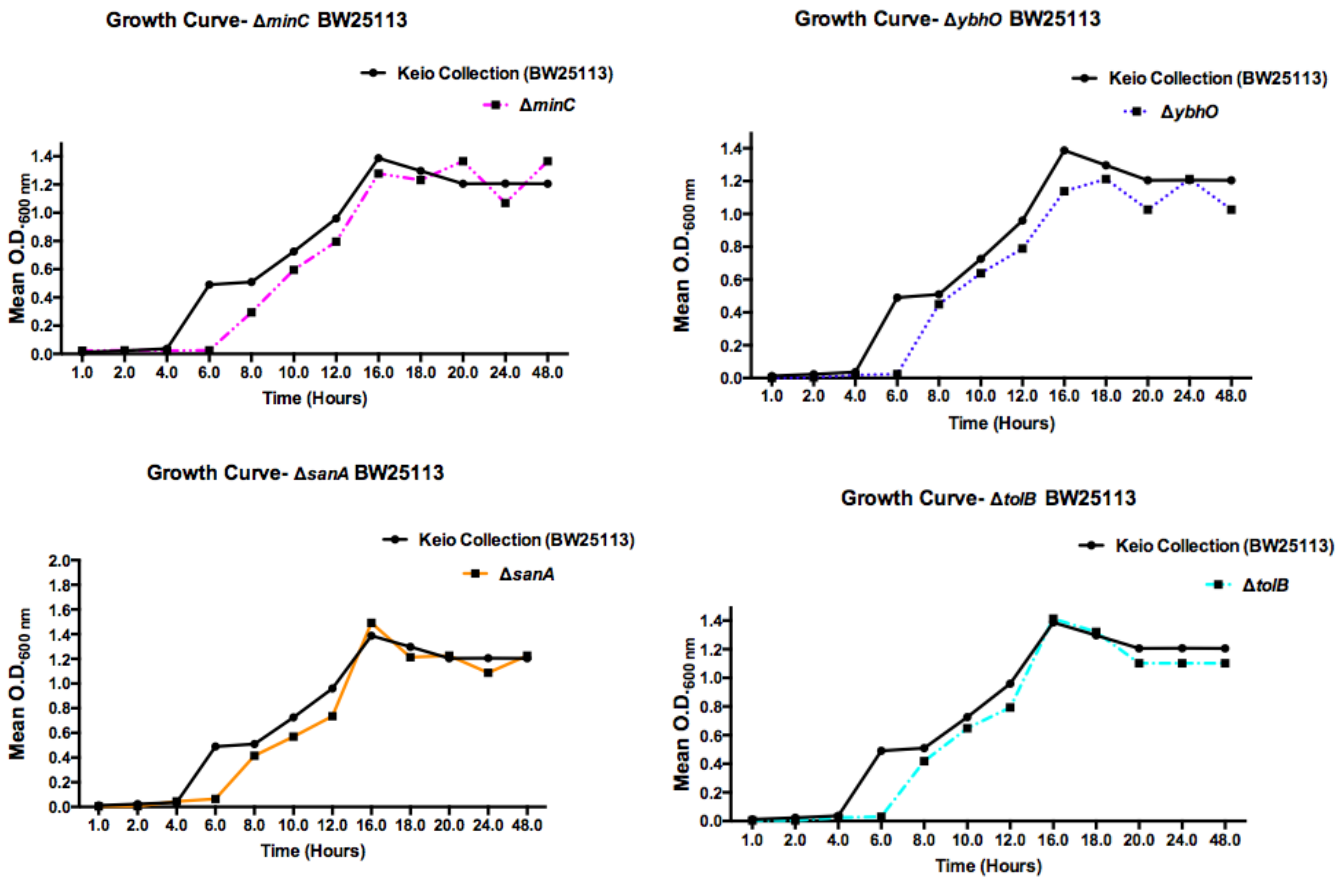

Figure B-1: Growth curve average of three biological each containing 3 technical trails, which measured OD_{600}nm readings of BW25113 Δ*minC*, Δ*sanA*, Δ*ybhO*, and Δ*tolB*.

Appendix C: Metal exposure response optical density values

Contains the remaining metal exposure-response data for the *E. coli* BW25113 mutants subjected to two-fold dilution challenge plates of three metal antimicrobials. the accumulation of cellular density was measured through optical density measurements and was proxy for observing sensitivity and resistance and change in cellular morphology.

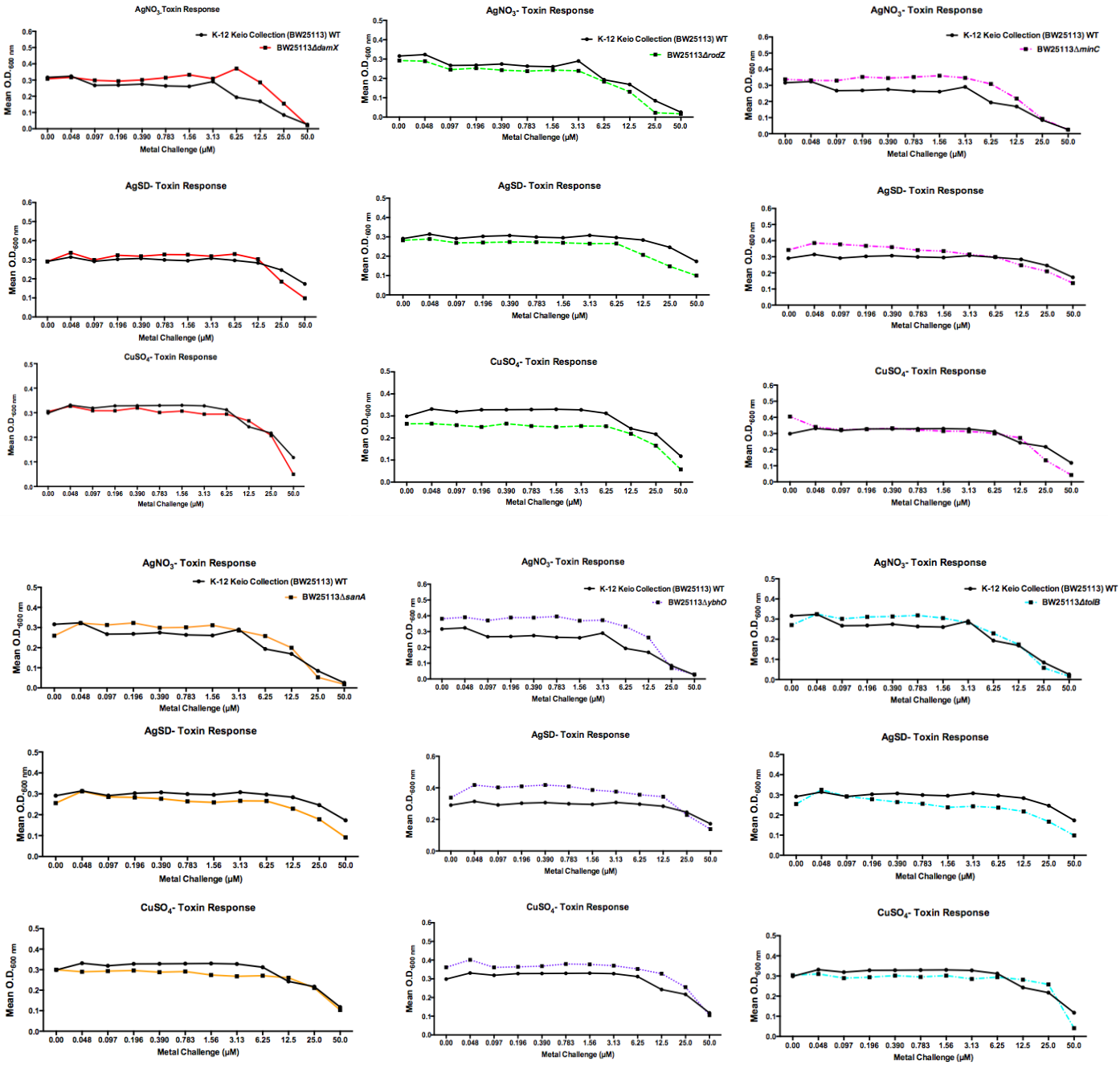

Figure C-1: Demonstrates the exposure-response relationship between K-12 BW25113 mutant's and K-12 BW25113 wild type planktonic cells, subjected to a 50 µM two- fold dilution antimicrobial gradient prepared on 96 well microtiter challenge plates (Figure 2.3) containing the three metal antimicrobials: $AgNO_3$, AgSD, and $CuSO_4$.

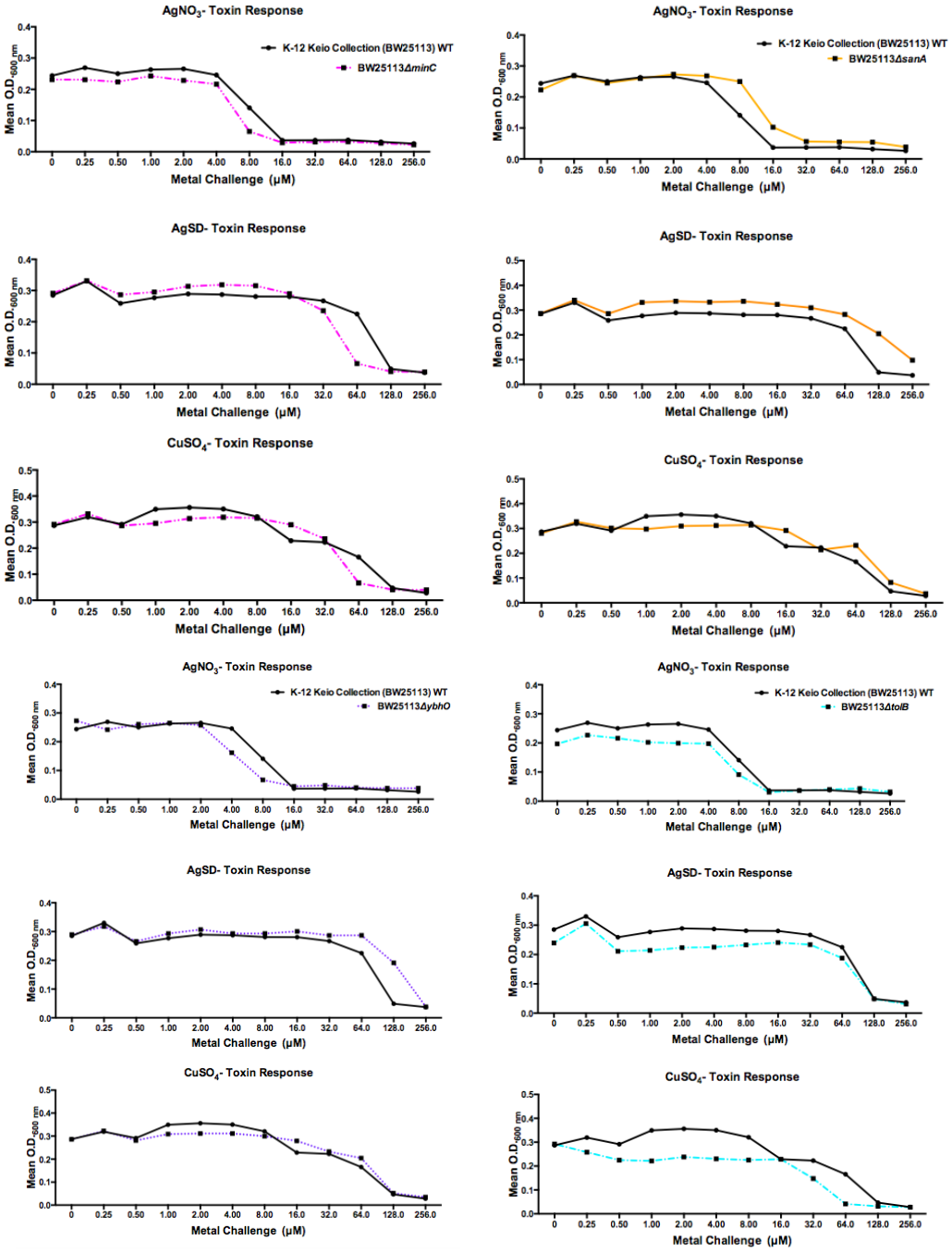

Figure C-2: Demonstrates the exposure-response relationship between K-12 BW25113 mutant's and K-12 BW25113 wild type planktonic cells, subjected to a 256 μM two- fold dilution antimicrobial gradient prepared on 96 well microtiter challenge plates (Figure 2.4) containing the three metal antimicrobials: $AgNO_3$, AgSD, and $CuSO_4$.

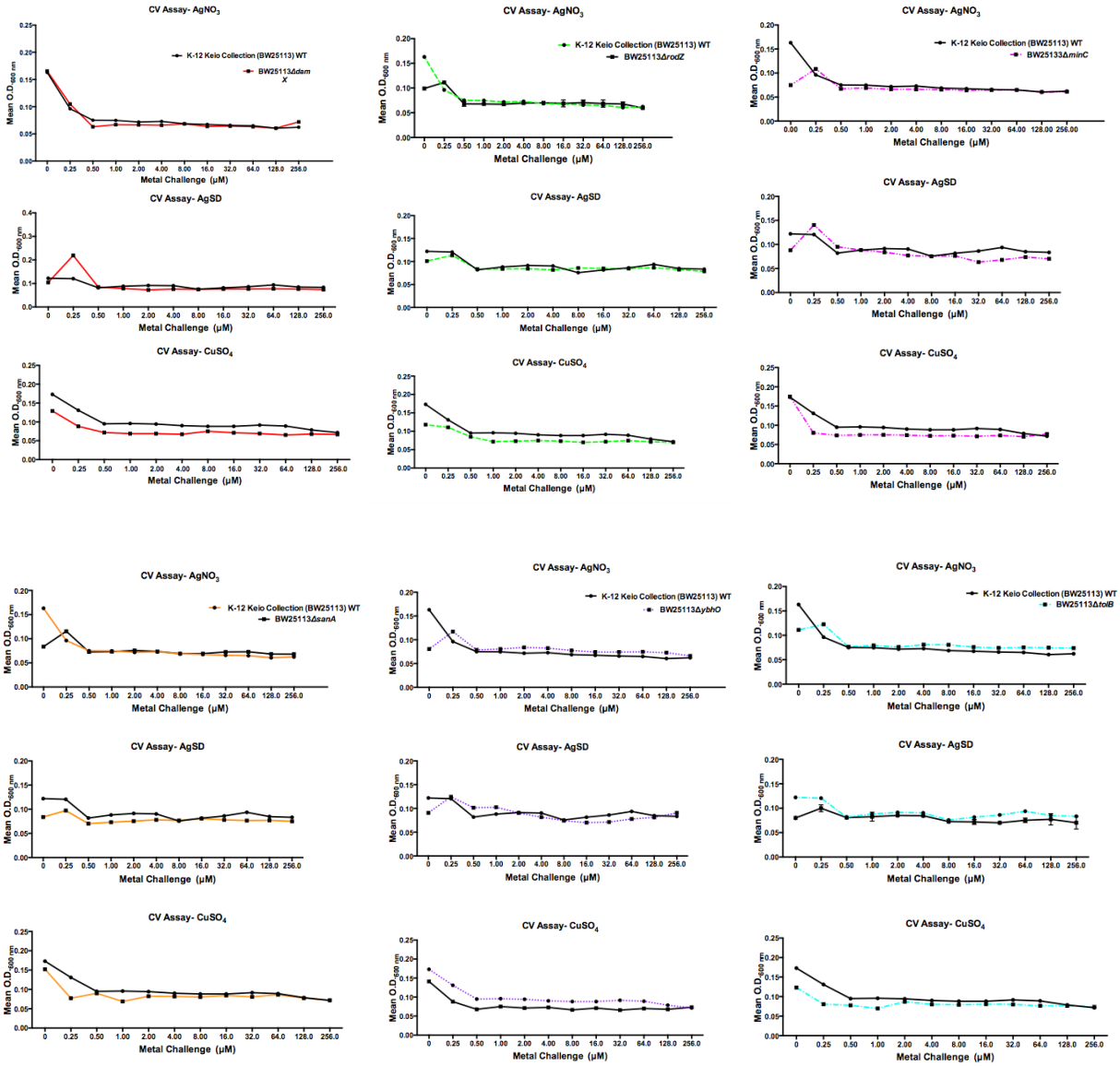

Figure C-3: Demonstrates the crystal violet assay of the BW25113 mutant's and wildtype biofilm cells grown for 24 hours in M9 media. The Δ*damX* cells were exposed to a 256 μM two-fold antimicrobial gradient (Figure 2.4) of the three antimicrobial metals.

Appendix D: Viable cell counts

Contains images of one biological trial of the viable cell counts for the *E. coli* BW25113 mutant's planktonic cells. Moreover, the log CFU/mL data representing planktonic cell viability in the presences of three metal antimicrobials is also present.

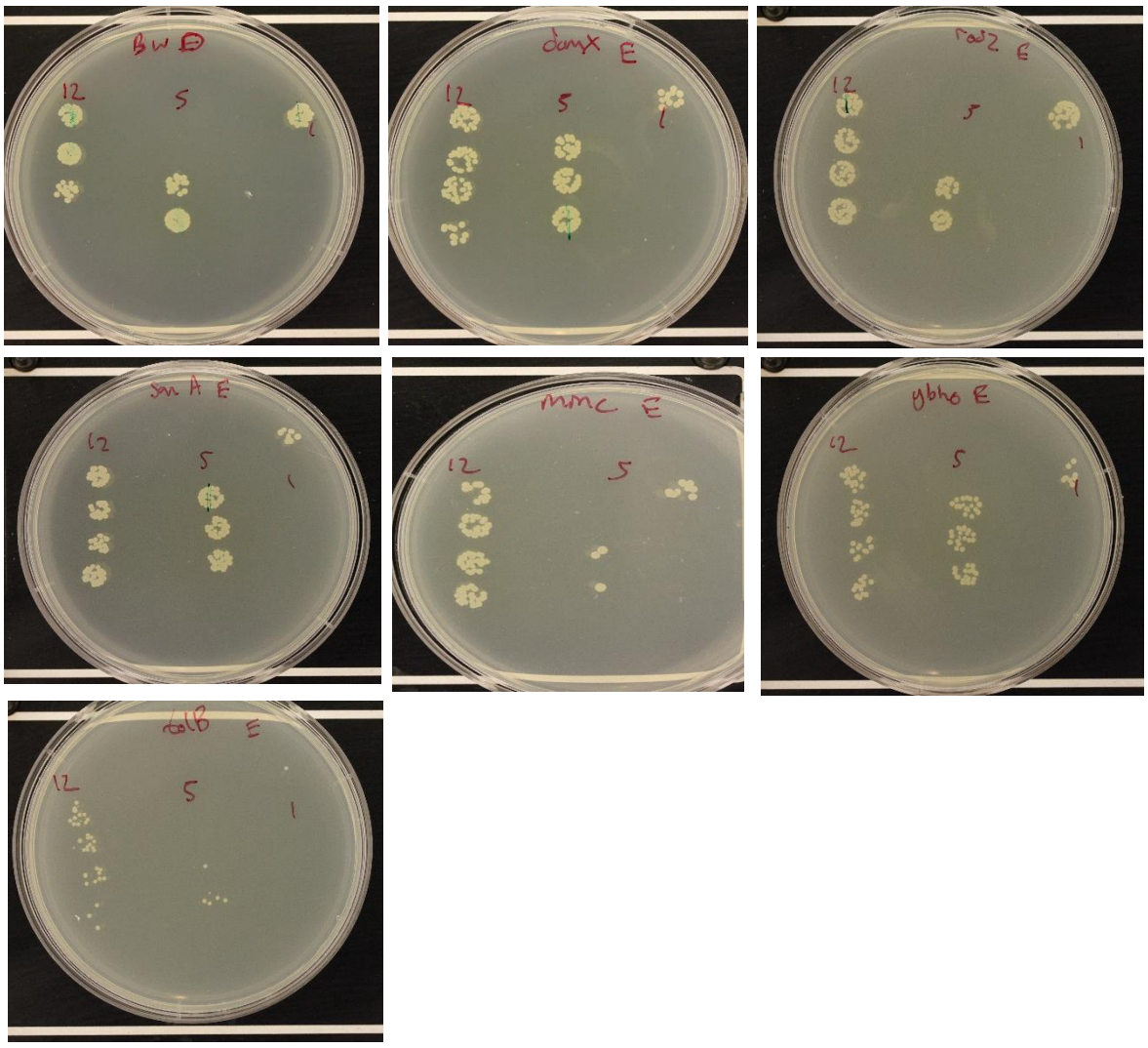

Figure D-1: One of three biological trails of viable cell counts for the 7 *E. coli* strains challenged by $AgNO_3$ that were spot plated (20 µL) onto 1.25% (w/v) LB agar.

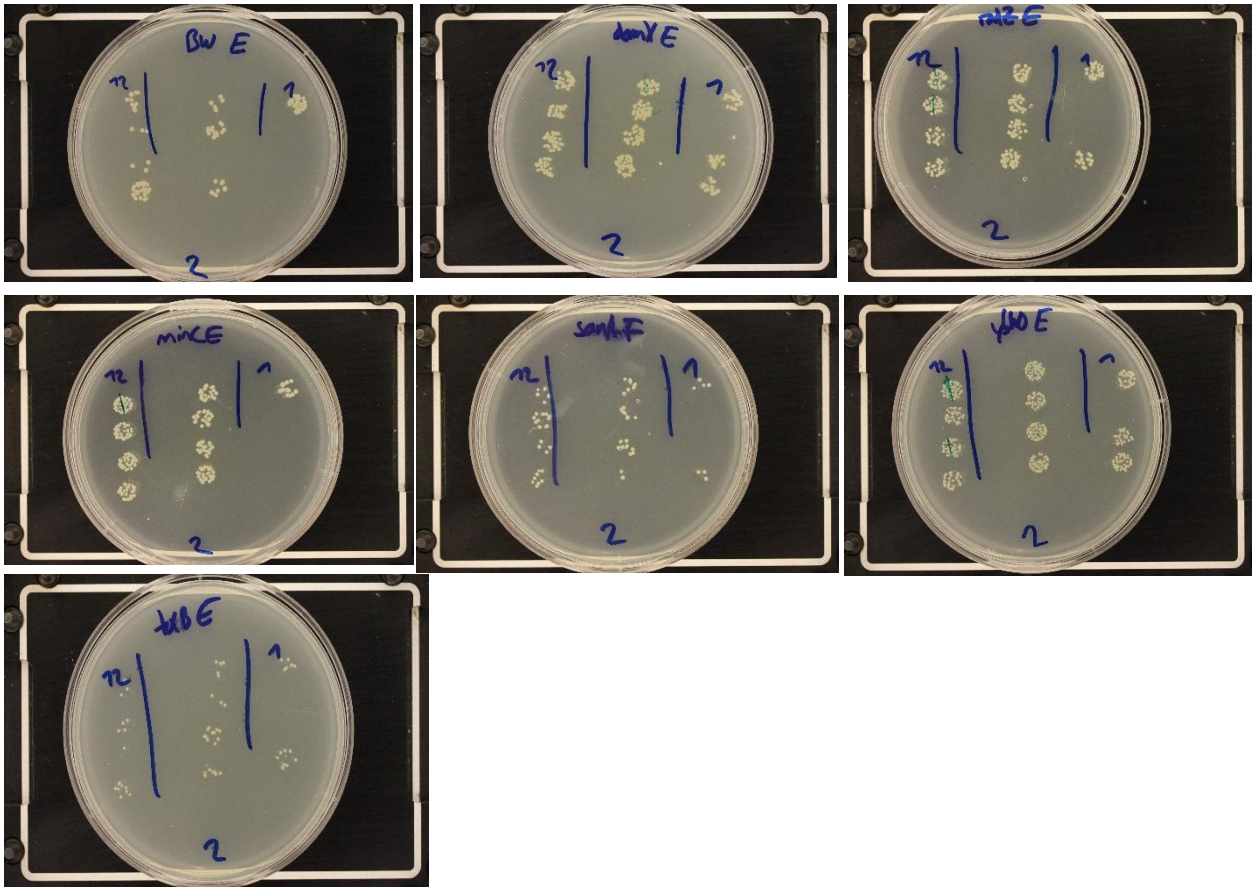

Figure D-2: One of three biological trails of viable cell counts for the 7 *E. coli* strains challenged by AgSD that were spot plated (20 µL) onto 1.25% (w/v) LB agar.

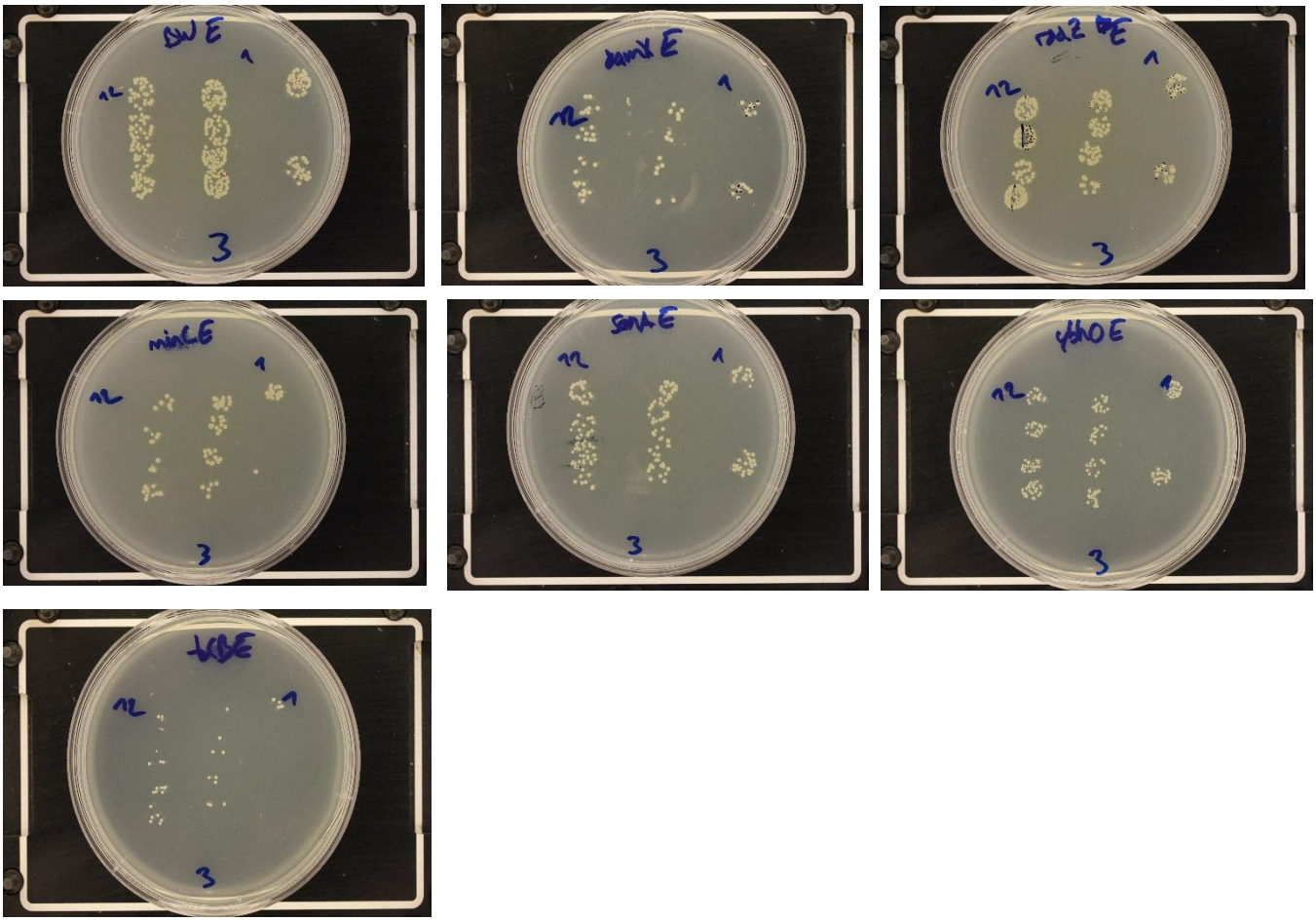

Figure D-3: One of three biological trails of viable cell counts for the 7 *E. coli* strains challenged by $CuSO_4$ that were spot plated (20 µL) onto 1.25% (w/v) LB agar.

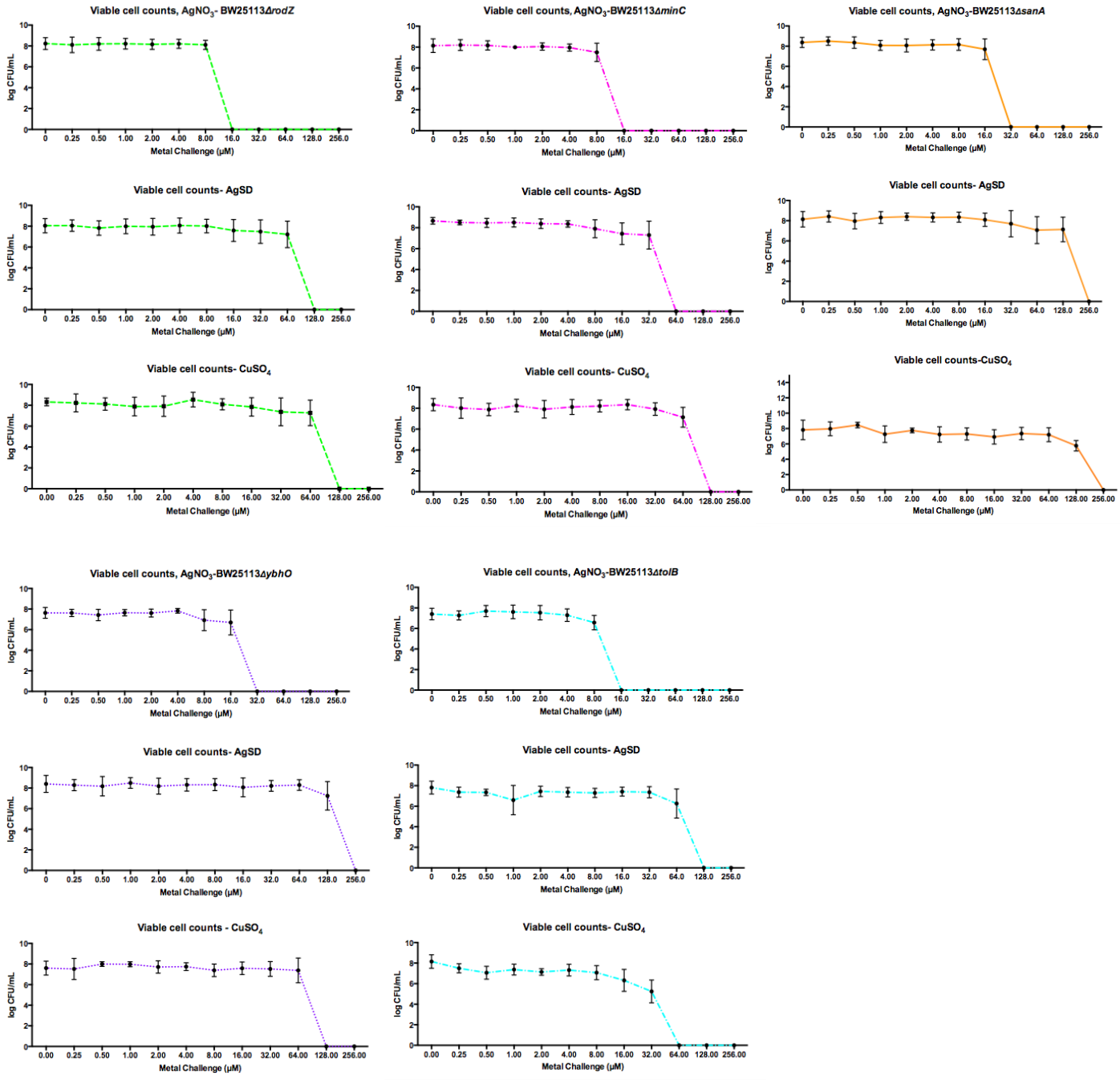

Figure E-4: log CFU/mL values generated for K-12 BW25113 mutant and wildtype *E. coli* cells exposed to three antimicrobial metals $AgNO_3$, AgSD, and $CuSO_4$. The Δ*rodZ* cells were exposed to a 256 μM two-fold antimicrobial gradient (Figure 2.4). These cultures were then diluted in dilution plates and 20 μL of culture was aliquoted onto 1.25% (w/v) LB agar plates (Figure 2.5). The CFU/mL was calculated by multiplying the number of viable bacteria colonies

by its respective dilution factor, divided by the total volume of the culture (180 µL). The CFU/mL was then expressed using logarithmic notation.

Appendix E: TEM Microscopy

Contains the comparison of TEM images of BW25113 wildtype and mutant's planktonic cells subjected to ±50 µM $AgNO_3$ challenge.

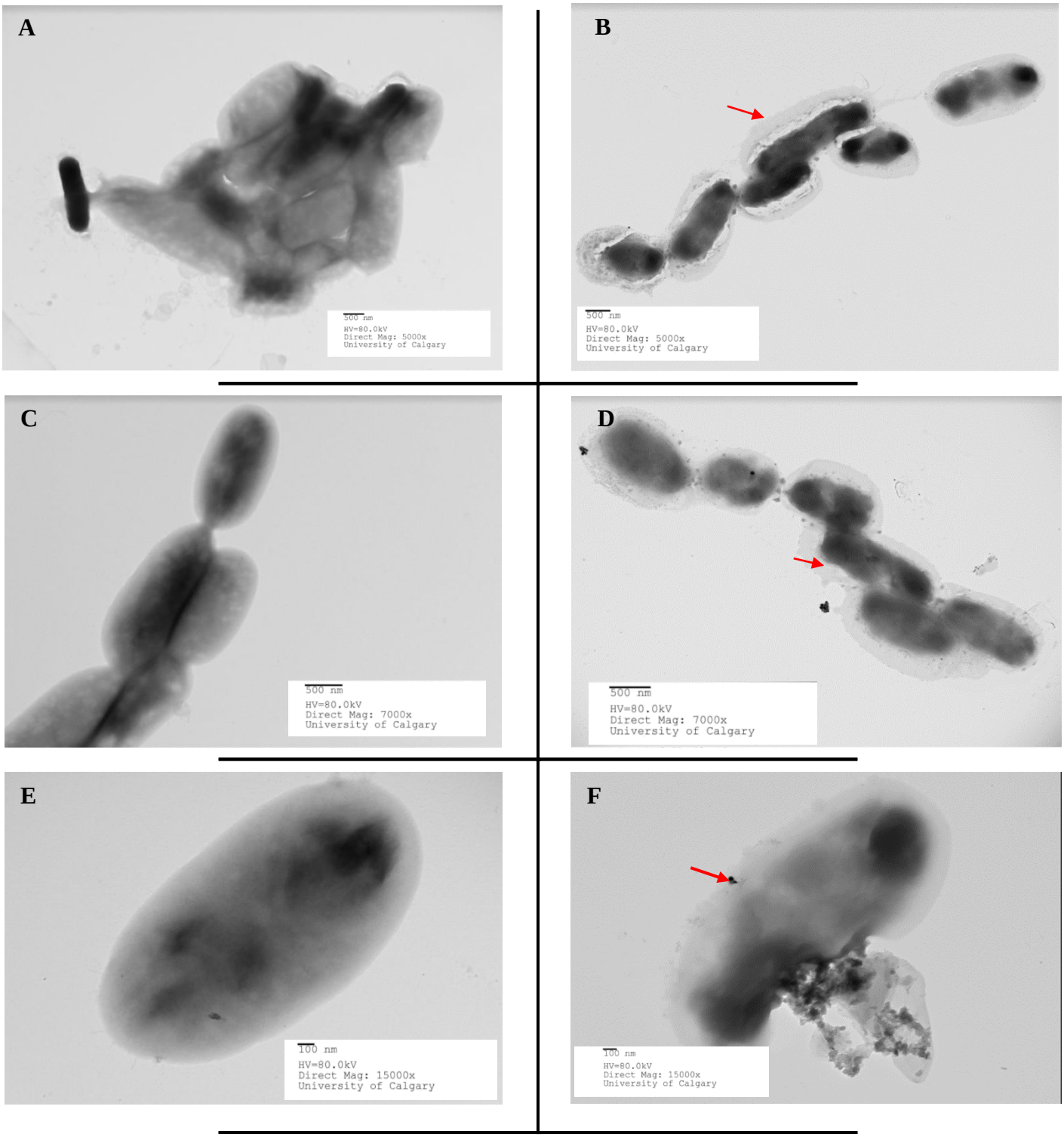

Figure E-1: External planktonic morphologies of 1.0% phosphotungstic acid stained wildtype BW25113 *E. coli* cells untreated (A, C, and E) and 50 µM $AgNO_3$ treated (B, D,

and F) observed by TEM. Images A and B, are imaged at 5000x mag, images C and D, were taken at 7000x mag, and images E and F, were taken at 15000x mag. Red arrows indicated electron-dense particles that were commonly found in treated TEM samples and areas of cell membrane separation. Some treated cells displayed either localized or complete separation of the cell membrane from the cell wall. plumes of cellular debris were also witnessed with accompanied electron-translucent cytoplasm and cellular disruption.

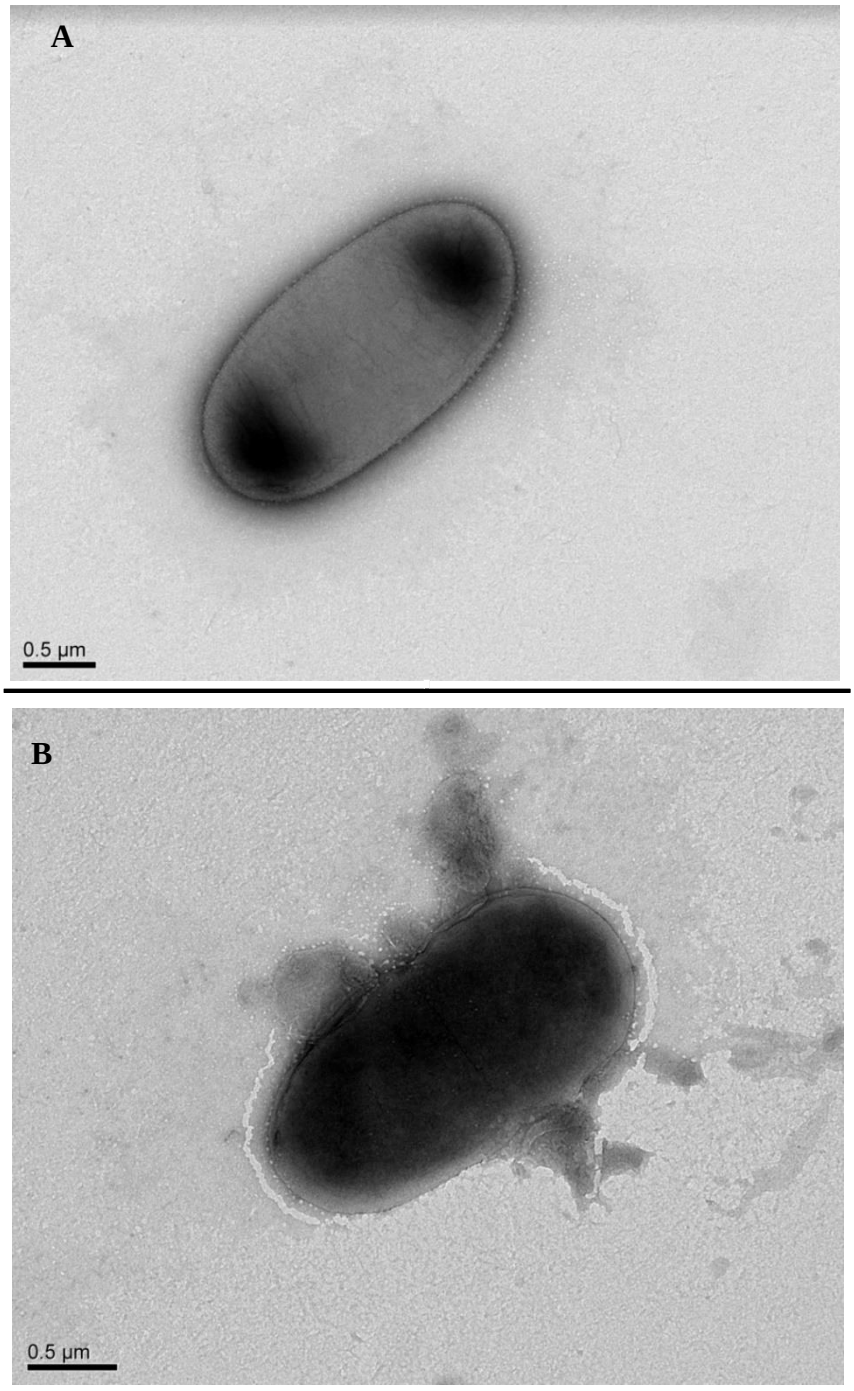

Figure E-2: External planktonic morphologies of 1.0% phosphotungstic acid stained BW25113Δ*minC E. coli* cells untreated (A) at 7800x magnification and 50 µM $AgNO_3$ treated (B) at 9600x magnification, observed by TEM. In untreated sample BW25113Δ*minC* confines to normal bacillus morphology. In contrast, treated BW25113Δ*minC* appear to have complete disruption and compromise of the cellular envelope.

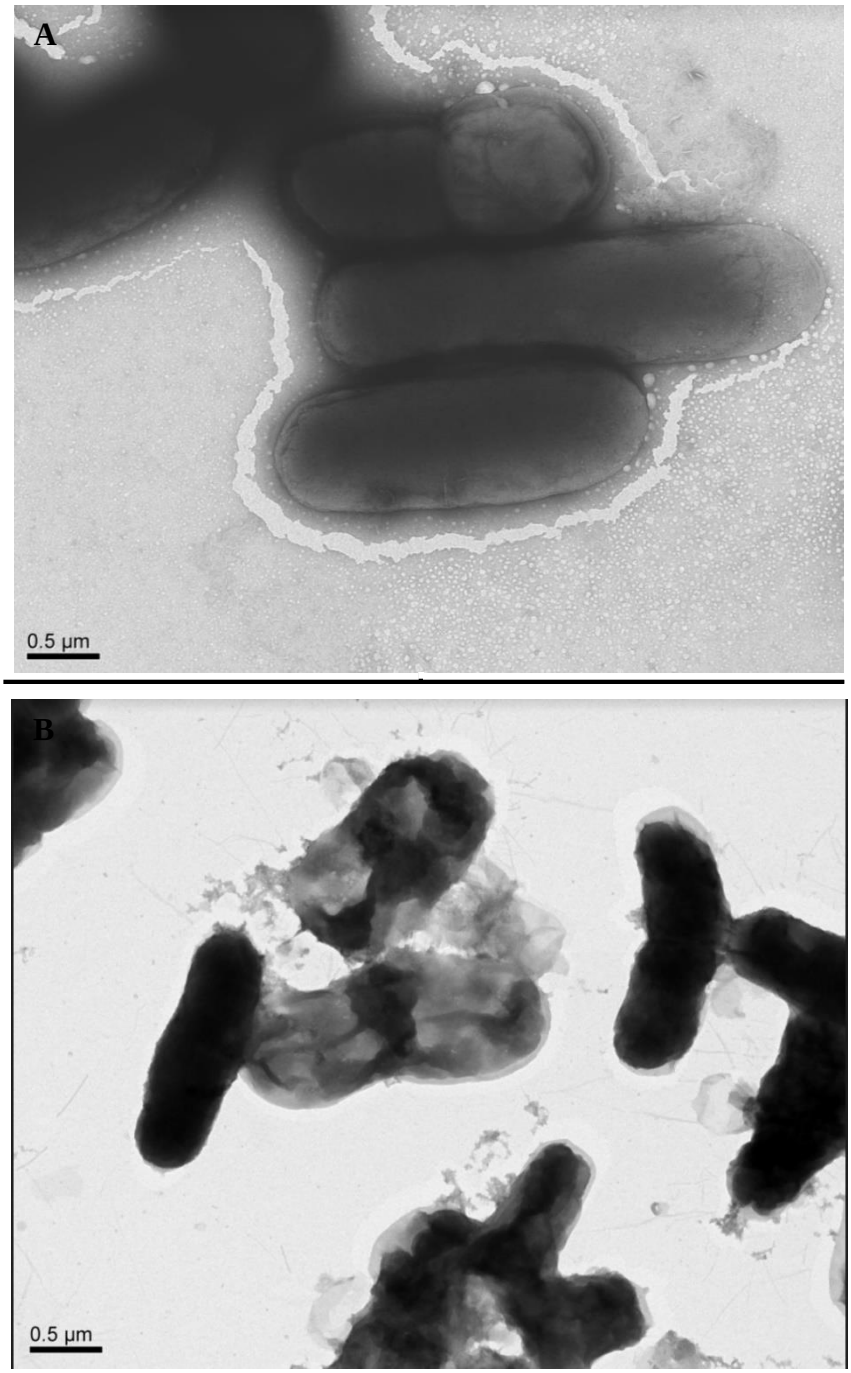

Figure E-3: External planktonic morphologies of 1.0% phosphotungstic acid stained BW25113Δ*sanA E. coli* cells untreated (A) and 50 µM $AgNO_3$ treated (B) observed by TEM at 7800 x magnification. In untreated sample BW25113Δ*minC* confines to normal bacillus morphology. In contrast, treated BW25113Δ*sanA* appear to have complete disruption of the cellular envelope.

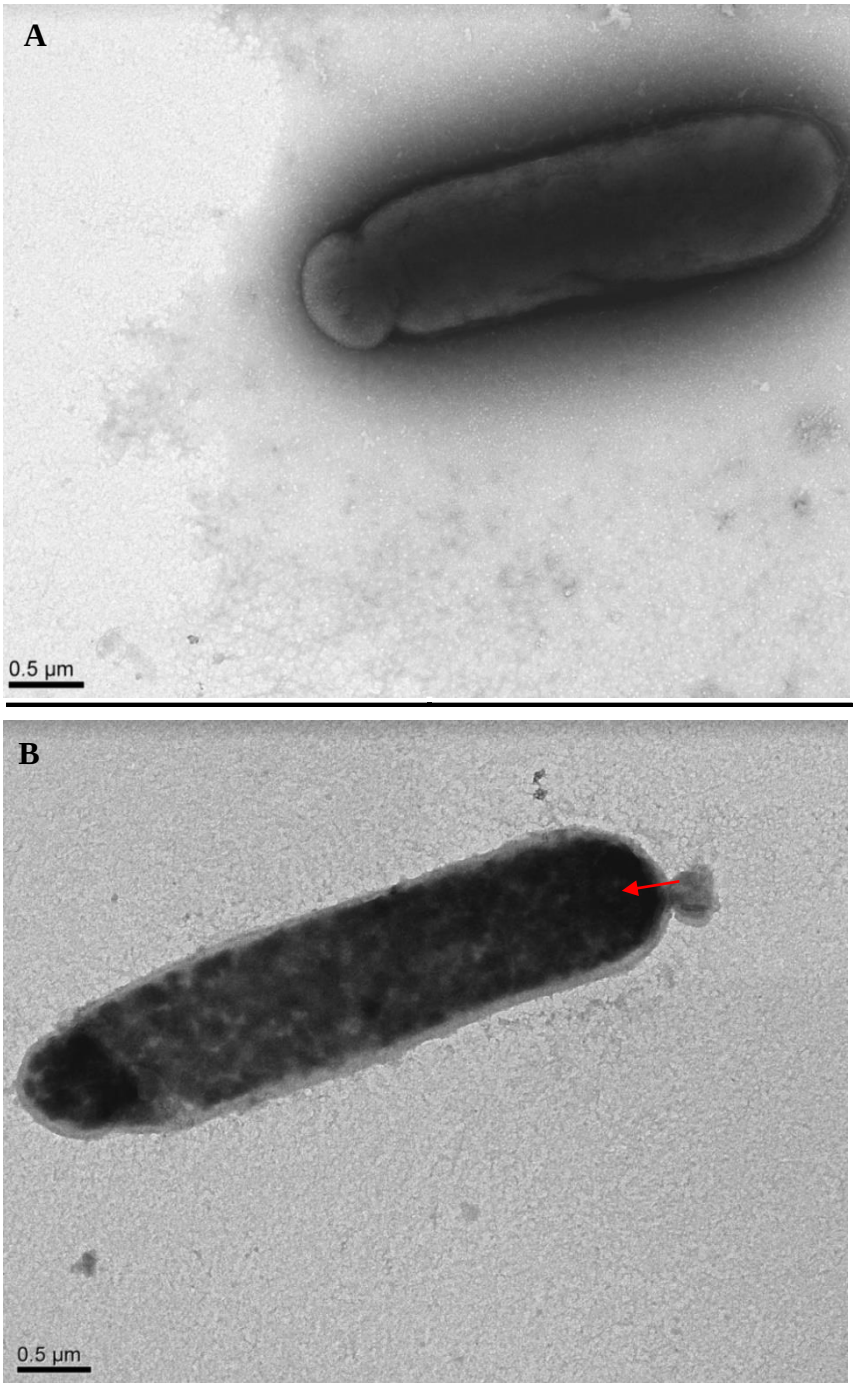

Figure E-4: External planktonic morphologies of 1.0% phosphotungstic acid stained BW25113Δ*ybhO E. coli* cells untreated at (A) and 50 µM $AgNO_3$ treated (B) observed by TEM at 7800 x magnification. In untreated sample BW25113Δ*ybhO* confines to normal bacillus morphology. In contrast, treated BW25113Δ*ybhO* appear to have localized disruption of the cellular envelope with plumes of cellular debris being released from cell (red arrow).

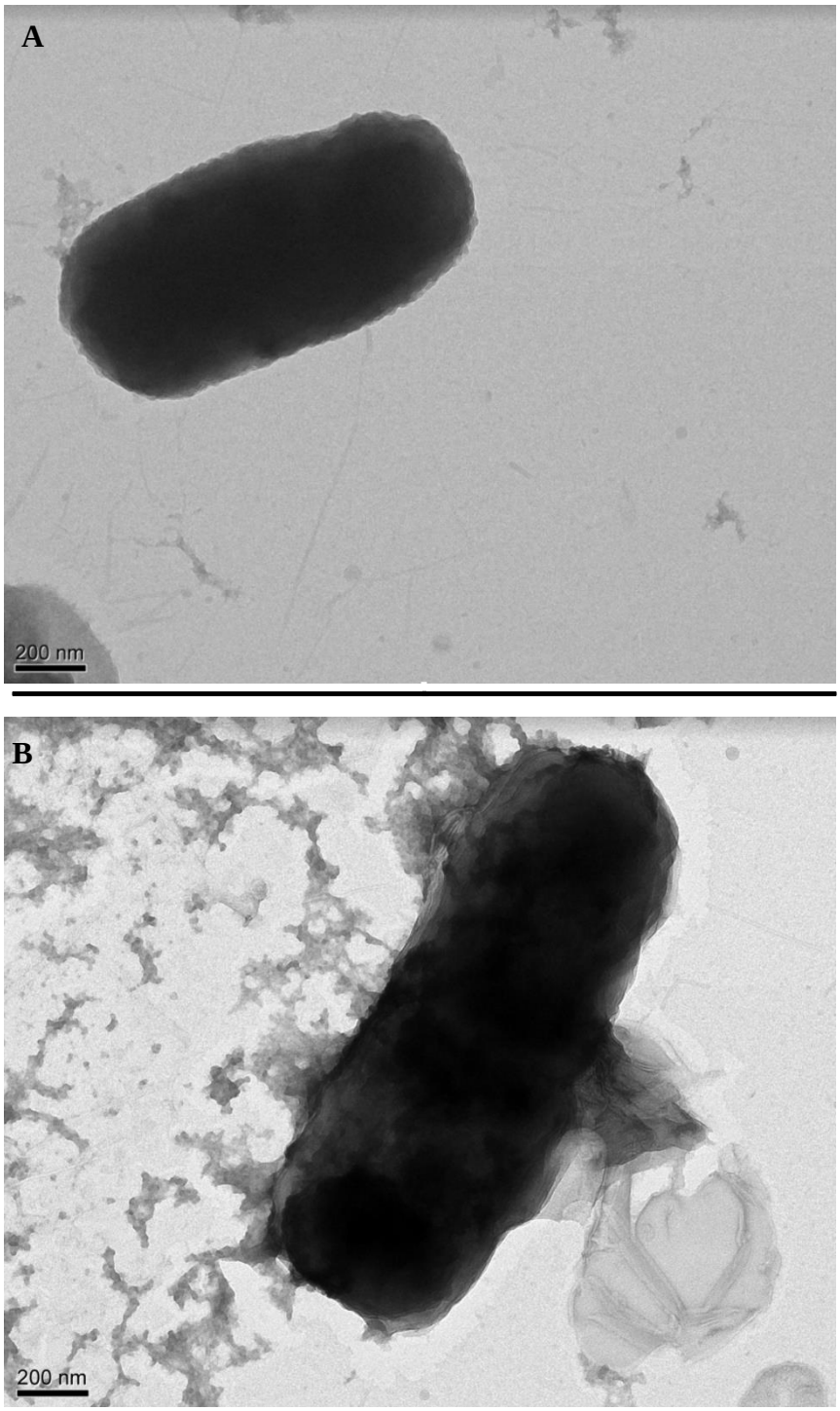

Figure E-5: External planktonic morphologies of 1.0% phosphotungstic acid stained BW25113Δ*tolB* *E. coli* cells untreated (A) and 50 µM $AgNO_3$ treated (B) observed by TEM, at 19000 x magnification. In untreated sample BW25113Δ*tolB* confines to normal bacillus morphology. In contrast, treated BW25113Δ*tolB* appear to have complete disruption of the cellular envelope.

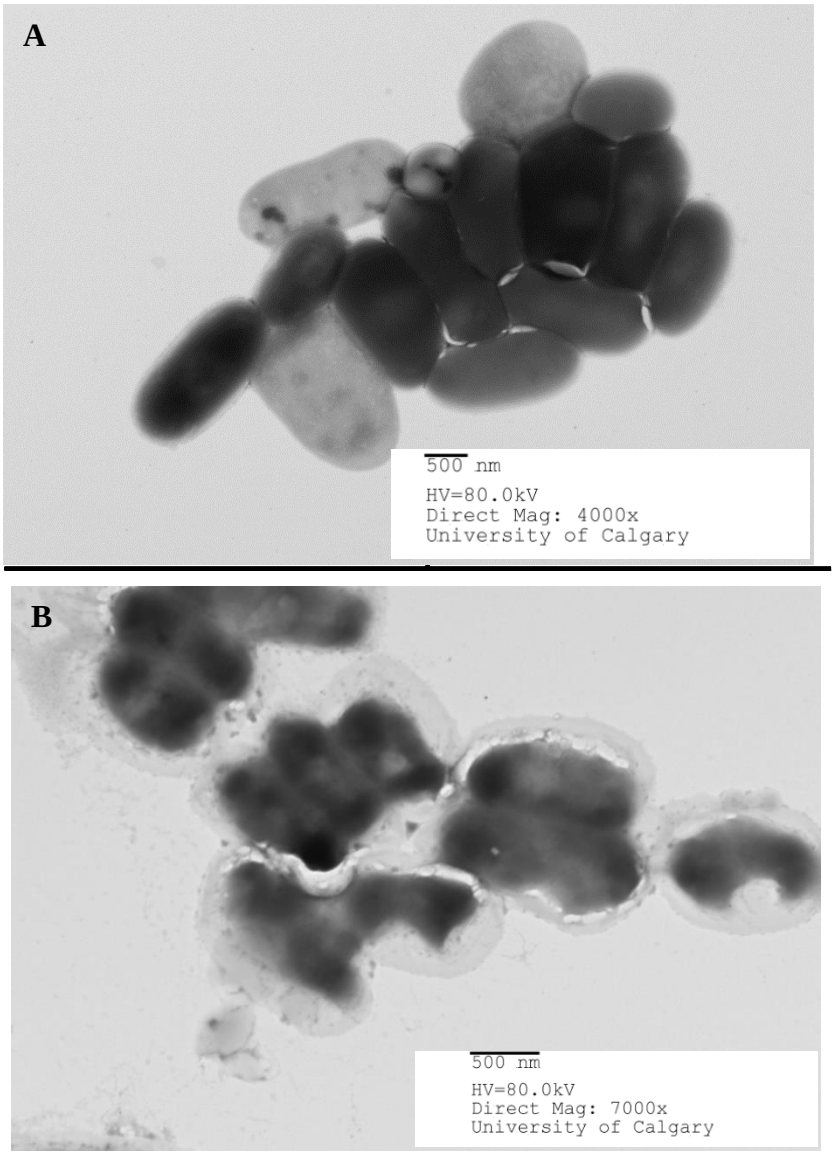

Figure E-6: External planktonic morphologies of 1.0% phosphotungstic acid stained wildtype K-12 MG1655 *E. coli* cells untreated (A) and 50 µM $AgNO_3$ treated (B) observed by TEM, at 4000 x magnification and 7000X magnification respectively. In the untreated sample, wildtype K-12 MG1655 cells appear to have a normal phenotype. In contrast, the treated cells displayed either localized or complete separation of the cell membrane from the cell wall.

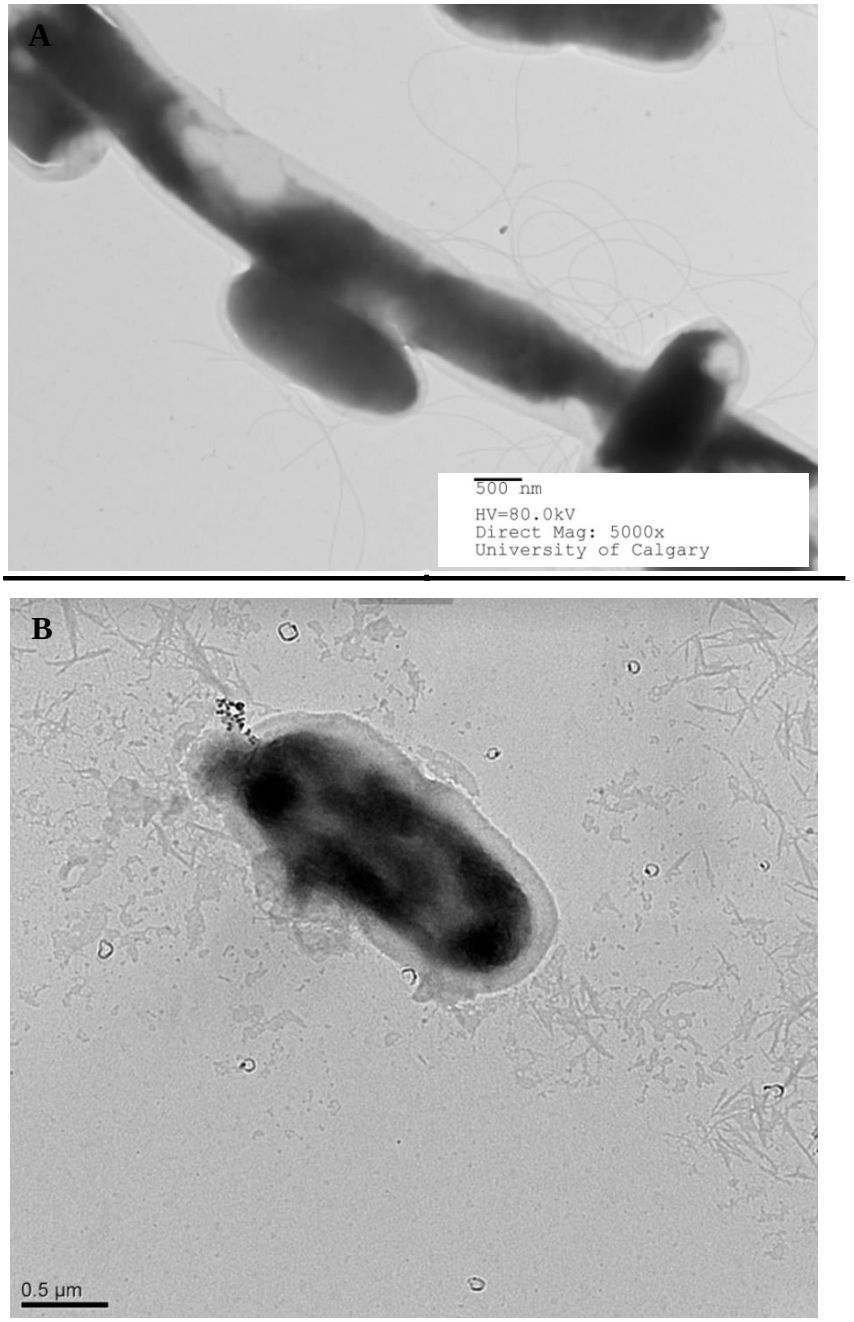

Figure E-7: External planktonic morphologies of 1.0% phosphotungstic acid stained K-12 MG1655Δ*rodZ E. coli* cells untreated (A) and 50 µM $AgNO_3$ treated (B) observed by TEM, at 5000 x magnification and 6500X magnification respectively. In the untreated cells, some of the mutant MG1655Δ*rodZ* cells displayed a mutant elongated bacillus phenotype, which was commonly found throughout the sample. In contrast the treated cells displayed either localized or complete separation of the cell membrane from the cell wall.

Appendix F: Disk diffusion assay

Contains images of one biological trial of the high throughput toxicological assay aimed to determine the sensitivity or resistance of the *E. coli* BW25113 ag-responsive mutants to various antimicrobial compounds.

Table F-1: Indicating the appropriate metal infused into sterile Sterile antimicrobial disks

Disk Number	Corresponding Challenge
1	$NaNO_3$
2	Na_2SO_4
3	$Ga(NO_3)_3 \cdot H_2O$
4	$CuSO_4$
5	$ZnSO_4$
6	Saline (NaCl)
7	$Al_2(SO_4)_3$
8	$NiSO_4 \cdot 6H_2O$
9	$AgNO_3$

*Metals were prepared following section *2.1.4.*

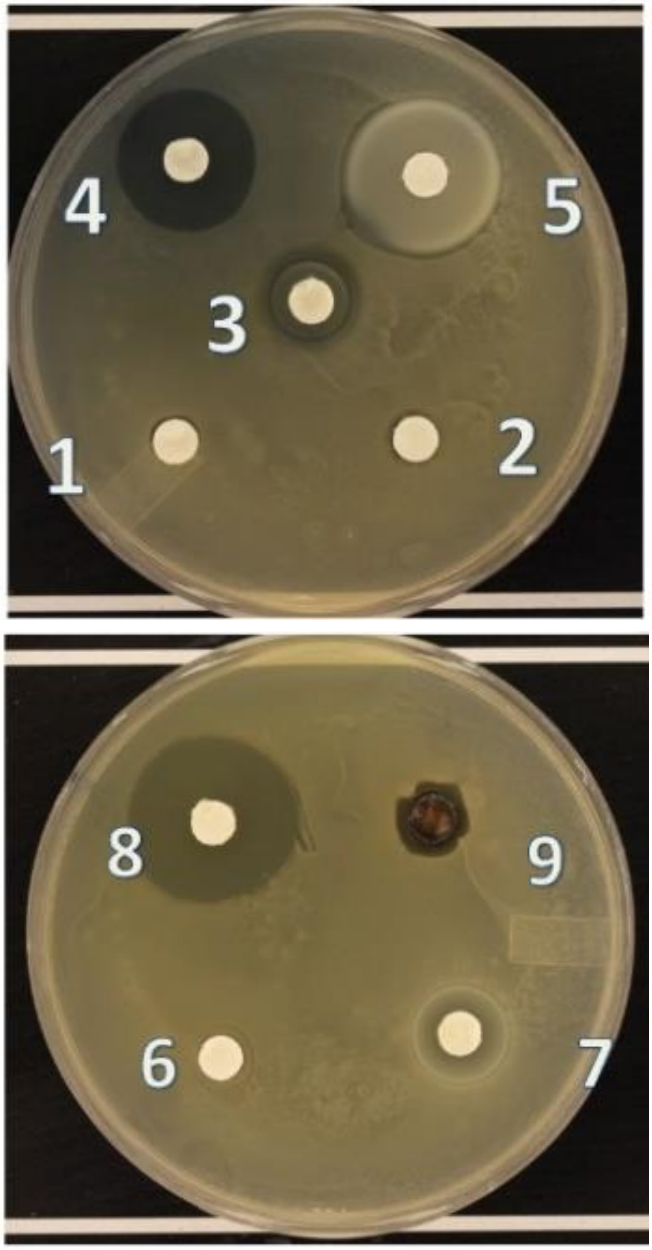

Figure F-1: Illustrates the disk diffusion assay conducted on wildtype BW25113 cells with the metals present in Table J-1.

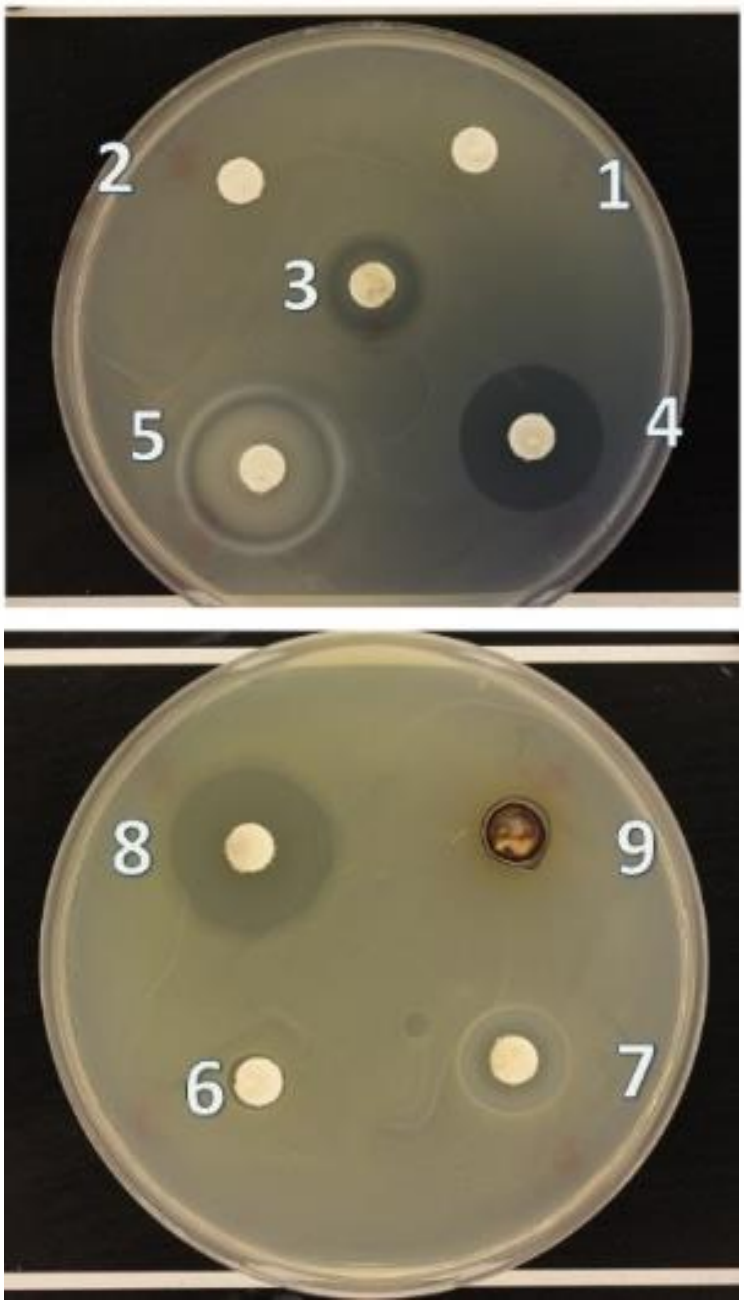

Figure F-2: Illustrates the disk diffusion assay conducted on wildtype BW25113Δ*damX* cells with the metals present in Table J-2.

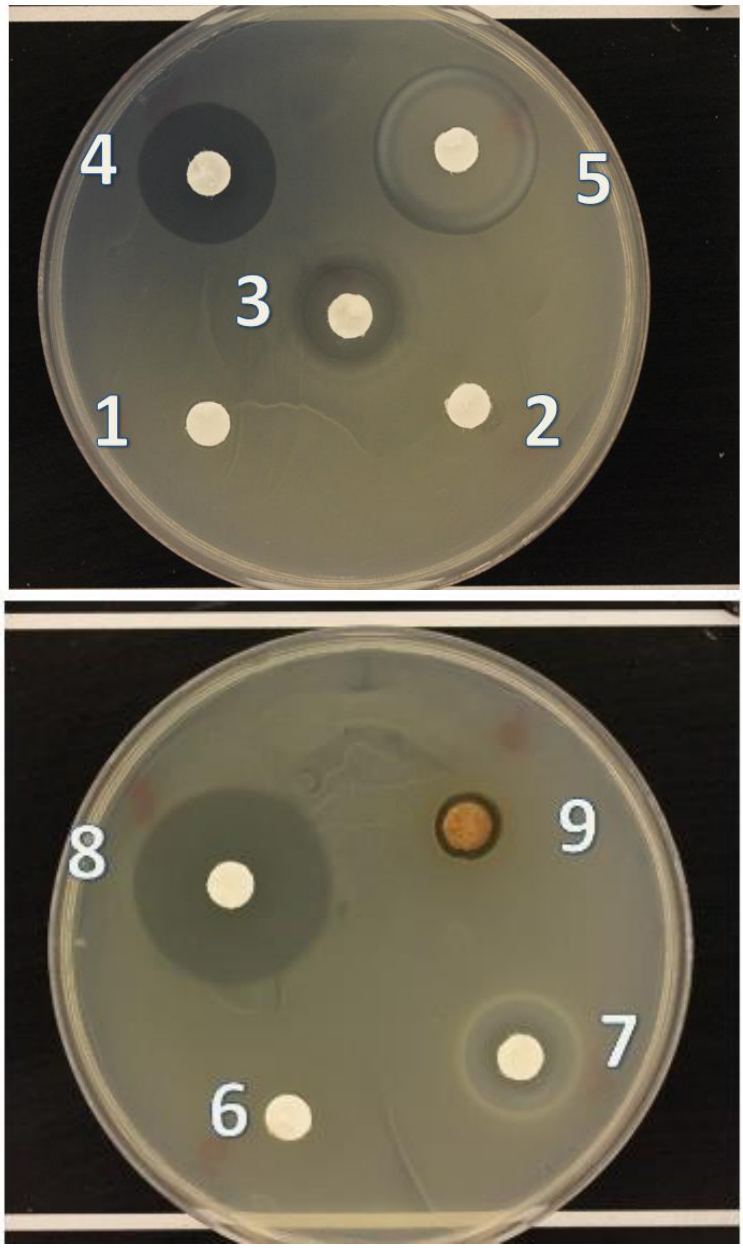

Figure F-3: Illustrates the disk diffusion assay conducted on wildtype BW25113Δ*rodZ* cells with the metals present in Table J-2.

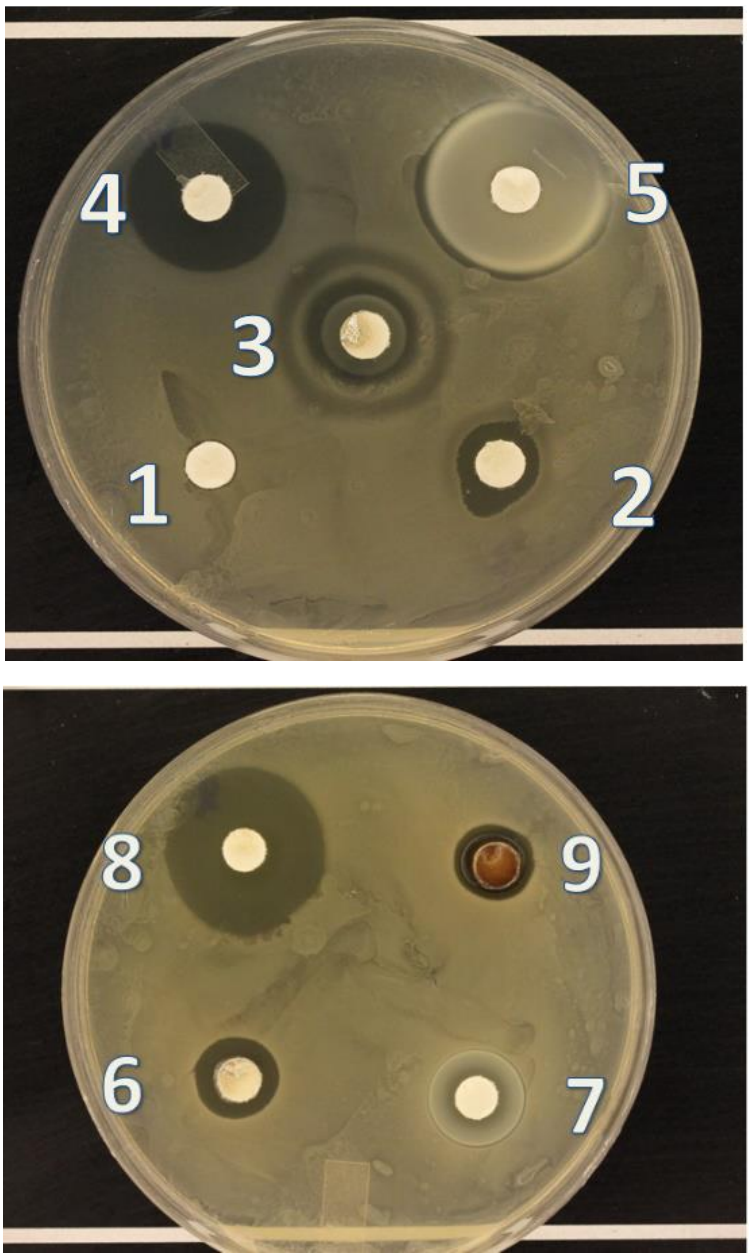

Figure F-4: Illustrates the disk diffusion assay conducted on wildtype BW25113Δ*minC* cells with the metals present in Table J-2.

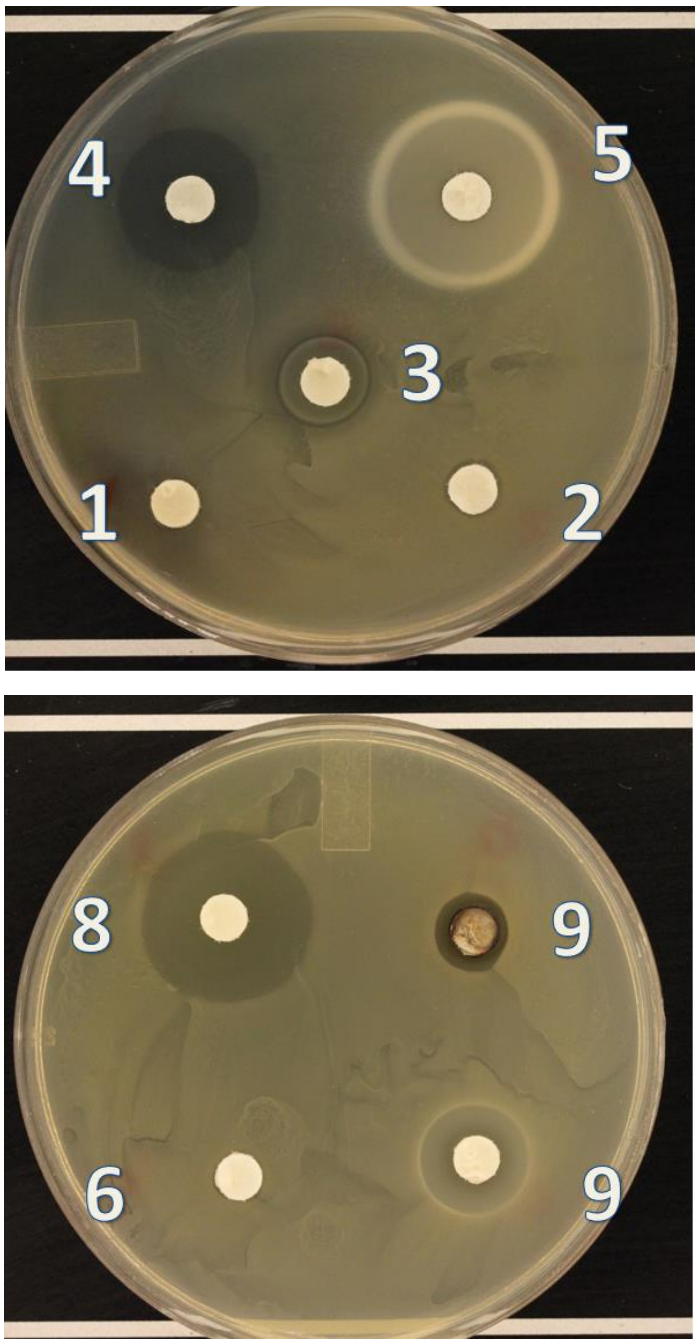

Figure F-5: Illustrates the disk diffusion assay conducted on wildtype BW25113Δ*SanA* cells with the metals present in Table J-2.

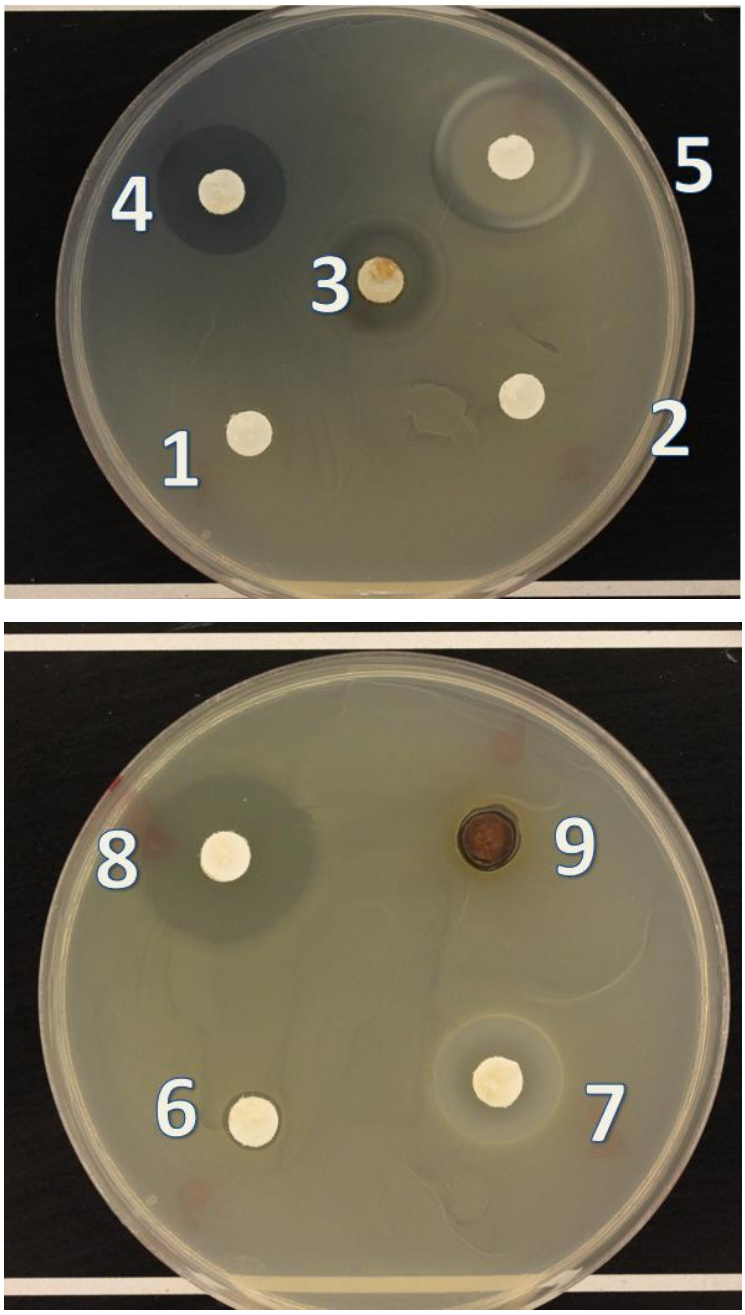

Figure F-6: Illustrates the disk diffusion assay conducted on wildtype BW25113Δ*ybhO* cells with the metals present in Table J-2.

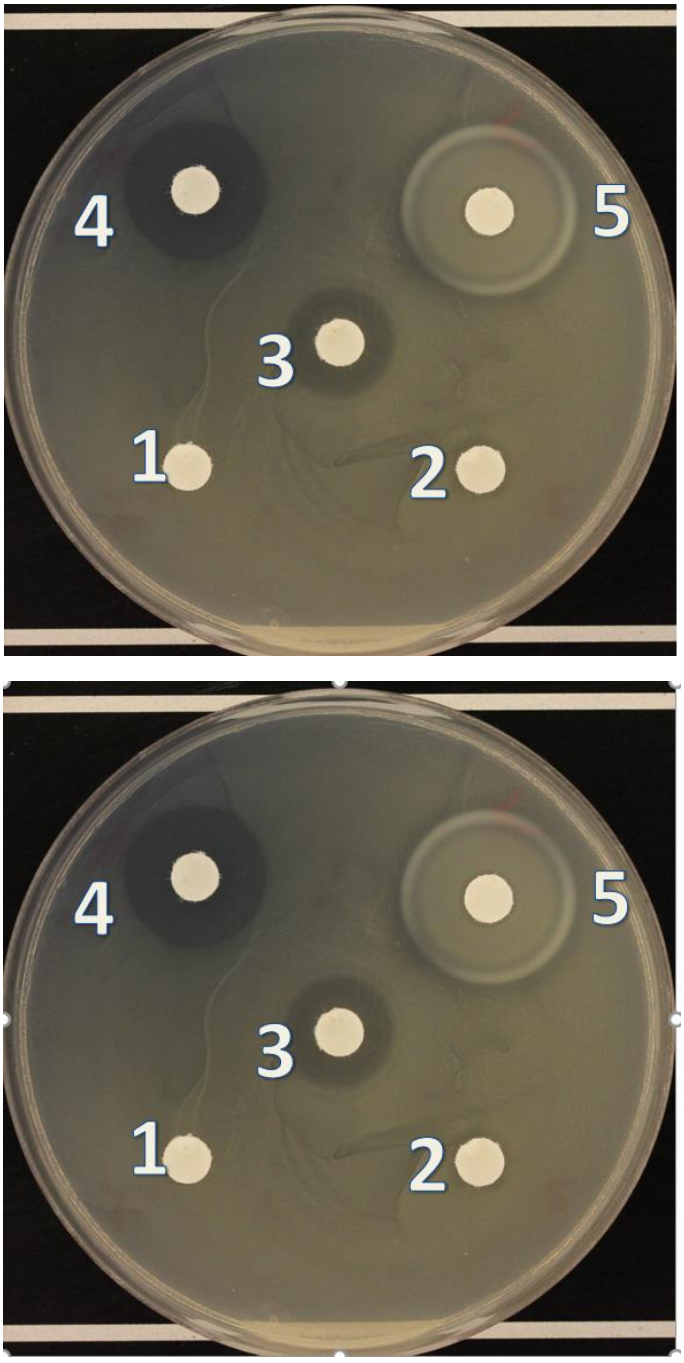

Figure F-7: Illustrates the disk diffusion assay conducted on wildtype BW25113Δ*tolB* cells with the metals present in Table J-2.